

การศึกษาการไฮเดรตของไอออนข้าวคู่อะลาตินโดยวิธีทฤษฎี

สุภาภรณ์ ดอกไม้ศรีจันทร์

วิทยานิพนธ์นี้เป็นส่วนหนึ่งของการศึกษาตามหลักสูตรปริญญาวิทยาศาสตรดุษฎีบัณฑิต

สาขาวิชาเคมี

มหาวิทยาลัยเทคโนโลยีสุรนารี

ปีการศึกษา 2548

ISBN 974-533-452-9

**A THEORETICAL STUDY ON HYDRATION OF
ALANINE ZWITTERION**

Supaporn Dokmaisrijan

**A Thesis Submitted in Partial Fulfillment of the Requirements for
the Degree of Doctor of Philosophy in Chemistry**

Suranaree University of Technology

Academic Year 2005

ISBN 974-533-452-9

**A THEORETICAL STUDY ON HYDRATION OF
ALANINE ZWITTERION**

Suranaree University of Technology has approved this thesis submitted in partial fulfillment of the requirements for the Degree of Doctor of Philosophy.

Thesis Examining Committee

M. Tangsathitkulchai

(Asst. Prof. Dr. Malee Tangsathitkulchai)

Chairperson

K. Sagarik

(Prof. Dr. Kritsana Sagarik)

Member (Thesis Advisor)

S. Hannongbua

(Assoc. Prof. Dr. Supot Hannongbua)

Member

A. Tongraar

(Assoc. Prof. Dr. Anan Tongraar)

Member

Visit Vao

(Asst. Prof. Dr. Visit Vao-soongnern)

Member

P. Suebka

(Assoc. Prof. Dr. Prasart Suebka)

S. Sujitjorn

(Assoc. Prof. Dr. Sarawut Sujitjorn)

Vice Rector for Academic Affairs

Dean of Institute of Science

สุภาภรณ์ ดอกไม้ศรีจันทร์ : การศึกษาการไฮเดรตของไอออนขั้วคู่อะลานีนโดยวิธีทฤษฎี

(A THEORETICAL STUDY ON HYDRATION OF ALANINE ZWITTERION)

อาจารย์ที่ปรึกษา : ศาสตราจารย์ ดร.กฤษณะ สาคริก, 99 หน้า. ISBN 974-533-452-9

งานวิจัยนี้ศึกษาโครงสร้างและพลังงานของโครงข่ายพันธะไฮโดรเจน (hydrogen bond network) ของโมเลกุลน้ำที่หมู่ฟังก์ชัน NH_3^+ และ COO^- ของไอออนขั้วคู่อะลานีน (alanine zwitterion) สองโครงรูปโดยใช้วิธีทฤษฎี การศึกษาเริ่มจากการสร้างศักย์ระหว่างโมเลกุลเพื่อใช้อธิบายอันตรกิริยาระหว่างไอออนขั้วคู่อะลานีนและน้ำ จากนั้นใช้วิธีการจำลองโมเลกุลพลวัต (molecular dynamics simulations) เพื่อศึกษาสมบัติของไอออนขั้วคู่อะลานีนในสารละลายน้ำ การวิเคราะห์โครงสร้างสามมิติและภูมิภาคพลังงานศักย์เฉลี่ยของโครงข่ายพันธะไฮโดรเจนของโมเลกุลน้ำทำโดยใช้แผนภาพการแจกแจงความน่าจะเป็น (probability distribution map) แบบต่างๆ

ผลจากการคำนวณโดยวิธีการจำลองโมเลกุลพลวัตแสดงว่า โครงรูปไอออนขั้วคู่อะลานีนที่มีโครงกระดูกแบนราบ (Alaz) มีเสถียรภาพการไฮเดรตโดยรวมสูงกว่าโครงรูปที่ระนาบ COO^- ทำมุม 90° กับระนาบ $\text{NC}^{\alpha}\text{C}$ (Alaz-R) อย่างไรก็ตาม พบว่าน้ำสามารถเข้าถึงโครงรูป Alaz-R ได้ดีกว่า การคำนวณยังแสดงด้วยว่า โมเลกุลน้ำสร้างโครงข่ายพันธะไฮโดรเจนรอบ Alaz และ Alaz-R ได้อย่างเป็นระเบียบโดยเฉพาะที่หมู่ NH_3^+ ทั้งนี้ โครงสร้างและพลังงานของโครงข่ายพันธะไฮโดรเจนของโมเลกุลน้ำที่หมู่ฟังก์ชัน NH_3^+ และ COO^- มีลักษณะแตกต่างกัน อันตรกิริยาระหว่างตัวถูกละลายและตัวทำละลายที่หมู่ NH_3^+ ของ Alaz และ Alaz-R แข็งแรงกว่าที่หมู่ COO^- ผลการคำนวณโดยวิธีการจำลองโมเลกุลพลวัตแสดงว่า โมเลกุลน้ำใช้เวลาอยู่ที่หมู่ NH_3^+ นานกว่าที่หมู่ COO^- และโครงสร้างการไฮเดรตที่หมู่ NH_3^+ ของ Alaz บางส่วนซ้อนเหลื่อมกับที่หมู่ COO^- ในขณะที่โครงสร้างการไฮเดรตที่หมู่ฟังก์ชันทั้งสองของ Alaz-R ค่อนข้างเป็นอิสระต่อกัน และโมเลกุลน้ำที่สร้างพันธะกับหมู่ NH_3^+ บางโมเลกุลสามารถเคลื่อนที่มาสร้างพันธะกับหมู่ COO^- ได้ ผลการคำนวณพบว่า หมู่ NH_3^+ และ COO^- มีแนวโน้มไม่สร้างพันธะไฮโดรเจนระหว่างกัน ในน้ำ

ผลการวิเคราะห์ภูมิภาคพลังงานศักย์เฉลี่ยของโครงข่ายพันธะไฮโดรเจนของโมเลกุลน้ำสรุปได้ว่า แม้ลักษณะของภูมิภาคพลังงานศักย์เฉลี่ยของโครงข่ายพันธะไฮโดรเจนของโมเลกุลน้ำค่อนข้างไม่สม่ำเสมอ แต่ภูมิภาคดังกล่าวสามารถอธิบายลักษณะจำเพาะและพฤติกรรมเชิงพลวัตของโมเลกุลน้ำได้โดยเฉพาะที่หมู่ฟังก์ชันของตัวถูกละลาย ผลการคำนวณโดยวิธีการจำลองโมเลกุลพลวัตกรณีสารละลายน้ำเสนอว่า หากต้องการข้อมูลเกี่ยวกับการ

ไฮดรตที่สมบูรณ์จะต้องนำโมเลกุลของน้ำและสมบัติเชิงพลวัตของมันมาร่วมพิจารณาในแบบจำลองด้วยเสมอ

สาขาวิชาเคมี

ปีการศึกษา 2548

ลายมือชื่อนักศึกษา Oliver Smita/Phu

ลายมือชื่ออาจารย์ที่ปรึกษา Dr. ลอรา

ลายมือชื่ออาจารย์ที่ปรึกษาร่วม Dr.

SUPAPORN DOKMAISRIJAN : A THEORETICAL STUDY ON
HYDRATION OF ALANINE ZWITTERION. THESIS ADVISOR :
PROF. KRITSANA SAGARIK, Ph.D. 99 PP. ISBN 974-533-452-9

ALANINE ZWITTERION/AMINO ACID/HYDROGEN BOND/T-MODEL/
HYDRATION/MD SIMULATIONS

This research focused on the study of the structures and energetic of hydrogen bond (H-bond) networks of water at the NH_3^+ and COO^- functional groups of two forms of alanine zwitterion using theoretical methods. The study started with the construction of intermolecular potentials between the alanine zwitterions and water, followed by molecular dynamics (MD) simulations of the aqueous solutions. The three-dimensional structures and the average potential energy landscapes of the H-bond networks of water were analyzed and visualized using various probability distribution (PD) maps.

The MD results revealed that the conformation with planar skeleton (Alaz) possesses larger overall stabilization by hydration, whereas the conformation with the COO^- plane being 90° with respect to the NC^αC backbone (Alaz-R) seems to be more accessible by water. The PD maps also showed that water forms well-defined H-bond networks around Alaz and Alaz-R, especially at the NH_3^+ group. The structures and energetic of the H-bond networks of water at the NH_3^+ and COO^- functional groups are quite different. The solute-solvent interaction at the NH_3^+ group of Alaz as well as Alaz-R is considerably stronger than at the COO^- group. The MD results revealed that water molecules spend longer time at the NH_3^+ group than at the COO^- group.

The MD results also showed that some parts of the hydration structures at the NH_3^+ group of Alaz overlap with some of that at the COO^- group; whereas the hydration structures at two functional groups of Alaz-R are quite independent. Some water molecules binding at the NH_3^+ group can translate to bind with the COO^- group. There was no direct evidence for the intramolecular H-bond formation between the NH_3^+ and COO^- groups.

The analysis of the average potential energy landscapes of the H-bond networks of water showed that, although their shapes are highly irregular, they can help characterize the dynamic behavior of water molecules especially at the functional groups of the solutes. The MD results led to the conclusion that complete information on molecular hydration can be obtained only when explicit water molecules, together with their hydration dynamics at the hydration sites, are considered in the model calculations.

School of Chemistry

Academic Year 2005

Student's Signature S. Dokmaimijan

Advisor's Signature H. Sepanik

Co-advisor's Signature A. Tonyasir

ACKNOWLEDGEMENTS

I am grateful to my thesis advisor, Prof. Dr. Kritsana Sagarik, for his valuable advices and comments for this research work. I would also like to thank the thesis examining committee for reading my thesis and for their useful suggestions.

My deep gratitude is extended to Assoc. Prof. Dr. Thanit Pewnim, a lecturer at Silpakorn University who encourage me to study in a Ph.D. program and Dr. Eckhard Spohr for his kindness, sincere advices and suggestions for my works and life when I did a research work at the Forschungszentrum Jülich, F. R. Germany.

I am thankful to all lecturers at School of Chemistry, Suranaree University of Technology for their useful comments. Special thanks for Assoc. Prof. Dr. Saowanee Rattanaphani, Assoc. Prof. Dr. Vichitr Rattanaphani and Asst. Prof. Dr. Malee Tangsathitkulchai for their kindness and suggestions about positive thinking.

The deepest gratitude to my family for their pure love, deep understanding and all supports.

Thanks for friendships and wonderful experiences we have shared to my unforgettable friends: Chulawadee Chantewalikhit, Pimolphan Nintasingh, Panita Decha, Jittima Chaodamrongsakul, Natthinee Supamethanont, Weenawan Somphon, Saiphon Schanpaka, Piyawan Tangkawanwanich, Montra Chairat, Rodjana Opassiri, Saowapa Chotisuwan, Thanaporn Tohsophon and Maslina Ibrahim.

I would like to thanks the Thailand Research Fund (TRF) for the Royal Golden Jubilee Ph.D. scholarship for financial supports. I would also like to thanks School of Chemistry, Suranaree University of Technology and Institute for Materials

and Processes in Energy System (IWV-3), Forschungszentrum Jülich, F. R. Germany
for research facilities for my research.

Supaporn Dokmaisrijan

CONTENTS

	Page
ABSTRACT IN THAI.....	I
ABSTRACT IN ENGLISH.....	III
ACKNOWLEDGEMENTS.....	V
CONTENTS.....	VII
LIST OF TABLES.....	IX
LIST OF FIGURES.....	X
LIST OF ABBREVIATIONS.....	XIV
LIST OF SYMBOLS.....	XVII
CHAPTER	
I INTRODUCTION.....	1
II THEORETICAL METHODS.....	9
2.1 The Alaz and Alaz-R conformations.....	9
2.2 The T-model Potential.....	11
2.3 Equilibrium structures of Alaz-H ₂ O and Alaz-R-H ₂ O 1 : <i>n</i> complexes.....	14
2.4 MD simulations.....	15
III RESULTS AND DISCUSSION.....	20
3.1 The Alaz-H ₂ O and Alaz-R-H ₂ O 1 : <i>n</i> complexes.....	20
3.2 MD simulations on [Alaz] _{aq} and [Alaz-R] _{aq}	24

CONTENTS (Continued)

	Page
3.2.1 Hydration structures and H-bond networks in aqueous solutions.....	26
3.2.1.1 [Alaz] _{aq}	26
3.2.1.2 [Alaz-R] _{aq}	34
3.2.2 Average potential energy landscapes at the H-bond networks.....	38
3.2.2.1 [Alaz] _{aq}	40
3.2.2.2 [Alaz-R] _{aq}	49
IV CONCLUSION	51
REFERENCES	54
APPENDICES	64
Appendix A Geometry of Alaz and the T-model parameters.....	65
Appendix B Additional information on the Alaz-H ₂ O and Alaz-R-H ₂ O 1 : <i>n</i> complexes.....	68
Appendix C Additional MD results on Alaz in aqueous solution.....	81
Appendix D Additional MD results on Alaz-R in aqueous solution.....	89
Appendix E Presentation and publication.....	97
CIRRICULUM VITAE	99

LIST OF TABLES

Table	Page
3.1 MD simulation parameters and results for [Alaz] _{aq} and [Alaz-R] _{aq}	25
3.2 The highest probabilities ($\langle P^{\text{PDO}} \rangle_{\text{max}}$) at the labeled areas on the PDO maps and the corresponding lowest average interaction energies ($\langle \Delta E_{\text{aq}}^{\text{X}} \rangle_{\text{min}}$) on the X maps in Figures 3.3-3.4.	29
3.3 Characteristic peak positions (R) related to H-bonds between water and the NH ₃ ⁺ , CH ₃ , CH and COO ⁻ groups, together with the corresponding running coordination number, n(R), obtained from MD simulations.....	33
3.4 Selected average H-bond distances ($\langle R_{\text{A-H...B}} \rangle$) and angles ($\langle \theta_{\text{A-H...B}} \rangle$), as well as the longest H-bond lifetimes ($\tau_{\text{A-H...B,max}}$) derived from MD simulations.....	41
A.1 Geometry of Alaz obtained from the neutron diffraction data.....	66
A.2 T-model parameters for Alaz and H ₂ O.....	67
B.1 Interaction energies and BSSE of Alaz-H ₂ O 1 : 1 complexes derived from the <i>ab initio</i> calculations.....	71
B.2 Interaction energies and BSSE of Alaz-R-H ₂ O 1 : 1 complexes derived from the <i>ab initio</i> calculations.....	77

LIST OF FIGURES

Figure	Page
1.1 Structures of the neutral form of twenty amino acids that differ in their side-chains.....	3
2.1 Two conformations of alanine zwitterion and the reference planes used in MD analyses.....	10
3.1 The absolute and some local minimum energy geometries of Alaz-H ₂ O and Alaz-R-H ₂ O 1 : 1 complexes computed from the T-model potentials.....	21
3.2 The absolute and some local minimum energy geometries of Alaz-H ₂ O and Alaz-R-H ₂ O 1 : 2 complexes computed from the T-model potentials.....	23
3.3 Selected PDO, AWPD and AW-WWPD maps for [Alaz] _{aq} obtained from MD simulations.....	27
3.4 Selected PDO, AWPD and AW-WWPD maps for [Alaz-R] _{aq} obtained from MD simulations.....	36
3.5 Cross section plots for the H-bond networks at the NH ₃ ⁺ group of [Alaz] _{aq} and [Alaz-R] _{aq}	43
3.6 Cross section plots for the H-bond networks at the COO ⁻ group of [Alaz] _{aq} and [Alaz-R] _{aq}	47

LIST OF FIGURES (Continued)

Figure	Page
B.1 The minimum energy geometries of the Alaz-H ₂ O 1 : 1 complexes obtained from T-model and MP2/6-311G(d,p) level.....	69
B.2 Equilibrium structures of the Alaz-H ₂ O 1 : 2 complexes derived from T-model.....	72
B.3 Equilibrium structures of the Alaz-H ₂ O 1 : 3 complexes derived from T-model.....	73
B.4 Equilibrium structures of the Alaz-H ₂ O 1 : 4 complexes derived from T-model.....	74
B.5 The minimum energy geometries of the Alaz-R-H ₂ O 1 : 1 complexes obtained from T-model and MP2/6-311G(d,p) level.....	75
B.6 Equilibrium structures of the Alaz-R-H ₂ O 1 : 2 complexes derived from T-model.....	78
B.7 Equilibrium structures of the Alaz-R-H ₂ O 1 : 3 complexes derived from T-model.....	79
B.8 Equilibrium structures of the Alaz-R-H ₂ O 1 : 4 complexes derived from T-model.....	80
C.1 PDO and PDH maps with respect to reference plane I for [Alaz] _{aq} obtained from MD simulations.	82
C.2 PDO and PDH maps with respect to reference plane II for [Alaz] _{aq} obtained from MD simulations.	83

LIST OF FIGURES (Continued)

Figure	Page
C.3 PDO and PDH maps with respect to reference plane III for [Alaz] _{aq} obtained from MD simulations.	84
C.4 AWPД and AW-WWPD maps with respect to reference plane I for [Alaz] _{aq} obtained from MD simulations.	85
C.5 AWPД and AW-WWPD maps with respect to reference plane II for [Alaz] _{aq} obtained from MD simulations.....	85
C.6 AWPД and AW-WWPD maps with respect to reference plane III for [Alaz] _{aq} obtained from MD simulations.	87
C.7 g(R) of [Alaz] _{aq} at 298 K derived from MD simulations	88
D.1 PDO and PDH maps with respect to reference plane I for [Alaz-R] _{aq} obtained from MD simulations.	90
D.2 PDO and PDH maps with respect to reference plane II for [Alaz-R] _{aq} obtained from MD simulations.....	91
D.3 PDO and PDH maps with respect to reference plane III for [Alaz-R] _{aq} obtained from MD simulations.	92
D.4 AWPД and AW-WWPD maps with respect to reference plane I for [Alaz-R] _{aq} obtained from MD simulations.....	93
D.5 AWPД and AW-WWPD maps with respect to reference plane II for [Alaz-R] _{aq} obtained from MD simulations.	94

LIST OF FIGURES (Continued)

Figure	Page
D.6 AWPD and AW-WWPD maps with respect to reference plane III for [Alaz-R] _{aq} obtained from MD simulations.....	95
D.7 $g(R)$ of [Alaz-R] _{aq} at 298 K derived from MD simulations.....	96

LIST OF ABBREVIATIONS

H-bond	=	Hydrogen Bond
NMR	=	Nuclear Magnetic Resonance
SCF-MO	=	Self-Consistent Field-Molecular Orbital
MC	=	Monte Carlo
Gly	=	Glycine
Ala	=	Alanine
Glyz	=	Glycine zwitterion
Alaz	=	Alanine zwitterion
Alaz-R	=	Alaz in which the COO ⁻ group is rotated to be 90°
AM1	=	Austin Model 1
PM3	=	Parameterized (NDDO) Model 3
NDDO	=	Neglect of Differential Diatomic Overlap
SCRf	=	Self-Consistent Reaction Field
B3LYP	=	Becke's Three parameter hybrid method using the Lee, Yang and Parr (LYP) correlation function
[Glyz] _{aq}	=	Glyz in aqueous solution
[Alaz] _{aq}	=	Alaz in aqueous solution
[Alaz-R] _{aq}	=	Alaz-R in aqueous solution
Glyz-H ₂ O 1 : <i>n</i> complexes	=	Cluster of the Glyz and water in the ratio of 1 : <i>n</i> where <i>n</i> is integer.

LIST OF ABBREVIATIONS (Continued)

Alaz-H ₂ O 1 : <i>n</i> complexes	=	Cluster of the Alaz and water in the ratio of 1 : <i>n</i> where <i>n</i> is integer.
Alaz-R-H ₂ O 1 : <i>n</i> complexes	=	Cluster of the Alaz-R and water in the ratio of 1 : <i>n</i> where <i>n</i> is integer.
T-model	=	Test-particle model
MD	=	Molecular Dynamics
PD	=	The probability distribution
PDO	=	The oxygen probability distribution
PDH	=	The hydrogen probability distribution
AWPD	=	The average solute-solvent interaction energy probability distribution
WWPD	=	The average solvent-solvent interaction energy probability distribution
AW-WWPD	=	The total-average interaction energy probability distribution
CHelpG	=	CHarges from electrostatic potentials using a Grid based method
MP2	=	The second order Møller-Plesset perturbation theory
B(T)	=	Second virial coefficient
CP	=	Counterpoise correction
BSSE	=	Basis Set Superposition Error

LIST OF ABBREVIATIONS (Continued)

PES	=	Potential Energy Surface
CP-PES	=	Counterpoise corrected- PES
NVE-MD	=	Microcanonical ensemble-MD
ps	=	pico second
fs	=	femto second
L	=	Simulation box length
MP2CP	=	Counterpoise correction energy at the MP2 level

LIST OF SYMBOLS

$^{\circ}$	=	Degrees
K	=	Kelvin
\AA	=	Angström
$\Delta E_{\text{T-model}}$	=	T-model interaction energy
ΔE_{SCF}^1	=	The first-order SCF interaction energy
ΔE^r	=	The higher-order energy term
ΔE_{MP2CP}	=	Counterpoise correction interaction energy at the MP2 level
SCF-X	=	SCF calculations using X basis set
SCFCP-X	=	SCF-X with BSSE correction
$\text{BSSE}_{\text{SCF-X}}$	=	BSSE at the SCF level using X basis set (SCF-X - SCFCP-X)
MP2-X	=	MP2 calculation using X basis set
MP2CP-X	=	MP2-X with BSSE correction
$\text{BSSE}_{\text{MP2-X}}$	=	BSSE at the MP2 level using X basis set (MP2-X - MP2CP-X)
$g(R)$	=	The atom-atom pair correlation function
$n(R)$	=	The average running coordination number of $g(R)$
R_{max}	=	Position of the maximum of the main peak of $g(R)$
R_{min}	=	Position of the minimum of the main peak of $g(R)$
$n(R_{\text{max}})$	=	The running coordination number at R_{max} of $g(R)$
$n(R_{\text{min}})$	=	The running coordination number at R_{min} of $g(R)$
$\langle E_{\text{aq}}^{\text{pot}} \rangle$	=	The average potential energy of aqueous solution

LIST OF SYMBOLS (Continued)

$\langle E_{\text{aq}}^{\text{solv-solv}} \rangle$	=	The average solvent-solvent interaction energy
$\langle R_{\text{A-H..B}} \rangle$	=	The average H-bond distance between molecules A and B
$\langle \theta_{\text{A-H..B}} \rangle$	=	The average H-bond angles
$\tau_{\text{A-H..B,max}}$	=	The longest H-bond lifetime
$\langle P^{\text{PDO}} \rangle_{\text{max}}$	=	The highest probabilities at the labeled areas on the PDO map
$\langle \Delta E_{\text{aq}}^{\text{X}} \rangle_{\text{min}}$	=	The lowest average interaction energies on the X map
$\langle \Delta E_{\text{aq}}^{\text{AWPD}} \rangle_{\text{min}}$	=	The lowest average interaction energy on the AWPD map
$\langle \Delta E_{\text{aq}}^{\text{WWPD}} \rangle_{\text{min}}$	=	The lowest average interaction energy on the WWPD map
$\langle \Delta E_{\text{aq}}^{\text{AW-WWPD}} \rangle_{\text{min}}$	=	The lowest average interaction energy on the AW-WWPD map
$\langle \Delta E_{\text{aq}}^{\text{X}} \rangle_{\text{min,av}}$	=	The average of $\langle \Delta E_{\text{aq}}^{\text{X}} \rangle$
	=	$\sum_{i=1}^N \frac{\langle E_{\text{aq}}^{\text{X}} \rangle_i}{N}$, N = number of the labeled area
$\langle \Delta E_{\text{aq}}^{\text{L}} \rangle$	=	The transition energy barriers to water exchange within the H-bond network
$\langle \Delta E_{\text{aq}}^{\text{T}} \rangle$	=	The transition energy barriers to water exchange between the H-bond network and the outside

CHAPTER I

INTRODUCTION

Proteins are essential components of living systems with the greatest functional range. Proteins consist of polypeptide chains that are made up of residues or amino acids linked together by peptide bonds. The polypeptide backbone is composed of repeating units that are identical, except for the chain termini. There are twenty common naturally occurring amino acids that differ in their side-chains as illustrated in Figure 1.1. The side-chains of those amino acids differ in size, shape, charge, hydrogen bond (H-bond) capacity, hydrophobicity and chemical reactivity. Individually and collectively, these side-chains contribute to the structure and function of proteins.

The study on the interactions of proteins with water molecules has been of interest for a long time. The most important consideration for understanding proteins is the influence of solvents such as water on the functional integrity and structural stability of them. This influence is manifested in a variety of different phenomena, ranging from marked solvent effects on conformation to the stabilization of oppositely charged side-chains. It is well known from X-ray diffraction experiments that structures of proteins in crystals depend largely on their conformations in aqueous solution from which they are grown (Baker, 1994). Several X-ray structural analyses also revealed that large solvent regions separate individual protein molecules in the crystal form (Billeter, 1995; Levitt and Park, 1993; Thanki, Thornton, and

Goodfellow, 1988). Since various experimental evidence has shown that solution properties can be consistently explained by crystal structures (Feig and Pettitt, 1998; Jiang and Brünger, 1994; Makarov, Pettitt, and Feig, 2002; Schoenborn, Garcia, and Knott, 1995), it has been proposed that protein structures in the crystal are essentially the same as in solution (Mathews, 1977; Rupley, 1969) and, in most cases, general phenomena of hydration as well as local hydration patterns can be discussed more accurately in the context of water distributions rather than individual water molecules (Makarov *et al.*). Nowadays, models for the hydration layers in close contact with the protein surface are described in terms of deviations from bulk solvent properties. Restricted motions, stronger binding and preferential binding sites are some of the properties that characterize well-ordered hydration layers (Schoenborn, Garcia, and Knott). Also experimental methods such as diffraction techniques and NMR or other spectroscopies have been applied to determining the structure of solvated proteins. However, the detailed analysis of arrangements of water in the crevices of proteins is limited due to the complexity of their structures.

In order to obtain more insight into the hydration of proteins as well as the role of water in its biological function and structure and the noncovalent forces stabilizing their native structures, it is necessary to study the hydration of the α -amino acids. Particularly the hydrophilic and/or hydrophobic hydration of the amino acids chains is interesting in view of the driving forces behind protein folding. Apart from this, the study of free amino acids is also interesting since there is a finite number of amino acids and they have tremendous biological and biochemical significant. Moreover, amino acids contain a variety of intramolecular and intermolecular interactions that lead to very flexible conformations. Their properties are thus not easily amenable to

experiments. However, the properties are accessible by the methods of computational chemistry, even up to high level *ab initio* calculations.

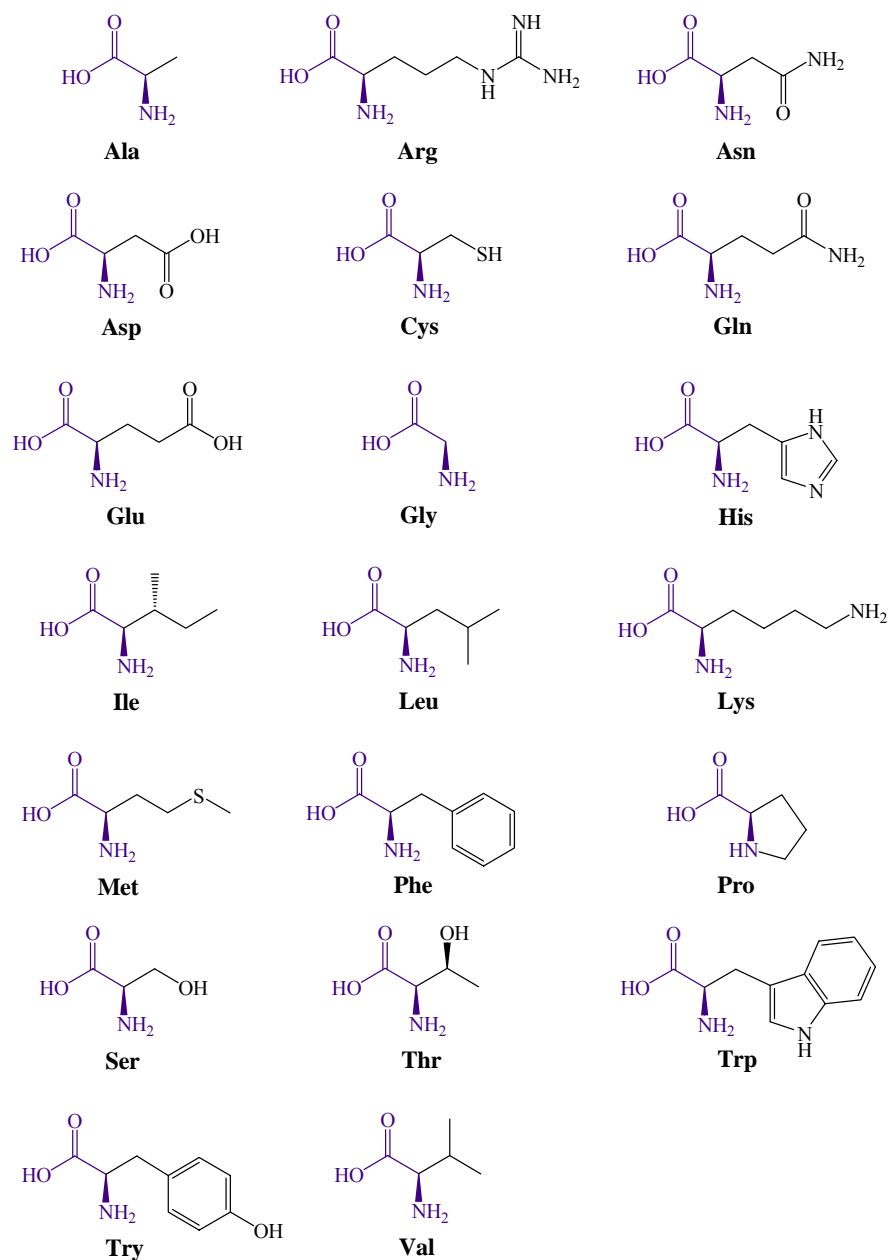


Figure 1.1 Structures of the neutral form of twenty amino acids that differ in their side-chains.

Attempts have been made to investigate hydration structures and energetic of amino acids in aqueous solution using various theoretical and experimental techniques (Alagona, Ghio, and Kollman, 1988; Castronuovo, Elia, and Velleca, 1996; Clementi, Cavallone, and Scordamaglia, 1977; Ding and Krogh-Jespersen, 1996; Förner, Otto, Bernhardt, and Ladik, 1981; Jensen and Gordon, 1995; Kalko, Guàrdia, and Padró, 1999; Kikuchi, Matsuoka, Sawahara, and Takahashi, 1994; Kikuchi, Watanabe, Ogawa, Takase, and Takahashi, 1997; Mark and Nilsson, 2001; Mezei, Mehrotra, and Beveridge, 1984; Park, Ahn, and Lee, 2003; Rzepa and Yi, 1991; Suzuki, Shigematsu, Fukunishi, and Kodama, 1997; Tajkhorshid, Jalkanen, and Suhai, 1998; Tuñón, Silla, Millot, Martins-Costa, and Ruiz-López, 1998; Watanabe, Hashimoto, Takase, and Kikuchi, 1997). One of the most pioneering computer simulations of amino acids in aqueous solution was put forward by Clementi *et al.* In Clementi *et al.*, intermolecular potentials for twenty-one amino acids were derived from Self-Consistent Field–Molecular Orbital (SCF-MO) calculations and some of them were applied in Monte Carlo (MC) simulations of aqueous solution (Clementi, 1980). Clementi suggested various possibilities to visualize and analyze hydration structures at functional groups of amino acids from SCF-MO calculations and MC simulations. It was also proposed for the first time that the detailed solvation structure is governed by a subtle balance between solute-solvent and solvent-solvent interactions and the H-bond filaments or H-bond networks of water are most likely the key aspect for fast and long distance deprotonation at one site and protonation at another site of biological molecules (Clementi). These imply the necessity to include explicitly water molecules in theoretical models and partly form the basis for the present investigation.

Glycine (Gly) and alanine (Ala) have been frequently chosen as model molecules in the study of amino acid in aqueous solution (Alagona *et al.*, 1988; Clementi *et al.*, 1977; Ding and Krogh-Jespersen, 1996; Förner *et al.*, 1981; Jensen and Gordon, 1995; Kikuchi *et al.*, 1994, 1997; Mezei *et al.*, 1984; Park *et al.*, 2003; Rzepa and Yi, 1991; Tajkhorshid *et al.*, 1998; Tuñón *et al.*, 1998; Watanabe *et al.*, 1997). It is well known that Gly and Ala exists in zwitterionic forms (Glyz and Alaz) in polar solvents and in the crystalline state (Gaffney, Pierce, and Friedman, 1977; Kimura, Nakamura, Eguchi, Sugisawa, Deguchi, Ebisawa, Suzuki, and Shoji, 1998; Lehmann, Koetzle, and Hamilton, 1972). At the earliest stage of theoretical studies, *ab initio* calculations with restricted basis sets were applied on the Glyz-H₂O 1 : *n* complexes (Clementi, 1980; Ding and Krogh-Jespersen; Förner *et al.*; Jensen and Gordon; Rzepa and Yi), from which structural properties in aqueous solution were anticipated. Based on the semi-empirical Austin Model 1 (AM1) and Parameterized (NDDO) Model 3 (PM3) as well as SCF-MO calculations, it was suggested that the microsolvated species of amino acids with fifteen water molecules can yield solvation energies close to the bulk solvation limit (Rzepa and Yi). The most probable microstructures of Glyz-H₂O are 1 : 7 and 1 : 15 complexes, which were found in Rzepa and Yi to be represented by a H-bond network of up to two water molecules linking together the NH₃⁺ and COO⁻ groups. However, numerous theoretical and experimental investigations have shown that the structures of such microsolvated species in the gas phase and in aqueous solution can be completely different (Desfrancois, Carles, and Schermann, 2000). The complicated H-bond networks in aqueous solution were pointed out to be responsible for the discrepancy (Desfrancois *et al.*).

Alagona *et al.* (1988) conducted a systematic analysis of water structures in the vicinities of the functional groups of Glyz in aqueous solution ($[\text{Glyz}]_{\text{aq}}$). They suggested four types of water molecules in $[\text{Glyz}]_{\text{aq}}$, namely those tightly bound to the oxygen atoms of the carboxyl group, those tightly bound to the ammonium group, those hydrophobically localized at the methylene group and those in the bulk. It was also concluded by Alagona *et al.* that the strong intramolecular H-bond between one of the oxygen atom in the COO^- group and the internal hydrogen atom in the NH_3^+ group prevents the formation of an intermolecular H-bond with water for both atoms.

Limited theoretical and experimental information is available for Ala compared to Gly. A detail analysis of the conformations of Glyz and Alaz in aqueous solution was reported (Kikuchi *et al.*, 1994, 1997; Watanabe *et al.*, 1997), based on the results of *ab initio* MO calculations with a continuum model and MC simulations. The authors concluded that the nearly planar skeleton is to be the most stable structure in aqueous solution and the stabilization by the aqueous solvent is larger in the conformation with the COO^- plane being 90° with respect to the NC^αC backbone plane. The latter conformation is regarded as Alaz-R in the present study. In contrast to the conclusion made by Alagona *et al.* (1988), Watanabe *et al.* pointed out the possibility for a water molecule to form a H-bond with the internal hydrogen atom of the NH_3^+ group. Additionally, they suggested that the hydrations at the COO^- and at the NH_3^+ groups are quite independent for Glyz.

The applicability of *ab initio* calculations with continuum models, such as the Self-Consistent Reaction Field (SCRF) method, has been frequently mentioned (Smith, 1994). This is due mainly to the fact that *ab initio* calculations with continuum models neglect specific short-range solute-solvent interactions as well as

temperature effects. These make them applicable only for systems, in which solvents act only as perturbation on the gas-phase property of the system (Smith). The effects of the presence of water molecules on the structure of Alaz were studied using *ab initio* calculations with Becke's Three parameter hybrid method using the Lee, Yang and Parr (LYP) correlation function (B3LYP) using the 6-31G* basis set. The calculations were compared to those within the Onsager continuum model (Tajkhorshid *et al.*, 1998). It was reported that the conformations of Alaz are strongly influenced by water molecules, mainly through the electrostatic, polarization and H-bond interactions. It was also shown that, in order to hydrate both NH_3^+ and COO^- groups, at least four water molecules have to be included in the model calculations (Tajkhorshid *et al.*). The three-dimensional structures of the H-bond networks of water in the vicinities of both NH_3^+ and COO^- groups of Alaz could not be presented due to the restricted number of water molecules considered in the theoretical investigation (Tajkhorshid *et al.*).

In the present work, structures and energetic of the H-bond networks in aqueous solution of Alaz ($[\text{Alaz}]_{\text{aq}}$) and Alaz-R ($[\text{Alaz-R}]_{\text{aq}}$) were studied. The two forms of the alanine zwitterion, Alaz and Alaz-R, were considered to investigate the effects of conformation change on the H-bond networks at the charged functional groups. The investigation started with the construction of intermolecular potentials to describe the interaction between Alaz and water, as well as Alaz-R and water, using the Test-particle model (T-model). The T-model potentials were tested in the calculations of the equilibrium structures and interaction energies of Alaz-H₂O and Alaz-R-H₂O 1 : *n* complexes, with *n* = 1 to 2. The computed T-model potentials were then applied in Molecular Dynamics (MD) simulations of $[\text{Alaz}]_{\text{aq}}$ and $[\text{Alaz-R}]_{\text{aq}}$.

In order to obtain information on the three-dimensional structures of the H-bond networks of water in the vicinities of the NH_3^+ and COO^- groups, the MD results were analyzed and visualized based on the oxygen (PDO) and hydrogen probability distribution (PDH) maps (Clementi, 1980). The interaction energy distributions in $[\text{Alaz}]_{\text{aq}}$ and $[\text{Alaz-R}]_{\text{aq}}$ were computed and displayed using the average solute-solvent (AWPD) and average solvent-solvent interaction energy probability distribution (WWPD) maps (Clementi). In order to provide insight into the stability and hydration dynamics of water molecules in the H-bond networks, the so-called total-average interaction energy probability distribution maps (AW-WWPD) were computed from the AWPD and WWPD maps. The results were discussed in comparison with available theoretical and experimental data of the same as well as similar systems.

CHAPTER II

THEORETICAL METHODS

In this chapter, the details of the research methods were explained. The calculations were divided into two parts, namely T-model and MD simulations. The derivation of the T-model parameters for Alaz, Alaz-R and H₂O molecules are briefly described.

2.1 The Alaz and Alaz-R conformations

Tajkhorshid, Jalkanen, and Suhai (1998) reported that the conformations of Alaz are strongly influenced by the presence of water molecules, and the results of geometry optimizations could be totally different after the inclusion of explicit water molecules in the calculation. The structure of Alaz in Figure 2.1 is in accordance with the experimental findings that, in the crystalline state and aqueous solution, the most probable structures of Glyz and Alaz consist of bifurcated-intramolecular H-bonds between the N-H groups and the oxygen atom (Lehmann, Koetzle, and Hamilton, 1972; Levy and Corey, 1941; Vishveshwara and Pople, 1977). The Alaz-R structure shown in Figure 2.1 was found in Tajkhorshid *et al.* to represent the lowest minimum energy geometry when four water molecules were included in *ab initio* geometry optimizations at the B3LYP/6-31G* level of theory. However, the Alaz structure became more stable when *ab initio* geometry optimizations in combination with the Onsager continuum model were conducted on Alaz with four water molecules

(Tajkhorshid *et al.*). We, therefore, adopted both Alaz and Alaz-R in the investigations of the effects of conformation change on the structures and energetic of the H-bond networks of water in aqueous solutions. The geometry of Alaz is given in Table A.1 in Appendix A.

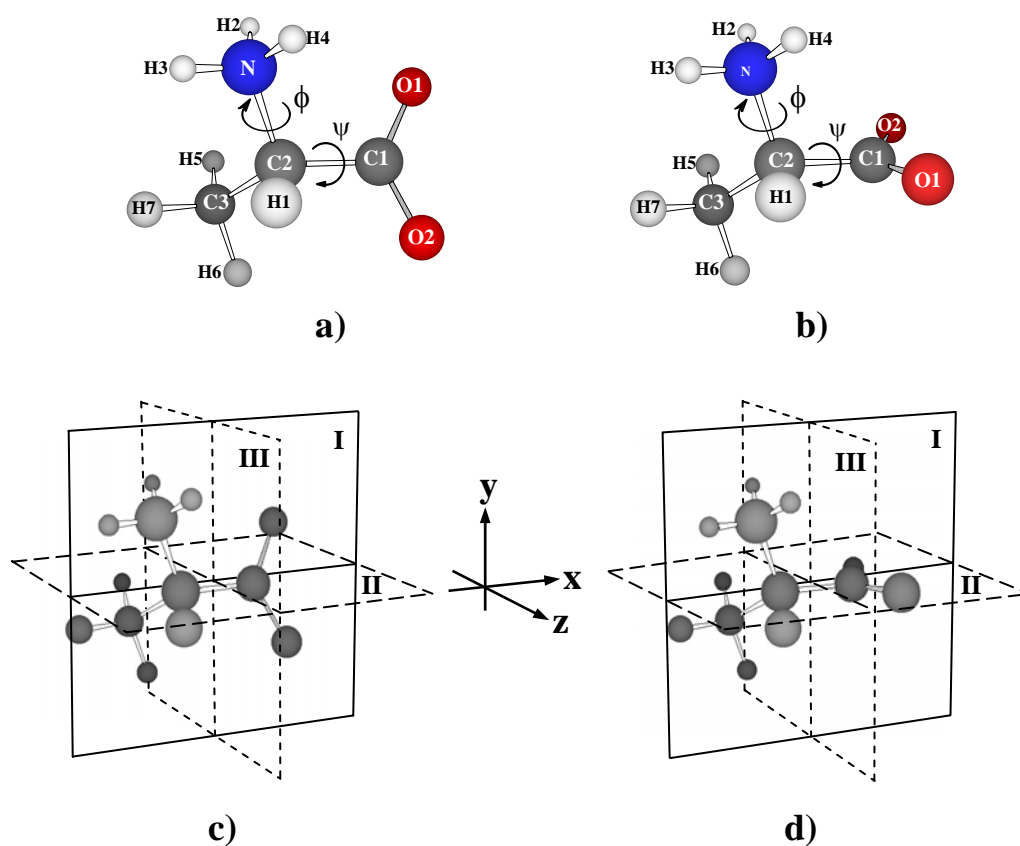


Figure 2.1 Two conformations of alanine zwitterion and the reference planes used in MD analyses.

- a) Alaz geometry with the nearly planar skeleton.
- b) Alaz-R geometry with the COO⁻ plane being 90° with respect to the NC^αC backbone plane.
- c) Reference planes for [Alaz]_{aq}.
- d) Reference planes for [Alaz-R]_{aq}.

2.2 The T-model potential

Based on the T-model potentials, various types of intermolecular interactions were investigated successfully, ranging from H-bonds between small molecules (Sagarik and Ahlrichs, 1987; Sagarik and Spohr, 1995; Sagarik, 1999) to $\pi-\pi$ interactions in phenol (Sagarik and Asawakun, 1997), benzoic acid (Sagarik and Rode, 2000) and benzene (Sagarik, Chaiwongwattana, and Sisot, 2004). It has been shown that the T-model potentials are suitable for the investigations of structures and energetics of both aqueous and nonaqueous solutions (Sagarik and Rode; Sagarik *et al.*, 2004), by means of statistical mechanical simulations. In the following subsections, some important aspects of the T-model and MD simulations will be summarized.

In the present investigation, the T-model was applied in the calculations of intermolecular potentials between Alaz and water, as well as between Alaz-R and water. Within the framework of the T-model, the interaction energy ($\Delta E_{\text{T-model}}$) between molecules A and B is written as a sum of the first-order interaction energy (ΔE_{SCF}^1) and a higher-order energy term (ΔE^r).

$$\Delta E_{\text{T-model}} = \Delta E_{\text{SCF}}^1 + \Delta E^r \quad (1)$$

ΔE_{SCF}^1 accounts for the exchange repulsion and electrostatic energies. It is computed from *ab initio* SCF calculations (Böhm and Ahlrichs, 1982) and takes the following analytical form:

$$\Delta E_{\text{SCF}}^{\text{l}} = \sum_{i \in A} \sum_{j \in B} \left[\exp\left(\frac{-R_{ij} + \sigma_i + \sigma_j}{\rho_i + \rho_j}\right) + \frac{q_i q_j}{R_{ij}} \right] \quad (2)$$

i and j in Equation (2) label the sites of molecules A and B . σ_i , ρ_i and q_i are the site parameters. R_{ij} is the site-site distance. The exponential term in Equation (2) represents the size and shape of the interacting molecules A and B . The point charges q_i and q_j are computed from the requirement that a point-charge model reproduces the electrostatic potentials of molecules of interest. In the present study, q_i and q_j for Alaz were determined by a fit of the electrostatic potentials at points selected according to the CHelpG scheme (Breneman and Wiberg, 1990) which has been embedded in the GAUSSIAN 98 package (Computer Program, 2001). The electrostatic potentials employed in the fit were derived from the density matrices computed from *ab initio* calculations at the level of second order Møller-Plesset perturbation theory (MP2) with the 6-311++G(2d,2p) basis set. About nine thousand electrostatic energies were used in the fit of the atomic charges. The dipole moment of Alaz computed from the CHelpG charges is 11.50 D, whereas those obtained from *ab initio* calculations and experiments in aqueous solutions are in the range of 10.8 and 15.7 D (Destro, Roversi, Barzaghi, and Marsh, 2000; Voogd, Derissen, and van Duijneveldt, 1981).

The higher-order energy contribution, ΔE^{r} in Equation (1), represents the dispersion and polarization contributions of the T-model potential. ΔE^{r} could be determined from both theoretical and experimental data. Our previous experience has shown that a calibration of the incomplete potential to the properties related to intermolecular interaction energies, such as the second virial coefficients (B(T)),

dimerization energies or potential energy of liquid *etc.* is the most appropriate choice.

ΔE^r takes the following form:

$$\Delta E^r = - \sum_{i \in A} \sum_{j \in B} C_{ij}^6 F_{ij}(R_{ij}) R_{ij}^{-6} \quad (3)$$

where

$$F_{ij}(R_{ij}) = \exp\left[-\left(1.28 R_{ij}^0/R_{ij} - 1\right)^2\right], R_{ij} < 1.28 R_{ij}^0 \quad (4)$$

$$= 1, \text{ elsewhere}$$

and

$$C_{ij}^6 = C_6 \frac{3}{2} \frac{\alpha_i \alpha_j}{(\alpha_i/N_i)^{1/2} + (\alpha_j/N_j)^{1/2}} \quad (5)$$

R_{ij}^0 in Equation (4) is the sum of the van der Waals radii of the interacting atoms.

Equation (5) is the Slater-Kirkwood relation. α_i and N_i in Equation (5) denote the atomic polarizability and the number of valence electrons of the corresponding atom, respectively. $F_{ij}(R_{ij})$ in Equation (4) is a damping function, introduced to correct the behavior of R_{ij}^{-6} at short R_{ij} distance. Only C_6 in Equation (5) is unknown.

The variation of C_6 within the range of 0.8 and 1.5 seems not to lead to significant change in the PES. For most of the microsolvated systems considered, the values of C_6 were determined to be 1.43 (Sagarik, Pongpitak, Chaiyapongs, Sisot, 1991). The same value was adopted for the Alaz-H₂O complexes. Previous experience has also demonstrated that the repulsion parameters and C_6 are not very sensitive to a slight conformational change, compared to the point charges. Therefore, only the

point charges of Alaz-R were recomputed using *ab initio* calculations at the MP2/6-311++G(2d,2p) level of theory. It turned out that the point charges of Alaz-R from the CHelpG scheme were not substantially different from those of Alaz, with the dipole moment of 11.52 D. Thus, in order to keep our T-model potential simple for further applications, we adopted the same point charges for both Alaz and Alaz-R. The T-model parameters for water (taken from Sagarik and Asawakun, 1997), Alaz as well as Alaz-R molecules are listed in Table A.2 in Appendix A.

2.3 Equilibrium structures of the Alaz-H₂O and Alaz-R-H₂O 1 : *n* complexes

The T-model potential constructed in the previous section was applied in the calculations of the equilibrium structures and interaction energies of the Alaz-H₂O and Alaz-R-H₂O 1 : *n* complexes, with *n* = 1 to 2. Rigid Alaz was placed at the origin of the Cartesian coordinate system and the coordinates of water were randomly generated in the vicinities of Alaz. Based on the T-model potential, the equilibrium structures of the Alaz-H₂O 1 : *n* complexes were searched using a minimization technique (Schlegel, 1982). A hundred starting configurations were generated for each intermolecular geometry optimization. Only some lowest-lying minimum energy geometries were discussed in details. The same procedure was applied to determine the equilibrium structure of the Alaz-R-H₂O complexes.

In order to test the reliability of the T-model potentials for Alaz-H₂O complexes and to obtain additional information on the minimum energy geometries on the *ab initio* PES of the Alaz-H₂O and Alaz-R-H₂O in the ratio of 1 : 1 complexes, all minimum energy geometries of those complexes obtained from T-model were

reoptimized at the MP2 level of theory with the 6-311G(d,p) basis set. Only the intermolecular geometrical parameters were considered in the *ab initio* gradient optimizations. Single-point counterpoise (CP) correction was applied to correct the BSSE. Single-point MP2 calculations were made on the MP2/6-311G(d,p) optimized geometry, using the 6-311G(2d,2p) and 6-311++G(2d,2p) basis sets. It should be noted that MP2 calculations employed in the present work were aiming only at checking the absolute and some local minimum energy geometries from the T-model PES. We are aware of the problem of Basis Set Superposition Error (BSSE) arising in *ab initio* standard gradient optimization of weakly interacting systems as addressed repeatedly by Hobza and Havlas (1998), and the fact that the quality of the MP2 calculations is very sensitive to the size of the basis sets. It appeared that, due to BSSE, PES obtained from *ab initio* gradient optimizations and the counterpoise corrected PES (CP-PES), for which the CP method is applied in each cycle, are not the same (Hobza and Havlas). It should be further stressed that the T-model and MP2 are obviously based on different levels of theory. One should not expect exactly the same PES from both methods.

2.4 MD simulations

Theoretical methods applied in the study of solvent effects on the static and dynamic properties of amino acids fall into two categories, depending on the treatment of the solvent molecules (Cramer and Truhlar, 1999; Kollman, 1993; Orozco and Luque, 2000). Microscopic methods treat solvent molecules and their interactions with the solute explicitly, whereas macroscopic methods consider solvent as a continuous medium characterized by a dielectric constant (Cramer and Truhlar;

Orozco and Luque). Both approaches have advantages and disadvantages (Leach, 2001). In aqueous solution, for example, the former can yield a deep insight into microscopic solvation structures, such as the three-dimensional structures of the H-bond networks of water in the vicinities of solute molecules. The latter has the advantage in free energy calculation. Since the three-dimensional structures of the H-bond networks of water in the first hydration sphere of the solutes were one of our prime interests, the former approach was adopted in the present work.

Based on the T-model potentials, microcanonical ensemble-MD (NVE-MD) simulations were performed on $[\text{Alaz}]_{\text{aq}}$ and $[\text{Alaz-R}]_{\text{aq}}$ at 298.15 K. In MD simulations, a rigid solute and 300 rigid water molecules were put in a cubic box subject to periodic boundary conditions. The center of mass of solute was placed at the center of the simulation box. In order to simplify the analysis of the hydration structures, the C1-C2-N backbone of Alaz was assumed to coincide with the XY plane of the box, with $Z = 0.20 \text{ \AA}$. The densities of $[\text{Alaz}]_{\text{aq}}$ and $[\text{Alaz-R}]_{\text{aq}}$ were maintained at 1.0 g cm^{-3} . The cut-off radius was half of the box length. The long-range Coulomb interaction was taken into account by means of the Ewald summations. The timestep used in solving the equations of motions was 0.5 fs. In MD simulations, 100,000 timesteps were devoted to the equilibration and additional 200,000 timesteps to property calculations. The latter corresponds to a simulation time of 100 ps.

General energetic results were computed from MD simulations, namely the average potential energy of aqueous solution ($\langle E_{\text{aq}}^{\text{pot}} \rangle$) and the average solute-solvent interaction energies ($\langle E_{\text{aq}}^{\text{solu-solv}} \rangle$), as well as the average solvent-solvent interaction

energies ($\langle E_{\text{aq}}^{\text{solv-solv}} \rangle$). These energy values were the results of the average over the timesteps and the number of water molecules. The structures of water molecules in the H-bond networks were initially characterized based on the average H-bond distances ($\langle R_{\text{A-H..B}} \rangle$) and angles ($\langle \theta_{\text{A-H..B}} \rangle$). $\langle \theta_{\text{A-H..B}} \rangle$ represent the angle between the A-H bond and the line connecting atoms A and B. Since NMR experiments (Otwinowski *et al.*, 1988; Sigler, 1992) suggested that hydration water can mediate protein-DNA recognition through specific H-bond formations which depend on the hydration dynamics of water molecules at particular hydration sites, it is interesting to estimate the duration of the H-bonding between individual water molecules and the NH_3^+ and COO^- groups from MD simulations. Due to the fact that the H-bond formations and disruptions take place quite often and very rapidly at the first hydration shell of proteins (Wüthrich, 1993), the residence times derived from MD simulations could vary in a wide range. Since NMR experiments can effectively detect the long-lived hydration water, it is reasonable to compare the longest H-bond lifetimes ($\tau_{\text{A-H..B,max}}$) obtained from MD simulations with the NMR average residence times (Brunner, Liepinsh, Otting, Wüthrich, and van Gunsteren, 1993). $\tau_{\text{A-H..B,max}}$ were approximated from the percentage of simulation steps, during which a specific pair of H-bond donor and acceptor were coming close enough to continuously engage in H-bonds. H-bond donor and acceptor in AMBER (Computer Program, 1999) were considered to engage in H-bond formation when the donor-acceptor distance was shorter than 4 Å.

The hydration structures and the H-bond networks of water around Alaz and Alaz-R were further analyzed in detail using the atom-atom pair correlation function

($g(R)$) and the average running coordination number ($n(R)$), as well as the PDO and PDH maps (Clementi, 1980). The PDO and PDH maps show the average three-dimensional structures of the H-bond networks at the functional groups of Alaz and Alaz-R. In the present work, three sets of the PDO and PDH maps were constructed, using the predefined reference planes I, II and III in Figure 2.1. In order to view the overall picture of hydration structures of Alaz and Alaz-R, the C1-C2-N backbone was chosen to form reference plane I. Since the second set of the PDO and PDH maps was aiming at the hydration structures at the NH_3^+ group, the XZ plane with $Y = 0.0 \text{ \AA}$ was defined as reference plane II. The YZ plane with $X = 0.0 \text{ \AA}$ was chosen as reference plane III to view of the hydration structures at the COO^- group.

In the calculations of the PDO and PDH maps, the volumes above and below the reference planes were divided into layers with the thickness of 1.0 \AA . In each layer, the PDO and PDH maps were computed at the 61×61 grid intersections, by following the trajectories of the oxygen and hydrogen atoms of water in the course of MD simulations. The PDO and PDH maps were represented by contour lines constructed using the SURFER program (Computer Program, 1997). For simplicity, the maximum and minimum of the contour lines, as well as the contour interval, was the same for all the PDO and PDH maps.

In order to obtain insight into the interaction energy distributions in aqueous solutions, a similar approach was adopted in the analysis of the average solute-solvent and average solvent-solvent interaction energies. The AWPD and WWPD maps (Clementi, 1980) for $[\text{Alaz}]_{\text{aq}}$ and $[\text{Alaz-R}]_{\text{aq}}$ were constructed with respect to reference planes I, II and III. The AWPD maps account for the average interaction energy between water molecule at the grid intersection and the solute molecule,

whereas the WWPD maps reveal the average interaction energy between water molecule at the grid intersection and all other water molecules in aqueous solution. Only negative interaction energies were employed in the calculations of the AWPD and WWPD maps. In order to obtain information on the hydration dynamics of water molecules and to view the average potential energy landscapes at the H-bond networks, the AW-WWPD maps were computed by combination of the AWPD and WWPD maps. Since in general the rate of water exchange and the mobility of water molecules depends on the transition energy barriers, the shapes of the average potential energy landscapes at the H-bond networks were analyzed in details using cross section plots. Various cross section plots were generated by taking vertical slices along predefined profile lines through the surfaces of the AW-WWPD, AWPD and WWPD maps. In the present work, the cross sections derived from the longitudinal profile lines on the AW-WWPD maps could be associated with the transition energy barriers to water exchange within the H-bond network ($\langle \Delta E_{\text{aq}}^{\text{L}} \rangle$). Whereas those computed from the transverse profile lines are attributed to the transition energy barriers to water exchange between the H-bond network and the outside ($\langle \Delta E_{\text{aq}}^{\text{T}} \rangle$). It should be noted that, when a particular water molecule leaves a hydration site, its place will be occupied nearly simultaneously by another water molecule. And since the rate of water exchange depends on the transition energy barriers, which is inversely proportional to $\tau_{\text{A-H..B,max}}$, the hydration dynamics of water molecules at the hydration sites are discussed based on $\tau_{\text{A-H..B,max}}$, $\langle \Delta E_{\text{aq}}^{\text{L}} \rangle$ and $\langle \Delta E_{\text{aq}}^{\text{T}} \rangle$.

CHAPTER III

RESULTS AND DISCUSSION

The results of the present work started with the T-model results of the Alaz-H₂O and the Alaz-R-H₂O 1 : *n* complexes, followed by the MD results of the [Alaz]_{aq} and [Alaz-R]_{aq} at 298.15 K. Some important data are displayed and discussed in this chapter and more results obtained from the calculations are enclosed in the Appendices.

3.1 The Alaz-H₂O and Alaz-R-H₂O 1 : *n* complexes

The absolute and two low lying minimum energy geometries, together with $\Delta E_{T\text{-model}}$, of the Alaz-H₂O and Alaz-R-H₂O 1 : *n* complexes, with *n* = 1 to 2 are illustrated in Figures 3.1-3.2. The atom numbering system employed in the discussion is shown in Figure 2.1.

The absolute minimum energy geometry of the Alaz-H₂O 1 : 1 complex from the T-model potential is structure **a** in Figure 3.1. Structure **a** consists of a cyclic H-bonded complex in which water acts simultaneously as proton acceptor and donor towards the NH₃⁺ and COO⁻ groups of Alaz, respectively. $\Delta E_{T\text{-model}}$ of structure **a** is -82.65 kJ mol⁻¹, with the N-H4..Ow and Ow-Hw..O1 H-bond distances of 2.65 and 2.71 Å, respectively. The cyclic H-bond in structure **b** is similar to structure **a**, with water molecule H-bonding at the H2 atom of Alaz. $\Delta E_{T\text{-model}}$ of structure **b** is 7.64 kJ mol⁻¹ higher than structure **a**. This could be attributed to weak repulsion between

the CH₃ group of Alaz and water in structure **b**. The N-H₂..O_w and O_w-H_w..O₁ H-bond distances are 2.81 and 2.69 Å, respectively. Structure **c** is considerably less stable than structures **a** and **b**. The water molecule in structure **c** acts only as a proton donor and forms H-bonds simultaneously with O₁ and O₂ of Alaz, with $\Delta E_{T\text{-model}}$

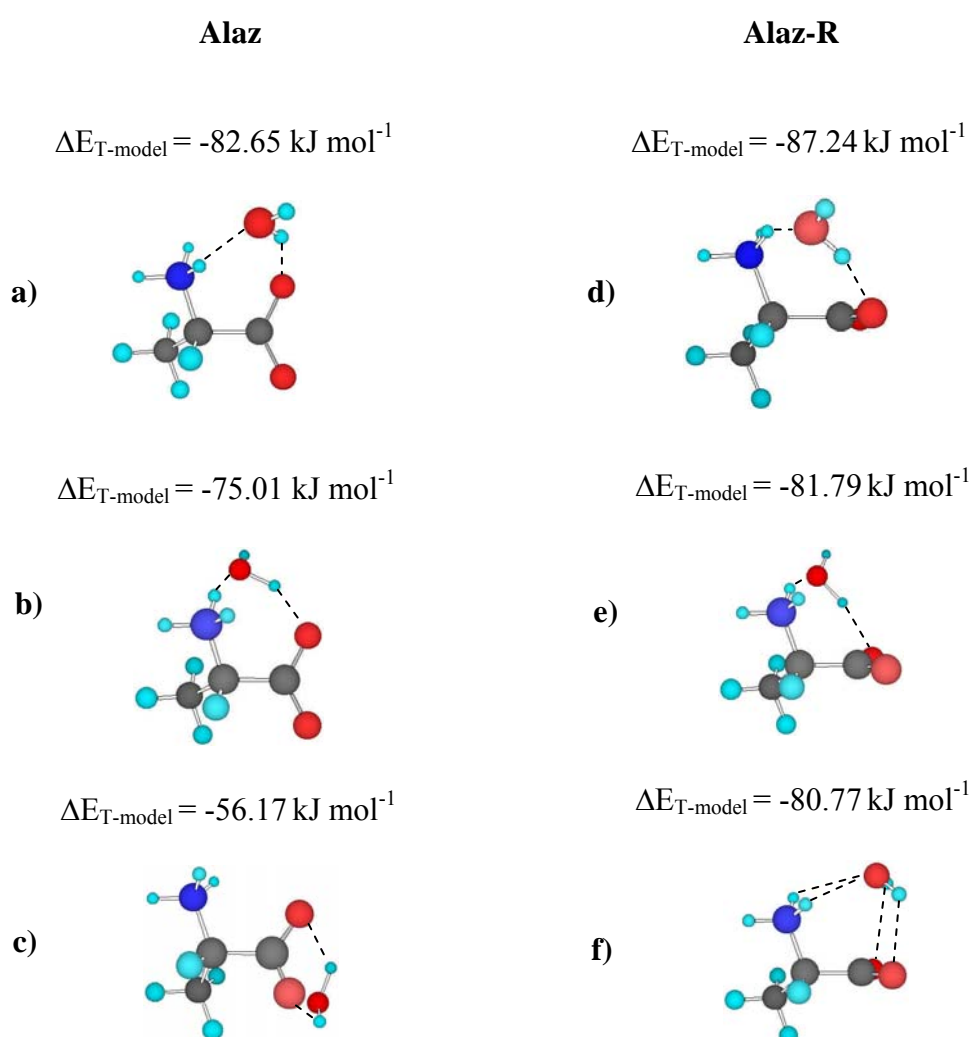


Figure 3.1 The absolute and some local minimum energy geometries of Alaz-H₂O and Alaz-R-H₂O 1 : 1 complexes computed from the T-model potentials. a) - c) Alaz-H₂O; d) - f) Alaz-R-H₂O.

of $-56.17 \text{ kJ mol}^{-1}$. Their interaction energies of structures **a** and **b** obtained from MP2/6-311++G(2d,2p)//MP2/6-311G(d,p) calculations are -83.12 and $-83.84 \text{ kJ mol}^{-1}$, respectively. With the single-point BSSE corrections, the interaction energies are reduced to -72.63 and $-72.43 \text{ kJ mol}^{-1}$, respectively.

For the Alaz-H₂O 1 : 2 complexes, both water molecules prefer to bridge between the NH₃⁺ and COO⁻ groups of Alaz, structure **a** in Figure 3.2. Structure **a**, which is the lowest minimum energy geometry, possesses $\Delta E_{\text{T-model}}$ of $-152.32 \text{ kJ mol}^{-1}$. Structure **a** is similar to that of the lowest energy conformer of the Glyz-H₂O and Alaz-H₂O 1 : 2 complex studied by Jensen and Gordon (1995) and Park *et al.* (2003), respectively.

The situations in the Alaz-R-H₂O complexes are similar to those in the Alaz-H₂O complexes. In general, the interaction energies of the Alaz-R-H₂O complexes are lower than the Alaz-H₂O complexes. The T-model potentials predict the structure in which water molecule H-bonds simultaneously at H4 and O1, structure **d** in Figure 3.1, to be the absolute minimum energy geometry of the Alaz-R-H₂O 1 : 1 complex. In this case, the interaction energy amounts to $-87.24 \text{ kJ mol}^{-1}$, with the Ow-Hw..O1 and N-H4..Ow distances of 2.72 and 2.74 \AA , respectively. The H-bond distances are slightly longer than those in structure **a** of the Alaz-H₂O dimer. The interaction energies of structures **e** and **f** are comparable and slightly higher than those of structure **d**. The H-bond features in structure **e** are similar to that of the Alaz-H₂O dimer, in which the water molecule bridges between H2 and O1. For structure **f**, the water molecule acts simultaneously as proton acceptor and donor forming four H-bonds with Alaz-R, two N-H..Ow H-bonds and two Ow-Hw..O H-bonds.

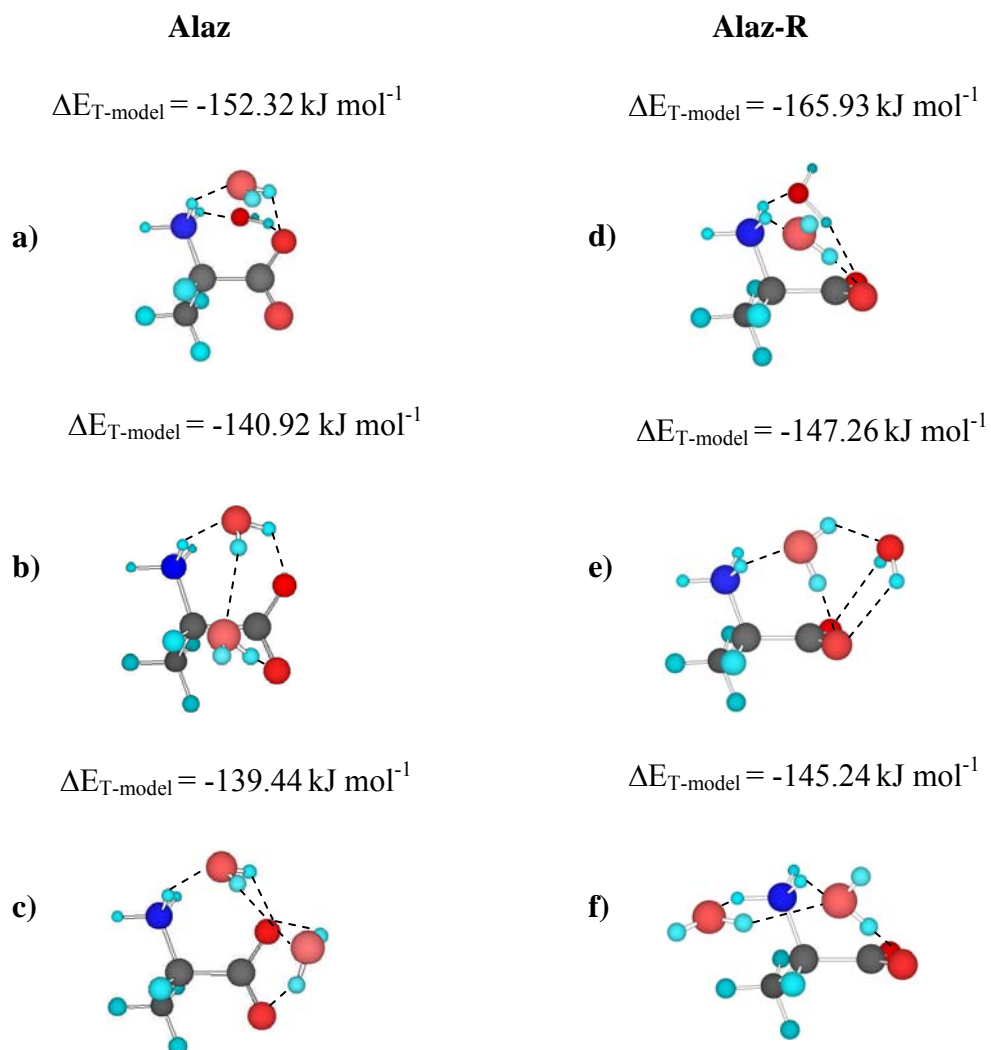


Figure 3.2 The absolute and some local minimum energy geometries of Alaz-H₂O and Alaz-R-H₂O 1 : 2 complexes computed from the T-model potentials. a) - c) Alaz-H₂O; d) - f) Alaz-R-H₂O.

The absolute minimum energy geometry of the Alaz-R-H₂O 1 : 2 complex is structure **d** in Figure 3.2. It is characterized by four H-bonds between water molecules bridging between the NH₃⁺ and COO⁻ groups of Alaz-R, similar to that in the Alaz-H₂O 1 : 2 complex. The interaction energy of structure **a** amounts to -165.93 kJ mol⁻¹.

3.2 MD simulations on [Alaz]_{aq} and [Alaz-R]_{aq}

The MD simulation parameters employed in the present work are given in Table 3.1, together with $\langle E_{\text{aq}}^{\text{pot}} \rangle$, $\langle E_{\text{aq}}^{\text{solv-solv}} \rangle$ and $\langle E_{\text{aq}}^{\text{solv-solv}} \rangle$. The PDO maps computed with respect to reference planes I, II and III for Alaz and Alaz-R are displayed in Figures 3.3 and 3.4, respectively. The corresponding AWPDP and AW-WWPDP maps for Alaz and Alaz-R are also shown in Figures 3.3 and 3.4, respectively. The WWPDP maps are not presented here to limit the number of figure. Some high-density contour areas on the PDO, AWPDP and AW-WWPDP maps in Figures 3.3 and 3.4 are labeled with letters. The values of the highest probabilities at the labeled areas on the PDO maps, as well as the corresponding lowest average interaction energies on the AWPDP, WWPDP and AW-WWPDP maps, are summarized in Table 3.2. They are denoted by $\langle P^{\text{PDO}} \rangle_{\text{max}}$, $\langle \Delta E_{\text{aq}}^{\text{AWPDP}} \rangle_{\text{min}}$, $\langle \Delta E_{\text{aq}}^{\text{WWPDP}} \rangle_{\text{min}}$ and $\langle \Delta E_{\text{aq}}^{\text{AW-WWPDP}} \rangle_{\text{min}}$, respectively. The structures of $g(R)$ of the NH₃⁺, CH₃, CH and COO⁻ groups for [Alaz]_{aq} and [Alaz-R]_{aq}, although they are not substantially different, and the corresponding $n(R)$, are shown in Figures C.7 (see Appendix C) and D.7 (see Appendix D), respectively. Some characteristic peak positions of $g(R)$ of the N, C and O atoms of those groups of [Alaz]_{aq} and [Alaz-R]_{aq}, directly related to the H-bonds

between water and the NH_3^+ , CH_3 , CH and COO^- groups together with $n(\text{R})$ are given in Table 3.3. Table 3.4 lists $\langle R_{\text{A-H..B}} \rangle$, $\langle \theta_{\text{A-H..B}} \rangle$ and $\tau_{\text{A-H..B,max}}$. The cross section plots for selected H-bond networks at the NH_3^+ and COO^- groups are displayed in Figures 3.5 and 3.6, respectively, with the lowest energy minima set to 0 kJ mol^{-1} to compare $\langle \Delta E_{\text{aq}}^{\text{L}} \rangle$ and $\langle \Delta E_{\text{aq}}^{\text{T}} \rangle$.

Table 3.1 MD simulation parameters and results for $[\text{Alaz}]_{\text{aq}}$ and $[\text{Alaz-R}]_{\text{aq}}$.

The number of water molecules in all MD simulations is three hundred.

Energies are in kJ mol^{-1} and all the definitions are in the text.

	L (Å)	$\langle E_{\text{aq}}^{\text{pot}} \rangle$	$\langle E_{\text{aq}}^{\text{solv-solv}} \rangle$	$\langle E_{\text{aq}}^{\text{solv-solv}} \rangle$
$[\text{Alaz}]_{\text{aq}}$	20.8888	-31.72 ± 0.22	-1.7326	-29.0697
$[\text{Alaz-R}]_{\text{aq}}$	20.8888	-31.58 ± 0.22	-1.7633	-28.9103

L = simulation box length.

$\langle E_{\text{aq}}^{\text{pot}} \rangle$ = average potential energy of aqueous solution.

$\langle E_{\text{aq}}^{\text{solv-solv}} \rangle$ = average solute-solvent interaction energy.

$\langle E_{\text{aq}}^{\text{solv-solv}} \rangle$ = average solvent-solvent interaction energy.

3.2.1 Hydration structures and H-bond networks in aqueous solutions

3.2.1.1 [Alaz]_{aq}

For [Alaz]_{aq}, the preferential hydration sites are labeled with **A** to **N** on the PDO maps in Figure 3.3. At least nine well-defined hydration sites are observed on the PDO maps of Alaz, five at the NH₃⁺ group and four at the COO⁻ group. The hydration sites labeled with **A**, **B**, **C**, **H** and **L** involve the NH₃⁺ group, whereas those with **D**, **E**, **F** and **J** are at the COO⁻ group. The PDO maps reveal that water molecules form more well defined H-bond networks at the NH₃⁺ group than at the COO⁻ group. According to $\langle P^{\text{PDO}} \rangle_{\text{max}}$ in Table 3.2, the order of the preferential hydration at the NH₃⁺ group is written as:

$$\mathbf{H} \geq \mathbf{L} > \mathbf{A} > \mathbf{C} > \mathbf{B}.$$

Combination of Figures 3.3a to 3.3e shows the three-dimensional structures of the H-bond networks at the NH₃⁺ group in details. The hydration sites labeled with **L**, **H** and **A** are located near H2, H4 and H3, respectively. Water molecules at **A** seem to bridge the NH₃⁺ and CH₃ groups, whereas the ones at **L** and **H** link between the NH₃⁺ and COO⁻ groups. These H-bonding features are similar to those observed in the Alaz-H₂O 1 : 1 and 1 : 2 complexes, Figures 3.1a, 3.1b and 3.2a, respectively. Figures 3.3b and 3.3f suggest that water molecules at **C** are located between and slightly above **L** and **H**. They also reveal the possibility for water molecules at **C** to bridge the NH₃⁺ and COO⁻ groups. This rules out the possibility to form an intramolecular H-bond between the NH₃⁺ and COO⁻ groups. The result is in accordance with the

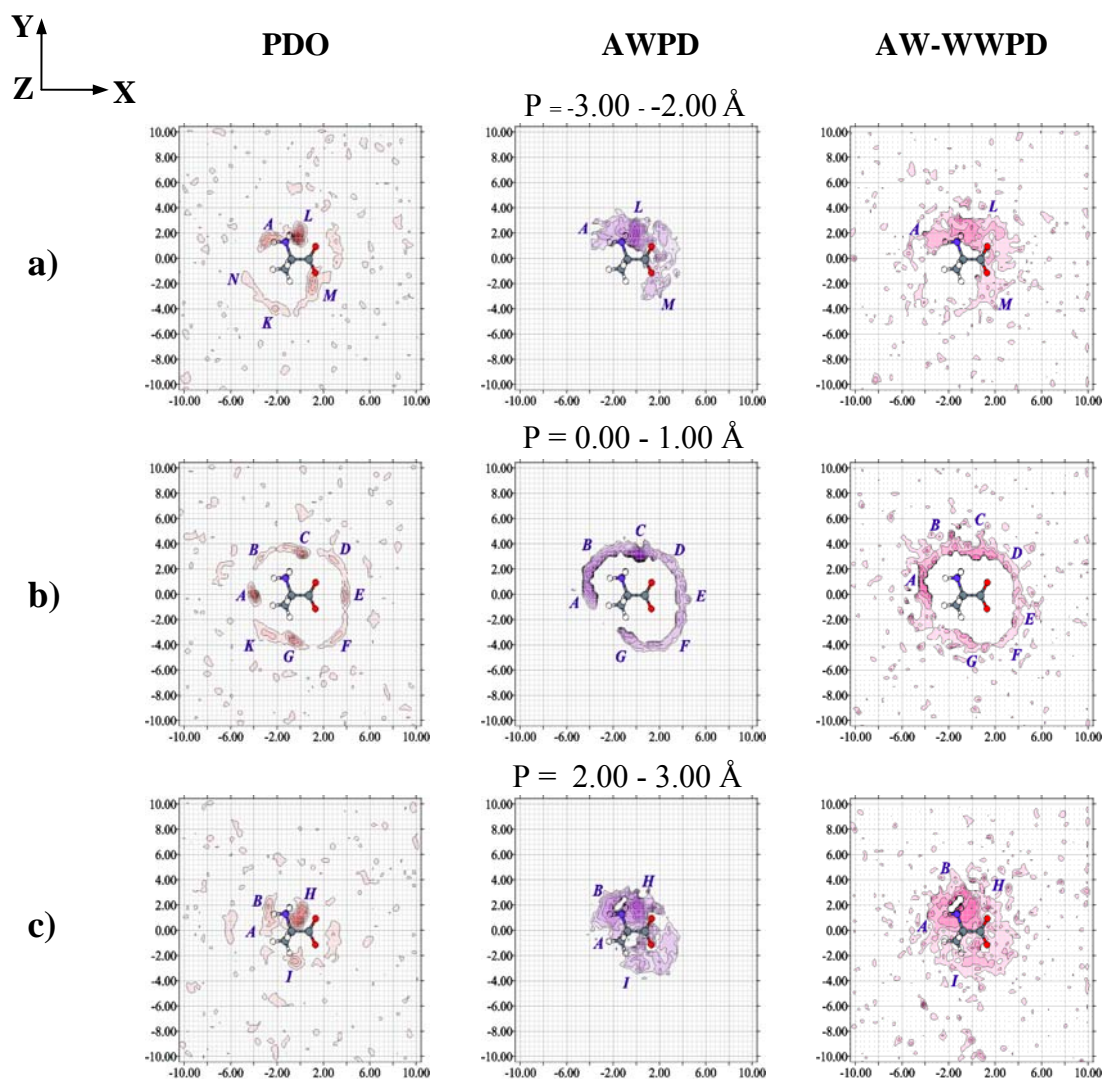


Figure 3.3 Selected PDO, AWP and AW-WWP maps for $[Alaz]_{aq}$ obtained

from MD simulations. X-, Y- and Z-axis are in Å.

a) – c) Results with respect to reference plane I.

d) – e) Results with respect to reference plane II.

f) – g) Results with respect to reference plane III.

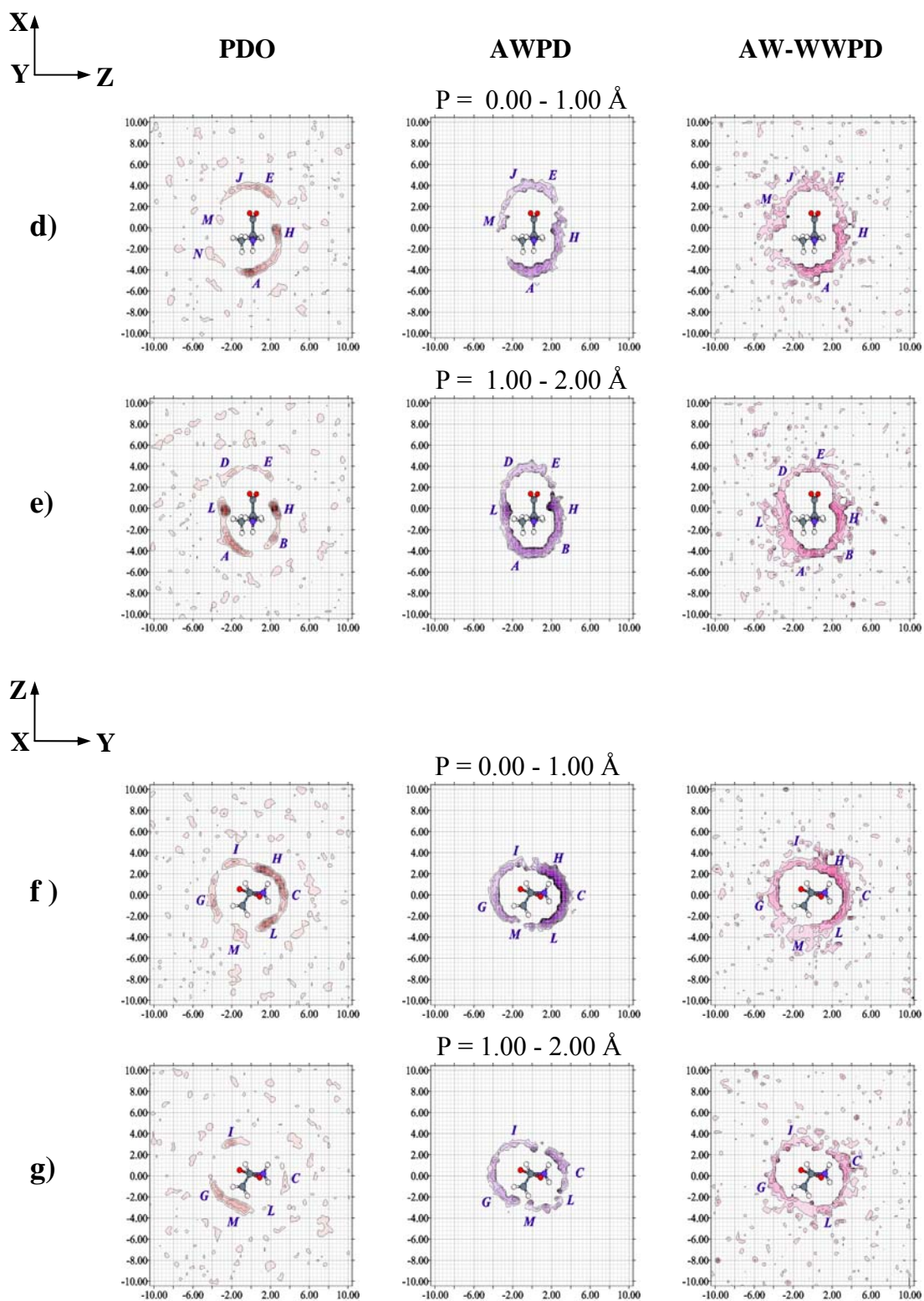


Figure 3.3 (Continued).

Table 3.2 The highest probabilities ($\langle P^{\text{PDO}} \rangle_{\text{max}}$) at the labeled areas on the PDO

maps and the corresponding lowest average interaction energies

($\langle \Delta E_{\text{aq}}^{\text{X}} \rangle_{\text{min}}$) on the X maps in Figures 3.3-3.4. X is AWPDP, WWPD orAW-WWPD. Energies are in kJ mol^{-1} .**a) [Alaz]_{aq}**

	$\langle P^{\text{PDO}} \rangle_{\text{max}}$	$\langle \Delta E_{\text{aq}}^{\text{AWPD}} \rangle_{\text{min}}$	$\langle \Delta E_{\text{aq}}^{\text{WWPD}} \rangle_{\text{min}}$	$\langle \Delta E_{\text{aq}}^{\text{AW-WWPD}} \rangle_{\text{min}}$
NH₃⁺				
A	0.066	-47.55	-77.58	-91.44
B	0.049	-47.27	-74.55	-90.25
C	0.051	-71.06	-74.77	-95.64
H	0.086	-67.27	-74.11	-87.74
L	0.084	-62.06	-79.92	-87.07
$\langle \Delta E_{\text{aq}}^{\text{X}} \rangle_{\text{min,av}}$		-59.04	-76.18	-90.43
COO⁻				
D	0.022	-37.60	-70.63	-88.86
E	0.034	-48.78	-84.31	-87.99
F	0.022	-36.92	-69.48	-86.06
J	0.036	-41.53	-75.30	-82.34
$\langle \Delta E_{\text{aq}}^{\text{X}} \rangle_{\text{min,av}}$		-41.21	-74.93	-86.31

Table 3.2 (Continued).**b) [Alaz-R]_{aq}**

	$\langle P^{\text{PDO}} \rangle_{\text{max}}$	$\langle \Delta E_{\text{aq}}^{\text{AWPD}} \rangle_{\text{min}}$	$\langle \Delta E_{\text{aq}}^{\text{WWPD}} \rangle_{\text{min}}$	$\langle \Delta E_{\text{aq}}^{\text{AW-WWPD}} \rangle_{\text{min}}$
NH₃⁺				
A	0.094	-52.64	-86.92	-96.07
B	0.041	-51.38	-73.74	-84.05
C	0.074	-70.84	-74.93	-87.15
H	0.097	-70.63	-76.01	-91.87
L	0.105	-68.32	-67.50	-86.40
$\langle \Delta E_{\text{aq}}^{\text{X}} \rangle_{\text{min,av}}$		-62.76	-75.82	-89.11
COO⁻				
D	0.024	-52.26	-65.55	-81.47
E	0.027	-36.94	-73.49	-84.01
F	0.022	-36.37	-68.65	-85.54
J	0.032	-37.58	-73.72	-82.11
O	0.042	-47.37	-63.31	-89.17
$\langle \Delta E_{\text{aq}}^{\text{X}} \rangle_{\text{min,av}}$		-42.10	-68.94	-84.46

$$\langle \Delta E_{\text{aq}}^{\text{X}} \rangle_{\text{min,av}} = \sum_{i=1}^N \frac{\langle E_{\text{aq}}^{\text{X}} \rangle_i}{N} : \quad N = \text{number of the labeled area.}$$

^{17}O -NMR relaxation study on $[\text{Gly}]_{\text{aq}}$ and MC results by Gerothanassis, Hunston, and Lauterwein (1982) and by Watanabe *et al.* (1997), respectively. Additional information on the hydration structures at the NH_3^+ group can be inferred from Figures 3.3a and 3.3c to 3.3e. The H-bond networks at **A** and **H** are linked together in Figures 3.3c and 3.3d. The H-bond networks bridging between **A** and **L** are recognized in Figures 3.3a and 3.3e.

Water molecules at **D**, **E**, **F** and **J** constitute the three-dimensional structures of the H-bond networks at the COO^- groups. $\langle P^{\text{PDO}} \rangle_{\text{max}}$ in Table 3.2 reveal the highest probability at **J**, followed by those at **E**, **D** and **F**, respectively. From Table 3.2, the order of the preferential hydration at the COO^- group is:

$$\mathbf{J} \geq \mathbf{E} > \mathbf{D} \approx \mathbf{F}.$$

Figure 3.3b suggest weak H-bond networks spanning from **D** to **E** to **F** in the vicinity of the COO^- groups, whereas Figure 3.3d suggest the possibility for a weak H-bond network linking between **J** and **E**. Weak H-bond networks are also recognized at the CH group. They span from **G** to **K**, as seen in Figure 3.3b.

Further information on the hydration structures of Alaz can be obtained from $g(R)$ in Figure C.7 (see Appendix C) and $n(R)$ data in Table 3.3. For $[\text{Alaz}]_{\text{aq}}$, the main peak of $g(R_{\text{N-Ow}})$ is located at $R = 2.76 \text{ \AA}$, with $n(R_{\text{N-Ow}})$ of about two (2.17). $n(R_{\text{N-Ow}})$ in this case represents the average number of water molecules in close contact with the NH_3^+ group. The integration of $g(R_{\text{N-Ow}})$ to the first minimum at $R = 3.61 \text{ \AA}$ yields more than six (6.34) water molecules in the first hydration shell of the NH_3^+ group. These could be attributed to the water molecules at **L**, **H**, **A**, **B** and **C** on

the PDO maps. The structures of the main peaks of $g(R_{O1-Ow})$ and $g(R_{O2-Ow})$ are quite similar. The main peaks of both $g(R_{O1-Ow})$ and $g(R_{O2-Ow})$ are located at $R = 2.81 \text{ \AA}$, with $n(R_{O1-Ow})$ and $n(R_{O2-Ow})$ of 1.49 and 1.38, respectively. Therefore, on average, more than one water molecule is in close contact with O1 and O2, and the degree of hydration at O1 is roughly 8% higher than at O2. The latter could result from the formation of well-defined H-bond networks linking between O1 and the NH_3^+ group. Combination of $g(R_{O1-Ow})$ and $g(R_{O2-Ow})$ is termed $g(R_{O-Ow})$, with the main peak position at 2.81 \AA and $n(R_{O-Ow})$ of 1.44. Since the C-H...O H-bond is weak in general, the hydration structures at the CH_3 and CH groups were not easy to elucidate. However, $n(R_{C2-Ow})$ and $n(R_{C3-Ow})$ indicate more than three (3.60) water molecules at the CH group and about three (2.95) water molecules at the CH_3 group.

Table 3.3 Characteristic peak positions (R) related to H-bonds between water and the NH_3^+ , CH_3 , CH and COO^- groups, together with the corresponding running coordination number, $n(R)$, obtained from MD simulations. Distances are in Å.

a) $[\text{Alaz}]_{\text{aq}}$

	R_{max}	$n(R_{\text{max}})$	R_{min}	$n(R_{\text{min}})$
$g(\text{R}_{\text{N-Ow}})$	2.76	2.17	3.61	6.34
$g(\text{R}_{\text{O1-Ow}})$	2.81	1.49	3.81	6.82
$g(\text{R}_{\text{O2-Ow}})$	2.81	1.38	3.96	7.25
$g(\text{R}_{\text{O-Ow}})$	2.81	1.44	3.96	7.35
$g(\text{R}_{\text{C2-Ow}})$	3.46	3.60	4.30	10.68
$g(\text{R}_{\text{C3-Ow}})$	3.21	2.95	4.01	8.54

b) $[\text{Alaz-R}]_{\text{aq}}$

	R_{max}	$n(R_{\text{max}})$	R_{min}	$n(R_{\text{min}})$
$g(\text{R}_{\text{N-Ow}})$	2.76	2.32	3.66	6.43
$g(\text{R}_{\text{O1-Ow}})$	2.81	1.46	4.06	8.09
$g(\text{R}_{\text{O2-Ow}})$	2.81	1.39	3.91	6.80
$g(\text{R}_{\text{O-Ow}})$	2.86	1.83	3.91	7.11
$g(\text{R}_{\text{C2-Ow}})$	3.41	3.52	3.81	6.48
$g(\text{R}_{\text{C3-Ow}})$	3.21	2.92	4.10	9.15

R_{max} = position of the maximum of the main peak.

R_{min} = position of the minimum of the main peak.

3.2.1.2 [Alaz-R]_{aq}

The hydration structures in [Alaz-R]_{aq} are slightly different from [Alaz]_{aq}. Since the COO⁻ plane in Alaz-R is 90° with respect to the NC^αC backbone plane, the distance between the NH₃⁺ and COO⁻ groups is larger than in Alaz. The O1..H4 and O2..H2 distances in Alaz-R are almost identical (about 2.98 Å). Thus, the steric effects at O1 due to H2 and H4 in Alaz are reduced in Alaz-R. The MD results show that the rotation of the COO⁻ plane allows the charged functional groups to be more exposed to water, which leads to an increase in the structure and the degree of hydration, especially at the NH₃⁺ group. The following discussion supports this scenario.

An increase in the degree of hydration at the NH₃⁺ group is recognized from the PDO maps in Figures 3.4a, 3.4b and 3.4e. Table 3.2 confirms that the probability distributions at **L**, **H**, **A** and **C** are higher than for [Alaz]_{aq}. Compared to [Alaz]_{aq}, $\langle P^{\text{PDO}} \rangle_{\text{max}}$ at **C** and **A** are increased by about 45 and 42%, respectively. At the NH₃⁺ group, only $\langle P^{\text{PDO}} \rangle_{\text{max}}$ at **B** is decreased, by about 16%. Thus, the order of the preferential hydration at the NH₃⁺ group in [Alaz-R]_{aq} is:

$$\mathbf{L} > \mathbf{H} \geq \mathbf{A} > \mathbf{C} > \mathbf{B}.$$

The degrees of hydration at the COO⁻ group are either increased or decreased due to the conformation change. The $\langle P^{\text{PDO}} \rangle_{\text{max}}$ values in Table 3.2 reveal that the degrees of hydration at **E** and **J** are decreased by about 21 and 11%, respectively, whereas at **D**. It is increased by about 9%. The rotation of the NC^αC backbone plane

creates a new H-bond network at region **O**. Table 3.2 shows that **O** possesses the highest $\langle P^{\text{PDO}} \rangle_{\text{max}}$ among the H-bond networks at the COO^- group. Water molecules at **O** link between the O2 atom and the CH_3 group of Alaz-R. Comparison of Figures 3.4a and 3.4b suggests that the H-bond network at **O** is similar to **G**, which links between the O2 atom and the CH group. According to $\langle P^{\text{PDO}} \rangle_{\text{max}}$, the order of the preferential hydration at the COO^- group in $[\text{Alaz-R}]_{\text{aq}}$ is:

$$\mathbf{O} > \mathbf{J} > \mathbf{E} \geq \mathbf{D} \geq \mathbf{F}.$$

$g(R)$ of the NH_3^+ , CH, CH_3 and COO^- groups of Alaz-R are shown in Figure D.7 (see Appendix D). The information in Table 3.3 also confirms the increase in the degrees of hydration at the NH_3^+ and COO^- groups. For $[\text{Alaz-R}]_{\text{aq}}$, the position of the main peak of $g(R_{\text{N-Ow}})$ is at $R = 2.76 \text{ \AA}$, with $n(R_{\text{N-Ow}})$ of 2.32. The value is about 7% higher than $[\text{Alaz}]_{\text{aq}}$. The number of water molecules in close contact with the COO^- group seems to be more strongly affected by the rotation of the $\text{NC}^{\alpha}\text{C}$ backbone plane. $n(R_{\text{O-Ow}})$ at the first maximum of $g(R_{\text{O-Ow}})$ amounts to 1.83, increased by about 27%. Therefore, on average, two water molecules are in close contact with the COO^- group in $[\text{Alaz-R}]_{\text{aq}}$.

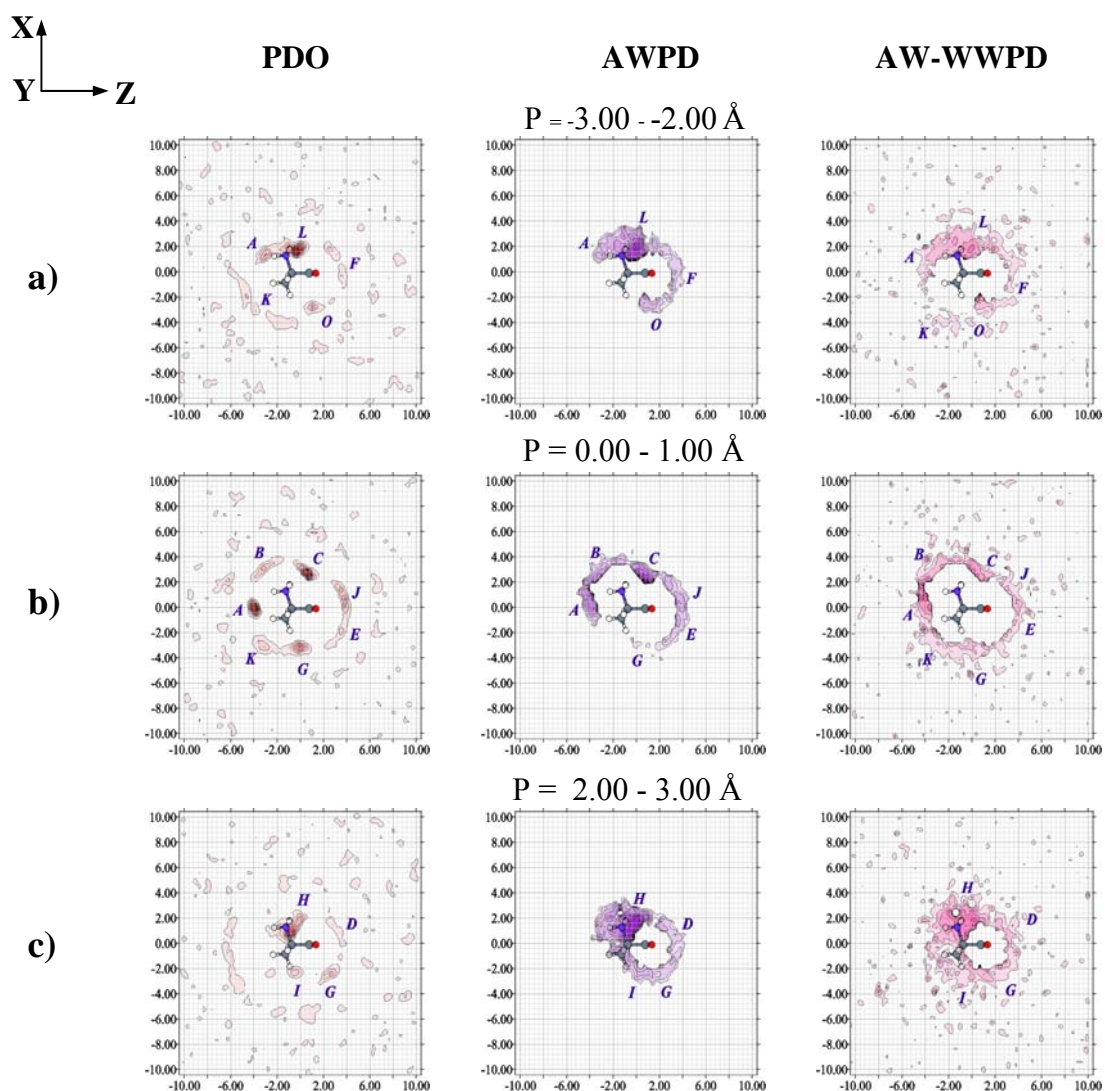


Figure 3.4 Selected PDO, AWP and AW-WWP maps for $[\text{Alaz-R}]_{\text{aq}}$ obtained

from MD simulations. X-, Y- and Z-axis are in Å.

a) – c) Results with respect to reference plane I.

d) – e) Results with respect to reference plane II.

f) – g) Results with respect to reference plane III.

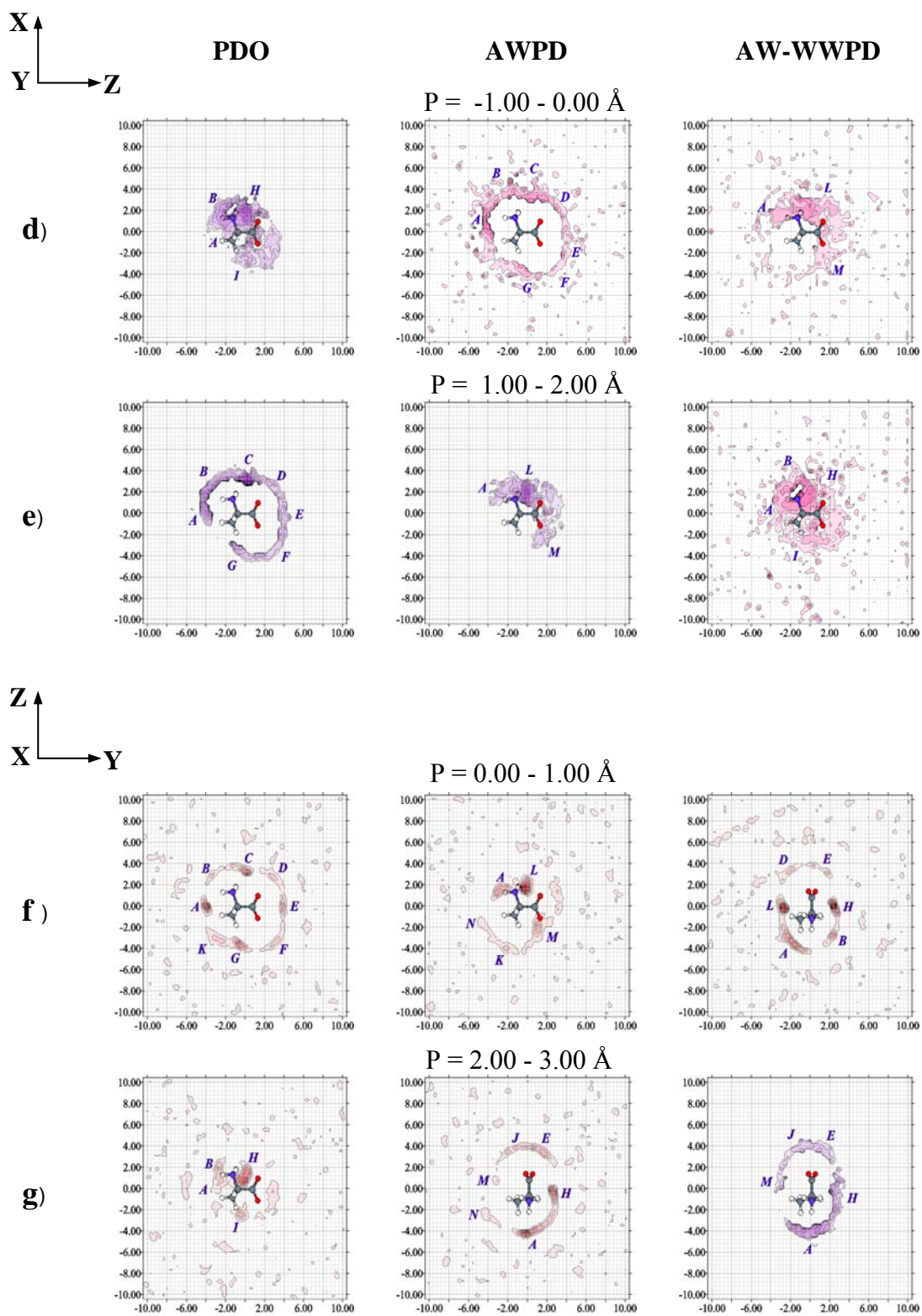


Figure 3.4 (Continued).

3.2.2 Average potential energy landscapes at the H-bond networks

General trends of the interaction energies of a polar solute in aqueous solutions were observed in $[\text{Alaz}]_{\text{aq}}$ and $[\text{Alaz-R}]_{\text{aq}}$. The preferential hydrations resulted more or less from the combined effects of solute-solvent and solvent-solvent interactions. The trend of $\langle E_{\text{aq}}^{\text{pot}} \rangle$ in Table 3.1 is in accordance with Kikuchi, Watanabe, Ogawa, Takase, and Takahashi (1997), in which the overall stabilization by hydration was reported to be slightly larger for $[\text{Alaz}]_{\text{aq}}$ than for $[\text{Alaz-R}]_{\text{aq}}$. $\langle E_{\text{aq}}^{\text{solu-solv}} \rangle$ in Table 3.1 suggests that the functional groups of Alaz-R is more accessible by water compared to Alaz.

It should be noted that the orders of the preferential hydration derived from the PDO maps and the stability orders from the AW-WWPD maps are not necessarily the same. This is due to the fact that the PDO maps represent the local probability distributions, which can be compared with the electron density maps obtained from the X-ray diffraction experiment. On the other hand, the minima of the AW-WWPD maps are associated with the interaction energy states, which may be occupied or unoccupied at any given MD timestep. Moreover, the occupancies of these interaction energy states depend primarily on the hydration dynamics of water molecules and the transition energy barriers connecting these states. Therefore, it is inappropriate to directly correlate these structural and energetic properties.

A similar argument was made on the hydration sites inferred from X-ray crystallography and NMR experiment. X-ray crystallography measures the extent to which a given hydration site is occupied by water molecules. It cannot distinguish a long-lived water molecule occupying a site from that involving rapid exchange. On the other hand, NMR experiments monitor a particular water molecule, which resides

sufficiently long at a hydration site before being replaced by another water molecule (Billeter, 1995). The NMR experiment is, therefore, more appropriate in the investigation of hydration dynamics of water molecules, such as the rate of water exchange or the residence times of water at specific functional groups of proteins.

Some additional remarks should be made on the energy values in Table 3.2 and the cross sections in Figures 3.5 and 3.6. Since the solute-solvent interactions are quite strong, especially at the NH_3^+ group, the minima on the AWPD and AW-WWPD maps are seen nearly at the same positions. In contrast, the minima on the WWPD maps are located at the boundary or outside the first hydration shells. These were recognized from the cross section plots derived from the transverse profile lines in Figure 3.5. The observations support the statement in Clementi (1980) that, in the first hydration shell, the stabilization by the solute-solvent interactions is accompanied by the destabilization of the solvent-solvent interactions and vice versa. In addition, it is also noticeable from the same cross section plots that the shapes of the average potential landscapes, especially in the first hydration shell of the NH_3^+ group, are determined by the solute-solvent interactions. On the other hand, Figure 3.6 suggested that the shapes of the average potential landscapes at the COO^- group are influenced by the solvent-solvent interactions. The following discussion will focus on the energetics of particular H-bond networks mentioned in the previous subsections.

3.2.2.1 $[\text{Alaz}]_{\text{aq}}$

Table 3.2 shows that, at the NH_3^+ group, water molecules at **C** possess the strongest solute-solvent interaction, followed by **H**, **L**, **A** and **B**, respectively. The solvent-solvent interactions are, however, strongest at **L**, followed by **A**, **C**, **B** and **H**

respectively. Based on $\langle \Delta E_{\text{aq}}^{\text{AW-WWPD}} \rangle_{\text{min}}$, the interaction energies at **A** and **B**, as well as **H** and **L**, are comparable and the stability order for the hydration at the NH_3^+ group is written as:

$$\mathbf{C} > \mathbf{A} \geq \mathbf{B} > \mathbf{H} \geq \mathbf{L}.$$

At the NH_3^+ group, $\langle \Delta E_{\text{aq}}^{\text{AWPD}} \rangle_{\text{min,av}}$, $\langle \Delta E_{\text{aq}}^{\text{WWPD}} \rangle_{\text{min,av}}$ and $\langle \Delta E_{\text{aq}}^{\text{AW-WWPD}} \rangle_{\text{min,av}}$ are -59.04, -76.18 and -90.43 kJ mol^{-1} , respectively.

Although the probability of finding water molecules at **H** is only slightly higher than at **L** according to the PDO maps, $\tau_{\text{A-H..B,max}}$ in Table 3.4 reveal that a particular water molecule stays at **H** much longer than at **L**. This indicates that water exchange takes place more often at **L** compared to **H**. $\tau_{\text{N-H2..Ow,max}}$ and $\tau_{\text{N-H4..Ow,max}}$ are approximately 3 and 21 ps, respectively. The latter is comparable with the average residence time for charged atoms reported in Brunne, Liepinsh, Otting, Wüthrich, and van Gunsteren (1993), approximately 19 ps. The shapes of the average potential energy landscapes in Figure 3.5 can help to provide insight into the discrepancy between the H-bond lifetimes at **L** and **H**.

Table 3.4 Selected average H-bond distances ($\langle R_{A-H...B} \rangle$) and angles ($\langle \theta_{A-H...B} \rangle$), as well as the longest H-bond lifetimes ($\tau_{A-H...B, \max}$) derived from MD simulations.

SD = Standard Deviation

A-H...B = H-bond donor-acceptor pair between molecules A and B

Distances and angles are in Å and degree, respectively.

a) [Alaz]_{aq}

		SD	
<hr/>			
NH ₃ ⁺			
N-H2..Ow	$\langle R_{N-H2..Ow} \rangle$	2.94	0.20
	$\langle \theta_{N-H2..Ow} \rangle$	15.23	5.20
	$\tau_{N-H2..Ow, \max}$	2.70	-
N-H3..Ow	$\langle R_{N-H3..Ow} \rangle$	2.88	0.23
	$\langle \theta_{N-H3..Ow} \rangle$	29.79	12.27
	$\tau_{N-H3..Ow, \max}$	19.44	-
N-H4..Ow	$\langle R_{N-H4..Ow} \rangle$	2.90	0.23
	$\langle \theta_{N-H4..Ow} \rangle$	27.24	10.76
	$\tau_{N-H4..Ow, \max}$	21.34	-
<hr style="border-top: 1px dashed black;"/>			
COO ⁻			
Ow-Hw..O1	$\langle R_{Ow-Hw..O1} \rangle$	2.95	0.26
	$\langle \theta_{Ow-Hw..O1} \rangle$	29.31	13.52
	$\tau_{Ow-Hw..O1, \max}$	5.08	-
Ow-Hw..O2	$\langle R_{Ow-Hw..O2} \rangle$	3.124	0.29
	$\langle \theta_{Ow-Hw..O2} \rangle$	31.20	13.91
	$\tau_{Ow-Hw..O2, \max}$	4.90	-
<hr/>			

Table 3.4 (Continued).

b) [Alaz-R] _{aq}			
			SD
NH ₃ ⁺			
N-H2..Ow	< R _{N-H2..Ow} >	2.86	0.21
	< θ _{N-H2..Ow} >	29.11	15.52
	τ _{N-H2..Ow, max}	3.95	-
N-H3..Ow	< R _{N-H3..Ow} >	2.85	0.25
	< θ _{N-H3..Ow} >	43.60	8.65
	τ _{N-H3..Ow, max}	17.93	-
N-H4..Ow	< R _{N-H4..Ow} >	2.87	0.28
	< θ _{N-H4..Ow} >	34.74	12.21
	τ _{N-H4..Ow, max}	13.87	-

COO ⁻			
Ow-Hw..O1	< R _{Ow-Hw..O1} >	2.96	0.26
	< θ _{Ow-Hw..O1} >	31.65	13.54
	τ _{Ow-Hw..O1, max}	4.77	
Ow-Hw..O2	< R _{Ow-Hw..O2} >	3.11	0.32
	< θ _{Ow-Hw..O2} >	31.59	13.94
	τ _{Ow-Hw..O2, max}	2.98	-

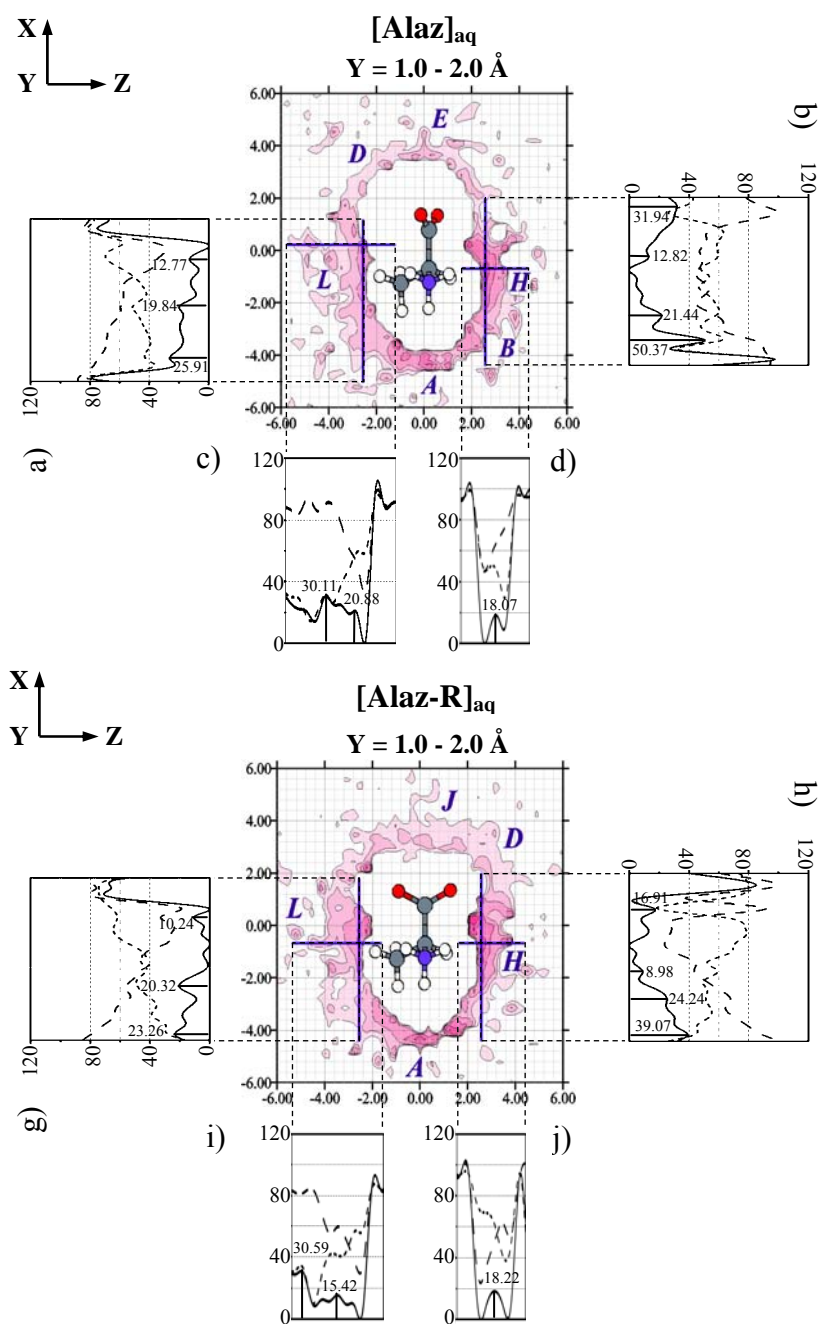


Figure 3.5 Cross section plots for the H-bond networks at the NH₃⁺ group of [Alaz]_{aq} and [Alaz-R]_{aq}. X-, Y- and Z-axis are in Å. The lowest energy minima of the cross sections were set to 0 kJ mol⁻¹ for comparison.

— for the AW-WWPD maps, - - - for the AWPD maps,
 - - - for the WWPD maps.

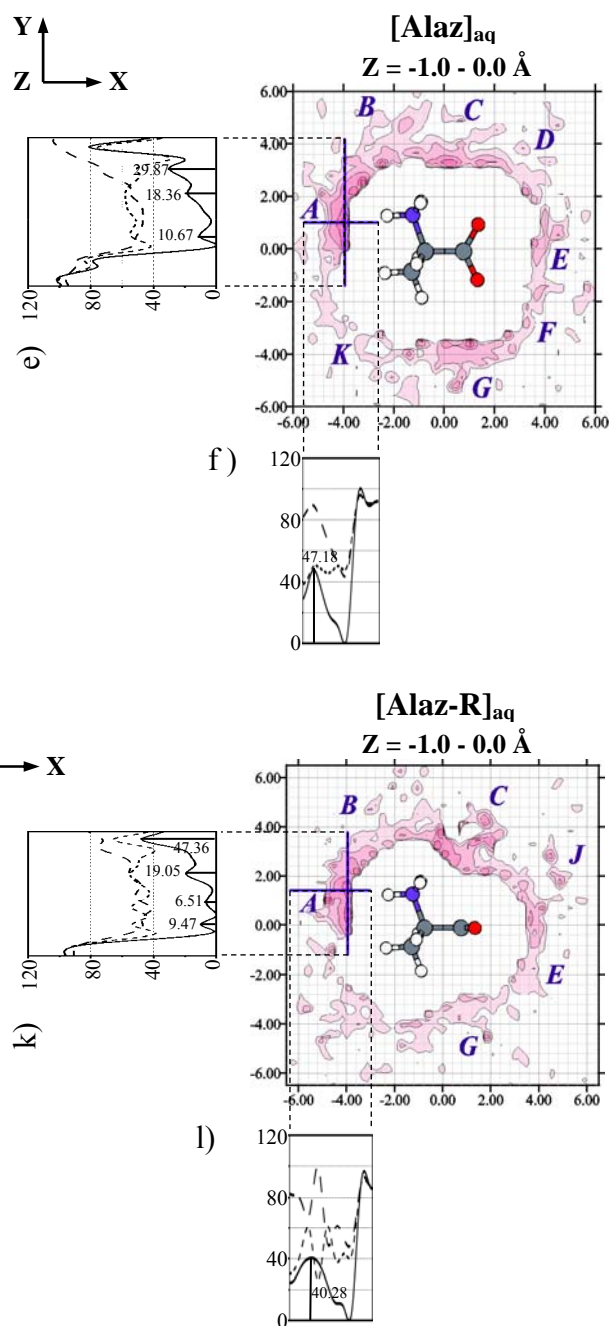


Figure 3.5 (Continued).

Investigation of Figure 3.5 and Table 3.4 suggests that the mobility of water molecules at specific hydration sites depend on the structures of the energy valleys of the H-bond networks. Figures 3.5a to 3.5d clearly show that the shapes of the average potential energy landscapes at **L** and **H** are different in details. Within the range from $X = 0.0$ to -4.0 \AA , for example, the transition energy barriers ($\langle \Delta E_{\text{aq}}^{\text{L}} \rangle$) at **L** vary approximately from 0 to 13 to 20 to 26 kJ mol^{-1} , whereas at **H** approximately from 13 to 0 to 50 kJ mol^{-1} , respectively. Figures 3.5c and 3.5d also reveal that $\langle \Delta E_{\text{aq}}^{\text{T}} \rangle$ at the boundary of **L** is only about 30 kJ mol^{-1} , whereas at **H** it amounts to about 100 kJ mol^{-1} . Since the transition energy barriers within and at the boundary of the H-bond network at **L** are lower, the mobility of water molecules at **L** is expected to be higher than at **H**. This should allow water exchange with the bulk to take place easier and faster at **L** compared to **H**. This discussion on the transition energy barriers explain why the H-bond lifetime at **L** is considerably shorter than **H**.

Figures 3.5b and 3.5d also suggest that the motion of water molecules at **H** is rather restricted, within a narrow energy valley of about 3 \AA width and about 4 \AA from the Alaz molecular plane. The latter supports the rough estimation in Clementi (1980) that the amino acid–water interaction drops sharply within 5 \AA , and the thickness of the perturbed water layer is about one water molecule. A similar explanation can be based on the average potential energy landscape at **A**. The shape of the average potential energy landscape at **A** is between that at **L** and at **H**. The cross section derived from the longitudinal profile line in Figure 3.5e is similar to Figure 3.5b, whereas that obtained from the transverse profile line in Figure 3.5f is similar to Figure 3.5c. This suggests that specific water molecules at **A** are more

localized compared to **L**, but less localized compared to **H**. $\tau_{\text{N-H3..Ow,max}}$ in Table 3.4 confirms this.

Due to weak H-bond interaction with water, the situation at the COO^- group is rather complicated. In Table 3.2, $\langle \Delta E_{\text{aq}}^{\text{AWPD}} \rangle_{\text{min,av}}$ for the interaction between the COO^- group and water is $-41.21 \text{ kJ mol}^{-1}$, about 18 kJ mol^{-1} higher than for the NH_3^+ group, whereas $\langle \Delta E_{\text{aq}}^{\text{WWPD}} \rangle_{\text{min,av}}$ is not substantially different from the NH_3^+ group. According to $\langle \Delta E_{\text{aq}}^{\text{AW-WWPD}} \rangle_{\text{min}}$, the stability order for the hydration at the COO^- group is found to be:

$$\mathbf{D} > \mathbf{E} > \mathbf{F} > \mathbf{J}.$$

Some difficulties are encountered in the analysis of the average potential energy landscapes at the COO^- group. Figure 3.6 shows energy valleys, which are not very well defined on the AW-WWPD maps. The fact that the O1 and O2 atoms are adjacent makes it difficult to specify the boundaries of the hydration shells. Therefore, an attempt will not be made to directly correlate $\tau_{\text{A-H...B,max}}$ with the size and shape of the cross sections at the COO^- group. It appears in general in Figures 3.6a to 3.6d that the energy valleys at the COO^- group are shallower compared to the NH_3^+ group. Hence, the shapes of the cross sections at the COO^- group allow water molecules to move in a wider range, especially within the areas between the O1 and O2 atoms. This could help promote the water exchanges at the COO^- group, both within and between the H-bond networks, as well as between the H-bond networks and the bulk. For example, the transition energy barrier for water exchange between the H-bond

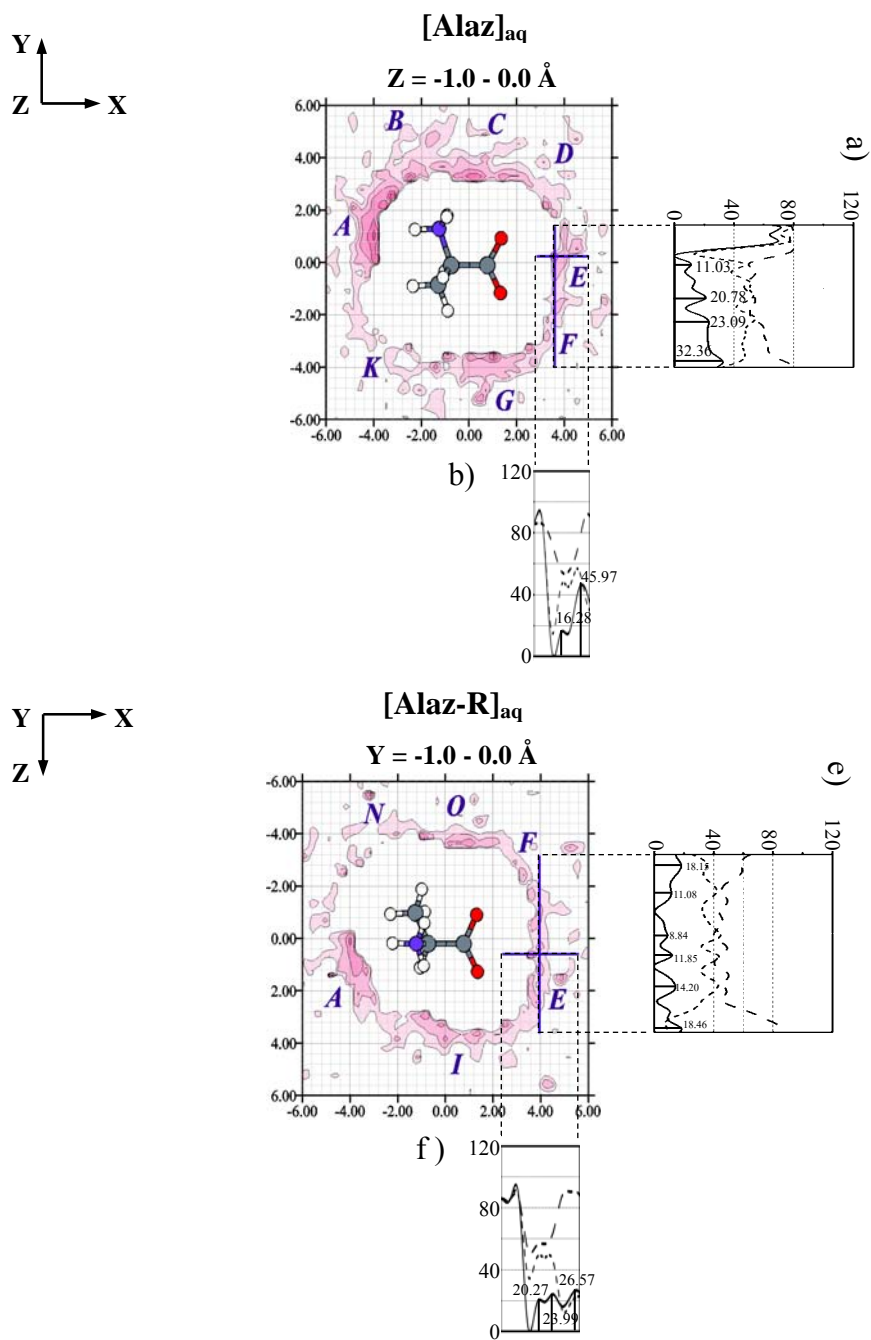


Figure 3.6 Cross section plots for the H-bond networks at the COO⁻ group of [Alaz]_{aq} and [Alaz-R]_{aq}. X-, Y- and Z-axis are in Å. The lowest energy minima of the cross sections were set to 0 kJ mol⁻¹ for comparison.

———— for the AW-WWPD maps, - - - for the AWPD maps,
- - - for the WWPD maps.

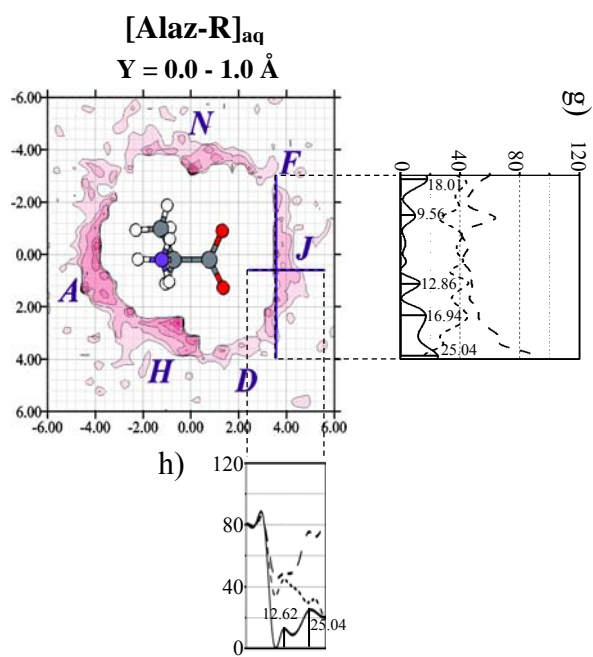
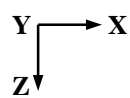
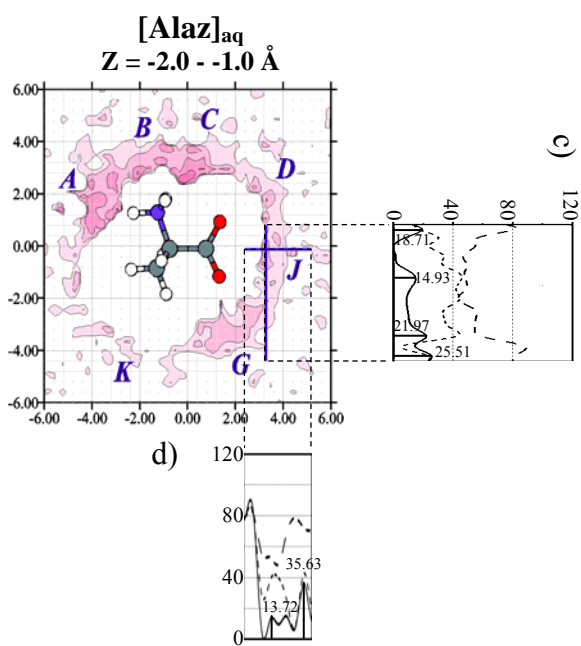
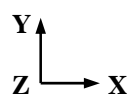


Figure 3.6 (Continued).

networks at **E** and **F** in Figure 3.5a is approximately 32 kJ mol^{-1} , and that between **J** and **G** is about 26 kJ mol^{-1} . These are in line with the values of $\tau_{\text{Ow-Hw..O1,max}}$ and $\tau_{\text{Ow-Hw..O2,max}}$, being only about 5 ps.

3.2.2.2 [Alaz-R]_{aq}

In general, the rotation of the COO^- plane led to slightly stronger solute-solvent interactions both at the NH_3^+ and COO^- groups. This is evident in Table 3.2, in which $\langle \Delta E_{\text{aq}}^{\text{AWPD}} \rangle_{\text{min,av}}$ at the NH_3^+ and COO^- groups is decreased by about 4 and 1 kJ mol^{-1} , respectively. $\langle \Delta E_{\text{aq}}^{\text{WWPD}} \rangle_{\text{min,av}}$ is nearly unchanged at the NH_3^+ group, whereas at the COO^- group is increased by about 6 kJ mol^{-1} .

Water molecules at **A** possess the lowest $\langle \Delta E_{\text{aq}}^{\text{AW-WWPD}} \rangle_{\text{min}}$, followed by **H**, **C**, **L** and **B**, respectively. Based on $\langle \Delta E_{\text{aq}}^{\text{AW-WWPD}} \rangle_{\text{min}}$, the stability order at the NH_3^+ group is:

$$\mathbf{A} > \mathbf{H} > \mathbf{C} > \mathbf{L} > \mathbf{B}.$$

The rotation of the COO^- plane brings about little change at the energy valleys at **L** and **A**. It, however, creates visible changes on the shapes of the cross section and $\langle \Delta E_{\text{aq}}^{\text{L}} \rangle$ at **H**. Within the range from $X = 0.0$ to -4.0 \AA , the highest $\langle \Delta E_{\text{aq}}^{\text{L}} \rangle$ at **H** reduces from approximately 50 kJ mol^{-1} in $[\text{Alaz}]_{\text{aq}}$ to 39 kJ mol^{-1} in $[\text{Alaz-R}]_{\text{aq}}$. This increases the mobility of water molecules at **H**, as is evident from the reduction of $\tau_{\text{N-H4..Ow,max}}$ from about 21 ps in $[\text{Alaz}]_{\text{aq}}$ to 14 ps in $[\text{Alaz-R}]_{\text{aq}}$.

Based on $\langle \Delta E_{\text{aq}}^{\text{AW-WWPD}} \rangle_{\text{min}}$, the stability order at the COO^- group is:

$$\mathbf{O} > \mathbf{F} > \mathbf{E} \geq \mathbf{J} > \mathbf{D}.$$

Figures 3.6a to 3.6h show that the rotation of the COO^- plane brings about remarkable changes in the cross sections at the COO^- group. The cross sections at **E** and **J** are discussed as examples. The energy barriers for the water exchange between the H-bond networks, discussed in the previous subsections, are considerably reduced in general. In Figure 3.6e, $\langle \Delta E_{\text{aq}}^{\text{L}} \rangle$ at **E** are about 18 kJ mol^{-1} at most. Figures 3.6d and 3.6h also illustrate that, upon rotation, $\langle \Delta E_{\text{aq}}^{\text{T}} \rangle$ at **J** is reduced, from about 36 to 25 kJ mol^{-1} . This should increase the rate of water exchange between the H-bond network and the bulk, as well as allow water molecules to move in a wider range in the area of the COO^- group, compared to $[\text{Alaz}]_{\text{aq}}$.

CHAPTER IV

CONCLUSION

Structures and energetics of the H-bond networks of water molecules at the charged functional groups of two forms of alanine zwitterions (Alaz and Alaz-R) were investigated, using intermolecular potentials derived from the T-model and MD simulations. In order to study the effects of conformation change on the structures and energetics of the H-bond networks, the MD results on [Alaz]_{aq} and [Alaz-R]_{aq} were analyzed extensively. General trends of the interaction energies of the polar solute in aqueous solutions are observed in the MD simulations. The preferential hydrations result more or less from combined effects of solute-solvent and solvent-solvent interactions, as well as the hydration dynamics of water molecules in the first hydration shell. The PDO maps clearly illustrate the three-dimensional structures of the H-bond networks of water at both the NH₃⁺ and the COO⁻ groups. It is recognized that water molecules establish more well-defined H-bond networks at the NH₃⁺ group, compared to the COO⁻ group. For both [Alaz]_{aq} and [Alaz-R]_{aq}, the PDO maps confirm that water molecules form H-bond networks between the NH₃⁺ and COO⁻ groups, which rules out the possibility for the two charged functional groups to form an intramolecular H-bond. This is in accordance with the previous ¹⁷O-NMR relaxation study and MC simulations on [Gly]_{aq}.

For [Alaz]_{aq}, at least five H-bond networks are observed at the NH₃⁺ group and four or more at the COO⁻ group. It is recognized that the orders of the preferential

hydration derived from the PDO maps and the stability orders inferred from the AWPD, WWPd and AW-WWPd maps are not the same. This is due to the fact that the minima on the AW-WWPd maps are associated with the interaction energy states, which might be occupied or unoccupied at a given MD timestep. The occupancies of the interaction energy states depend on the hydration dynamics of individual water molecule, as well as on the transition energy barriers interconnected these states.

Attempt was made in the present work to correlate the sizes and shapes of the average potential energy landscapes at the H-bond networks with the H-bond lifetimes. To serve this purpose, cross section plots at the H-bond networks are constructed from the AW-WWPd maps. The mobility of water molecules and the possibilities for the water exchanges within and between the H-bond networks, as well as between the H-bond networks and the outsides, are discussed based on $\tau_{A-H...B,max}$, $\langle \Delta E_{aq}^L \rangle$ and $\langle \Delta E_{aq}^T \rangle$. The structures of the energy valleys suggest that, at the NH_3^+ group, water exchanges within the H-bond networks seem to take place easier and faster than between the H-bond networks and the bulk. On the other hand, water molecules at the COO^- group cannot move or exchange very rapidly within a wider range.

The rotation of the COO^- plane 90° with respect to the $NC^\alpha C$ backbone seems to create changes more or less in both the structures and the energetics of the H-bond networks. It is confirmed in the present work that, although the functional groups of Alaz-R are more accessible by water, the overall stabilization by hydration is larger for $[Alaz]_{aq}$ than the $[Alaz-R]_{aq}$. On average, the solute-solvent interactions are stronger and the solvent-solvent interactions are weaker at the H-bond networks of both NH_3^+ and COO^- groups. The rotation of the COO^- plane creates an additional

well-defined H-bond network at the COO^- group, and brings about changes in $\langle \Delta E_{\text{aq}}^{\text{L}} \rangle$ and $\langle \Delta E_{\text{aq}}^{\text{T}} \rangle$. They are considerably reduced at the COO^- group, allowing water molecules to move or exchange within a wider range. The present results imply that complete information on molecular hydration can be obtained only when explicit water molecules, together with their hydration dynamics at the hydration sites, are considered in the model calculations.

REFERENCES

REFERENCES

- Alagona, G., Ghio, C., and Kollman, P. A. (1988). Monte Carlo simulation studies of the solvation of ions. 2. Glycine zwitterion. **Journal of Molecular Structure (THEOCHEM)** 166: 385-392.
- Baker, E. N. (1994). Solvent interactions with proteins as revealed by X-ray crystallographic studies. In Gregory, R. B. (Ed.). **Protein-solvent interactions** (pp. 143-189). New York: Marcel Dekker.
- Billeter, M. (1995). Hydration water molecules seen by NMR and by X-ray crystallography. **Progress in Nuclear Magnetic Resonance Spectroscopy** 27: 635-645.
- Böhm, H. J., and Ahlrichs, R. (1982). A study of short-range repulsions. **Journal of Chemical Physics** 77: 2028-2034.
- Breneman, C. M., and Wiberg, K. B. (1990). Determining atom-centred monopoles from molecular electrostatic potentials. The need for high sampling density in formamide conformational analysis. **Journal of Computational Chemistry** 11: 361-373.
- Brunne, R. M., Liepinsh, E., Otting, G., Wüthrich, K., and van Gunsteren, W. F. (1993). Hydration of proteins. A comparison of experimental residence times of water molecules solvating the Bovine Pancreatic Trypsin inhibitor with theoretical model calculations. **Journal of Molecular Biology** 231: 1040-1048.

- Case, D. A., Pearlman, D. A., Caldwell, J. W., Cheatham III, T. E., Ross, W. S., Simmerling, C. L., Darden, T. A., Merz, K. M., Stanton, R. V., Cheng, A. L., Vincent, J. J., Crowley, M., Tsui, V., Radmer, R. J., Duan, Y., Pitera, J., Massova, I., Seibel, G. L., Singh, U. C., Weiner, P. K., and Kollman, P. A. (1999). **AMBER** (version 6.0) [Computer software]. San Francisco: University of California.
- Castronuovo, G., Elia, V., and Velleca, F. (1996). Preferential configurations in solution. Calorimetric study of ternary aqueous systems containing a destructuring agent and derivatives of α -amino acids at 298 K. **Journal of Chemical Society, Faraday Transaction** 92: 4215-4218.
- Clementi, E. (1980). **Computational Aspects for Large Chemical Systems, Lecture Notes in Chemistry 19**. Berlin: Springer-Verlag.
- Clementi, E., Cavallone, F., and Scordamaglia, R. (1977). Analytical potentials from “*ab Initio*” computations for the Interaction between biomolecules. 1. water with amino acids. **Journal of the American Chemical Society** 99: 5531-5545.
- Cramer, C. J., and Truhlar, D. G. (1999). Implicit solvation models: equilibria, structure, spectra, and dynamics. **Chemical Reviews** 99: 2161-2200.
- Desfrancois, C., Carles, S., and Schermann, J. P. (2000). Weakly bound clusters of biological interest. **Chemical Reviews** 100: 3943-3962.
- Destro, R., Roversi, P., Barzaghi, M., and Marsh, R. E. (2000). Experimental charge density of α -glycine at 23 K. **The Journal of Physical Chemistry A** 104: 1047-1054.

- Ding, Y., and Krogh-Jespersen, K. (1996). The 1:1 glycine zwitterion-water complex: an *ab initio* electronic structure study. **Journal of Computational Chemistry** 17: 338-349.
- Feig, M., and Pettitt, B. M. (1998). Crystallographic water sites from a theoretical perspective. **Structure** 6: 1351-1354.
- Förner, W., Otto, P., Bernhardt, J., and Ladik, J. (1981). A model study of the intermolecular interactions of amino acids in aqueous solution: the glycine-water system. **Theoretica Chimica Acta (Berlin)** 60: 269-281.
- Frisch, M. J., Trucks, G. W., Schlegel, H. B., Scuseria, G. E., Robb, M. A., Cheeseman, J. R., Zakrzewski, V. G., Montgomery, J. A. Jr., Stratmann, R. E., Burant, J. C., Dapprich, S., Millam, J. M., Daniels, A. D., Kudin, K. N., Strain, M. C., Farkas, O., Tomasi, J., Barone, V., Cossi, M., Cammi, R., Mennucci, B., Pomelli, C., Adamo, C., Clifford, S., Ochterski, J., Petersson, G. A., Ayala, P. Y., Cui, Q., Morokuma, K., Salvador, P., Dannenberg, J. J., Malick, D. K., Rabuck, A. D., Raghavachari, K., Foresman, J. B., Cioslowski, J., Ortiz, J. V., Baboul, A. G., Stefanov, B. B., Liu, G., Liashenko, A., Piskorz, P., Komaromi, I., Gomperts, R., Martin, R. L., Fox, D. J., Keith, T., Al-Laham, M. A., Peng, C. Y., Nanayakkara, A., Challacombe, M., Gill, P. M. W., Johnson, B., Chen, W., Wong, M. W., Andres, J. L., Gonzalez, C., Head-Gordon, M., Replogle, E. S., and Pople, J. A., **Gaussian 98** (Revision A.5), Gaussian, Inc., Pittsburgh PA, 2001.
- Gaffney, J. G., Pierce, R. C., and Friedman, L. (1977). Mass spectrometer study of evaporation of α -amino Acids. **Journal of the American Chemical Society** 99: 4293-4298.

- Gerothanassis, I. P., Hunston, R., and Lauterwein, J. (1982). 175. ¹⁷O-NMR. of enriched acetic acid, glycine, glutamic acid and aspartic acid in aqueous solution. II. Relaxation studies. **Helvetica Chimica Acta** 65: 1774-1784.
- Hobza, P., and Havlas, Z. (1998). Counterpoise-corrected potential energy surfaces of simple H-bonded systems. **Theoretica Chimica Acta** 99: 372-377.
- Jensen, J. H., and Gordon, M. S. (1995). On the number of water molecules necessary to stabilize the glycine zwitterion. **Journal of the American Chemical Society** 117: 8159-8170.
- Jiang, J. -S., and Brünger, A. T. (1994). Protein hydration observed by X-ray diffraction solvation properties of penicillopepsin and neuraminidase crystal structures. **Journal of Molecular Biology** 243: 100-115.
- Kalko, S. G., Guàrdia, E., and Padró, J. A. (1999). Molecular Dynamics Simulation of the Hydration of the Alanine Dipeptide. **The Journal of Physical Chemistry B** 103: 3935-3941.
- Kikuchi, O., Matsuoka, T., Sawahara, H., and Takahashi, O. (1994). *Ab initio* molecular orbital calculations including solvent effects by generalized Born formula. Conformation of zwitterionic forms of glycine, alanine and serine in water. **Journal of Molecular Structure (THEOCHEM)** 305: 79-87.
- Kikuchi, O., Watanabe, T., Ogawa, Y., Takase, H., and Takahashi, O. (1997). *Ab initio* MO and Monte Carlo simulation study on the conformation of L-alanine zwitterion in aqueous solution. **Journal of Physical Organic Chemistry** 10: 145-151.

- Kimura, H., Nakamura, K., Eguchi, A., Sugisawa, H., Deguchi, K., Ebisawa, K., Suzuki, E., and Shoji, A. (1998). Structural study of α -amino-acid crystals by ^1H CRAMPS NMR spectroscopy. **Journal of Molecular Structure** 447: 247-255.
- Kollman, P. A. (1993). Free energy calculations: applications to chemical and biological phenomena. **Chemical Reviews** 93: 2395-2417.
- Leach, A. R. (2001). **Molecular Modelling**. (2nd ed.). England: Pearson Education.
- Lehmann, M. S., Koetzle, T. F., and Hamilton, W. C. (1972). Precision neutron diffraction structure determination of protein and nucleic acid components. I. The crystal and molecular structure of the amino acid L-alanine. **Journal of the American Chemical Society** 94: 2657-2660.
- Levitt, M., and Park, B. H. (1993). Water: now you see it, now you don't. **Structure** 1: 223-226.
- Levy, H. A., and Corey, R. B. (1941). The crystal structure of *dl*-alanine. **Journal of the American Chemical Society** 63: 2095-2108.
- Makarov, V., Pettitt, B. M., and Feig, M. (2002). Solvation and hydration of proteins and nucleic acids: a theoretical view of simulation and experiment. **Accounts of Chemical Research** 35: 376-384.
- Mark, P., and Nilsson, L. (2001). Molecular dynamics simulations of the ala-pro dipeptide in water: conformational dynamics of trans and cis isomers using different water models. **The Journal of Physical Chemistry B** 105: 8028-8035.
- Mathews, B. W. (1977). In Neurath, H., and Hill, R. L. (Eds.). **The Proteins** (pp. 403-590). New York: Academic Press.

- Mezei, M., Mehrotra, P. K., and Beveridge, D. L. (1984). Monte Carlo computer simulation of the aqueous hydration of the glycine zwitterion at 25°C. **Journal of Biomolecular Structure and Dynamics** 2: 1-26.
- Orozco, M., and Luque, F. J. (2000). Theoretical methods for the description of the solvent effects in biomolecular systems. **Chemical Reviews** 100: 4187-4225.
- Otwinowski, Z., Schevitz, R. W., Zhang, R. G., Lawson, C. L., Joachimiak, A., Marmorstein, R. Q., Luisi B. F., and Sigler, B. P. (1988). Crystal structure of *trp* repressor/operator complex at atomic resolution. **Nature** 335: 321.
- Park, S. -W., Ahn, D. -S., and Lee, S. (2003). Dynamic paths between neutral alanine-water and zwitterionic alanine-water clusters: single, double and triple proton transfer. **Chemical Physics Letter** 371: 74-79.
- Rupley, J. A. (1969). In Timasheff, S. N., and Fasman, G. D. (Eds.). **Structure and Stability of Biological Macromolecules** (pp. 291-352). New York: Marcel Dekker.
- Rzepa, H. S., and Yi, M. Y. (1991). An AM1 and PM3 molecular orbital and self-consistent reaction-field study of the aqueous solvation of glycine, alanine and proline in their neutral and zwitterionic forms. **Journal of Chemical Society, Perkin Transaction** 2: 531-537.
- Sagarik, K. P. (1999). Theoretical studies on hydrogen bonding in hydroxylamine clusters and liquid. **Journal of Molecular Structure (THEOCHEM)** 465: 141-155.

- Sagarik, K. P., and Ahlrichs, R. (1987). A test particle model potential for formamide and molecular dynamics simulations of the liquid. **Journal of Chemical Physics** 86: 5117–5126.
- Sagarik, K. P., and Asawakun, P. (1997). Intermolecular potential for phenol based on the test particle model. **Chemical Physics** 219: 173-191.
- Sagarik, K. P., and Rode, B. M. (2000). Intermolecular potential for benzoic acid-water based on the test-particle model and statistical mechanical simulations of benzoic acid in aqueous solutions. **Chemical Physics** 260: 159-182.
- Sagarik, K. P., and Spohr, E. (1995). Statistical Mechanical simulations on properties of liquid pyridine. **Chemical Physics** 199: 73-82.
- Sagarik, K. P., Chaiwongwattana, S., and Sisot, P. (2004). A theoretical study on clusters of benzoic acid-water in benzene solution. **Chemical Physics** 306: 1-12.
- Sagarik, K. P., Pongpituk, V., Chiyapongs, S., and Sisot, P. (1991). Test-particle model potentials for hydrogen-bonded complexes: complexes formed from HCN, HF, H₂O, NH₃, HCONH₂, HCONHCH₃, guanine and cytosine. **Chemical Physics** 156: 439-456.
- Schlegel, H. B. (1982). Optimization of equilibrium geometries and transition structures. **Journal of Computational Chemistry** 3: 214-218.
- Schoenborn, B. P., Garcia, A., and Knott, R. (1995). Hydration in protein crystallography. **Progress in Biophysics and Molecular Biology** 64: 105-119.

- Sigler, P. B. (1992). The Molecular Mechanism of *trp* repression. In McKnight, S. L., and Yamamoto, K. R. (Eds.). **Transcriptional regulation** New York: Cold Spring Harbor Laboratory Press.
- Smith, D. A. (1994). **Modeling the Hydrogen-Bond**. Washington DC: American Chemical Society.
- SURFER** for Windows (version. 6.04) [Computer software]. (1997). USA: Golden Software.
- Suzuki, M., Shigematsu, J., Fukunishi, Y., and Kodama, T. (1997). Hydrophobic hydration analysis on amino acid solutions by the microwave dielectric method. **The Journal of Physical Chemistry B** 101: 3839-3845.
- Tajkhorshid, E., Jalkanen, K. J., and Suhai, S. (1998). Structure and vibrational spectra of the zwitterion L-alanine in the presence of explicit water molecules: a density functional analysis. **The Journal of Physical Chemistry B** 102: 5899-5913.
- Thanki, N., Thornton, J. M., and Goodfellow, J. M. (1988). Distributions of water around amino acid residues in proteins. **Journal of Molecular Biology** 202: 637-657.
- Tuñón, I., Silla, E., Millot, C., Martins-Costa, M. T. C., and Ruiz-López, M. F. (1998). Intramolecular proton transfer of glycine in aqueous solution using Quantum Mechanics-Molecular Mechanics simulations. **The Journal of Physical Chemistry A** 102: 8673-8678.
- Vishveshwara, S., and Pople, J. A. (1977). Molecular orbital theory of the electronic structures of organic compounds. 32. Conformations of glycine and related systems. **Journal of the American Chemical Society** 99: 2422-2426.

- Voogd, J., Derissen, J. L., and van Duijneveldt, F. B. (1981). Calculation of proton-transfer energies and electrostatic lattice energies of various amino acids and peptides using CNDO/2 and ab Initio SCF methods. **Journal of the American Chemical Society** 103: 7701-7706.
- Watanabe, T., Hashimoto, K., Takase, H., and Kikuchi, O. (1997). Monte Carlo simulation study on the conformation and interaction of the glycine zwitterion in aqueous solution. **Journal of Molecular Structure (THEOCHEM)** 397: 113-119.
- Wüthrich, K. (1993). **NMR in structural biology, World Scientific Series in 20th Century Chemistry** (pp. 647-655). Vol. 5. Singapore: World Scientific.

APPENDICES

APPENDIX A

GEOMETRY OF ALAZ AND

THE T-MODEL PARAMETERS

Table A.1 Geometry of Alaz obtained from the neutron diffraction data^a.

Bond length		Bond angle		Torsion angle	
	(Å)		(°)		(°)
C1-C2	1.5310	C1C2C3	111.0699	C1C2NH2	58.30
C1-O1	1.2420	C1C2H1	108.5576	C1C2NH3	178.8450
C1-O2	1.2580	C2C1O1	118.3900	C1C2NH4	297.7545
C2-N	1.4870	C2C1O2	115.97	NC2C3H5	57.6002
C2-H1	1.0930	O1C1O2	125.6398	NC2C3H6	177.3002
C2-C3	1.5240	C2NH2	111.3300	NC2C3H7	297.8700
N-H2	1.0225	C2NH3	108.5774	NC2C1O1*	341.3373
N-H3	1.0225	C2NH4	108.5775	NC2C1O2*	161.5001
N-H4	1.0225	C3C2H1	110.40		
C3-H5	1.0810	NC2C3	109.74		
C3-H6	1.0820	NC2C1	110.0639		
C3-H7	1.0810	NC2H1	106.9150		
		H2NH3	109.4424		
		H2NH4	109.4424		
		H3NH4	109.4424		
		C2C3H5	110.33		
		C2C3H6	110.57		
		C2C3H7	110.37		
		H5C3H6	108.2344		
		H5C3H7	108.3615		
		H6C3H8	108.9102		

^a Taken from Lehmann, Koetzle, and Hamilton (1972).

(Three N-H bond lengths and HNH angles were adjusted to be equal.)

* For Alaz-R: NC2C1O1 = 90.0° and NC2C1O2 = 270.16°.

Table A.2 T-model parameters for Alaz and H₂O. Values are in atomic units.

Molecule	Atom	σ_i	ρ_i	q_i
Alaz				
	N	1.353868	0.218911	-0.525237
	C1	0.787583	0.339274	0.761047
	C2	0.917581	0.263135	0.080266
	C3	1.214082	0.260744	-0.148352
	O1	1.144134	0.241377	-0.708529
	O2	1.112793	0.247678	-0.702305
	H1	0.061947	0.284460	0.041066
	H2	-0.499160	0.371735	0.323706
	H3	-0.102376	0.270691	0.354676
	H4	-0.164475	0.271370	0.342286
	H5	0.036322	0.293167	0.064755
	H6	-0.049472	0.305756	0.088530
	H7	0.021921	0.308578	0.028090
H₂O				
	Ow	1.284091	0.200370	-0.451660
	Hw	-0.318644	0.331849	0.514110
	D			-0.576560

Note D is a dummy charge on the C₂ axis of H₂O, 0.26 Å from oxygen and in the opposite direction of the lone pair. The solute-solvent exchange repulsion energy was scaled with a factor of 0.70.

APPENDIX B

ADDITIONAL INFORMATION ON THE ALAZ-H₂O

AND ALAZ-R-H₂O 1 : N COMPLEXES

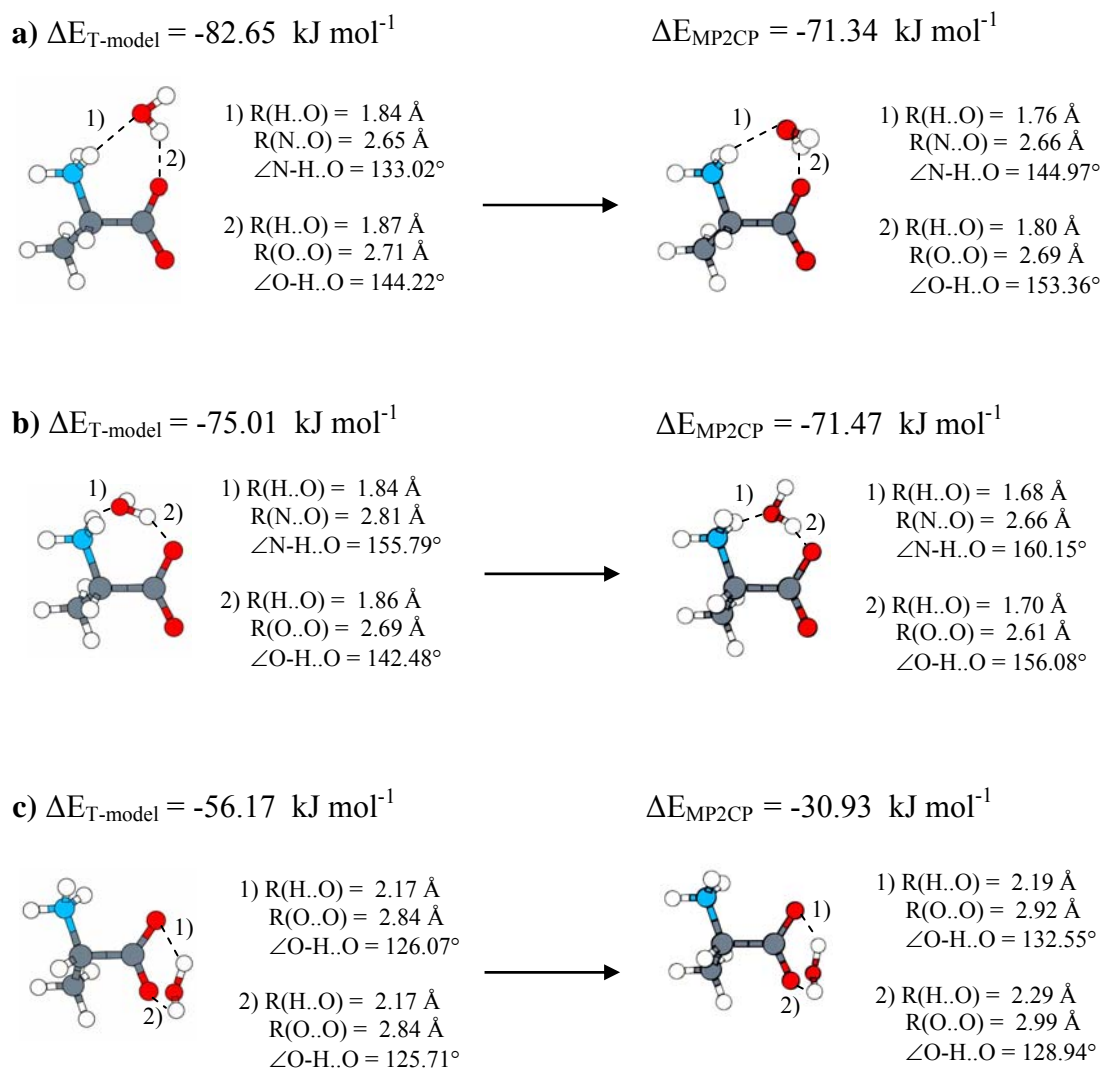


Figure B.1 The minimum energy geometries of the Alaz-H₂O 1 : 1 complexes obtained from T-model and MP2/6-311G(d,p) level.

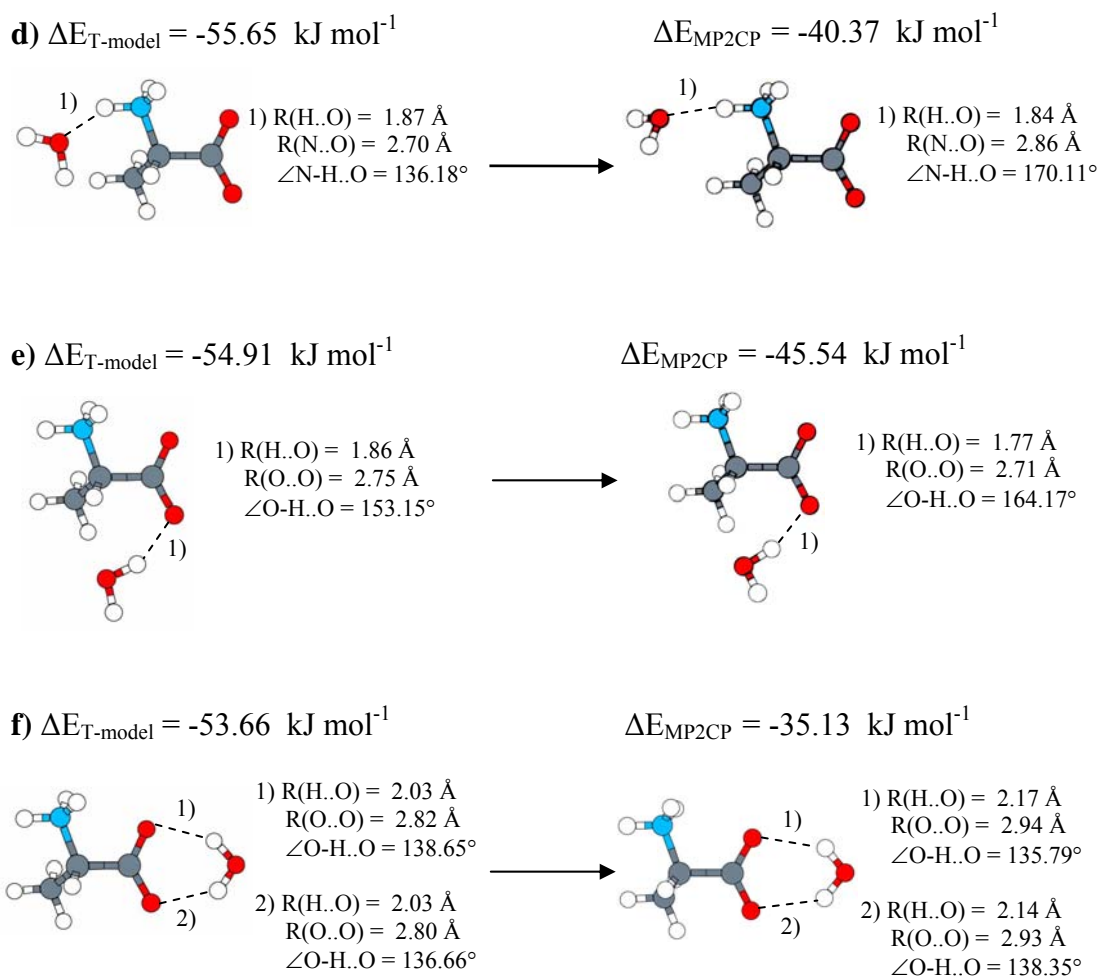


Figure B.1 (Continued).

Table B.1 Interaction energies and BSSE of Alaz-H₂O 1 : 1 complexes derived from the *ab initio* calculations. Energy is in kJ mol⁻¹.

Method	Structure						Mean	SD
	a	b	c	d	e	f		
SCF-A	-80.12	-80.03	-46.27	-45.98	-55.68	-48.43		
SCFCP-A	-64.68	-64.25	-30.37	-36.95	-43.36	-37.87		
BSSE _{SCF-A}	-15.44	-15.78	-15.90	-9.03	-12.32	-10.55	-13.17	2.97
MP2-A	-101.21	-103.21	-59.51	-56.76	-69.46	-54.40		
MP2CP-A	-71.34	-71.47	-30.93	-40.37	-45.54	-35.13		
BSSE _{MP2-A}	-29.87	-31.73	-28.58	-16.39	-23.92	-19.27	-24.96	6.16
SCF-B	-76.68	-75.84	-43.84	-41.55	-53.99	-44.90		
SCFCP-B	-61.91	-60.99	-29.13	-32.35	-41.67	-34.17		
BSSE _{SCF-B}	-14.77	-14.84	-14.71	-9.19	-12.32	-10.73	-12.76	2.42
MP2-B	-102.30	-103.98	-59.81	-55.16	-72.61	-53.76		
MP2CP-B	-74.47	-74.72	-34.39	-38.42	-49.44	-35.33		
BSSE _{MP2-B}	-27.83	-29.26	-25.42	-16.74	-23.17	-18.43	-23.48	5.04
SCF-C	-63.20	-61.88	-32.09	-33.28	-44.21	-37.61		
SCFCP-C	-59.96	-58.81	-29.45	-31.42	-42.15	-35.55		
BSSE _{SCF-C}	-3.24	-3.07	-2.64	-1.85	-2.06	-2.06	-2.49	0.58
MP2-C	-83.12	-83.84	-43.73	-42.71	-59.22	-43.79		
MP2CP-C	-72.63	-72.43	-36.16	-37.25	-51.29	-38.36		
BSSE _{MP2-C}	-10.49	-11.41	-7.57	-5.46	-7.93	-5.43	-8.05	2.49

SCF-X = SCF calculations using X basis set

SCFCP-X = SCF-X with BSSE correlation

BSSE_{SCF-X} = (SCF-X) - (SCFCP-X)

MP2-X = MP2 calculation using X basis set

MP2CP-X = MP2-X with BSSE correction

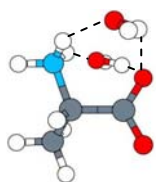
BSSE_{MP2-X} = (MP2-X) - (MP2CP-X)

X = A = *ab initio* calculations with MP2/6-311G(d,p)

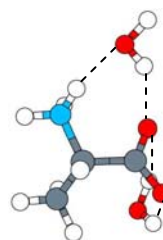
B = *ab initio* calculations with MP2/6-311G(2d,2p)//MP2/6-311G(d,p)

C = *ab initio* calculations with MP2/6-311++G(2d,2p)//MP2/6-311G(d,p)

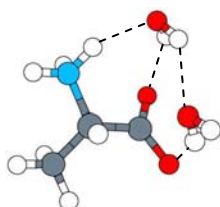
a) $\Delta E_{T\text{-model}} = -152.32 \text{ kJ mol}^{-1}$



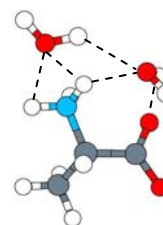
d) $\Delta E_{T\text{-model}} = -136.61 \text{ kJ mol}^{-1}$



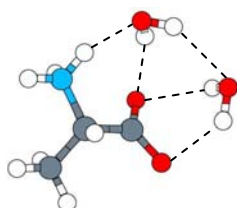
b) $\Delta E_{T\text{-model}} = -140.92 \text{ kJ mol}^{-1}$



e) $\Delta E_{T\text{-model}} = -136.30 \text{ kJ mol}^{-1}$



c) $\Delta E_{T\text{-model}} = -139.44 \text{ kJ mol}^{-1}$



f) $\Delta E_{T\text{-model}} = -136.04 \text{ kJ mol}^{-1}$

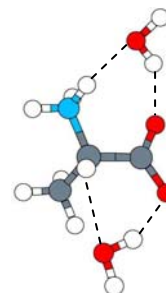
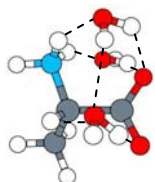
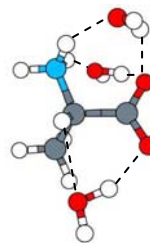


Figure B.2 Equilibrium structures of the Alaz-H₂O 1 : 2 complexes derived from T-model.

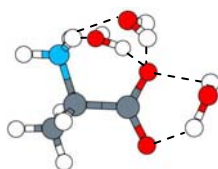
a) $\Delta E_{T\text{-model}} = -210.57 \text{ kJ mol}^{-1}$



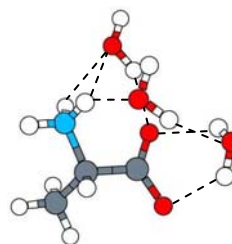
d) $\Delta E_{T\text{-model}} = -203.76 \text{ kJ mol}^{-1}$



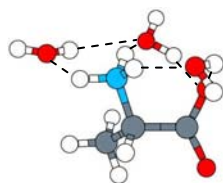
b) $\Delta E_{T\text{-model}} = -207.84 \text{ kJ mol}^{-1}$



e) $\Delta E_{T\text{-model}} = -202.97 \text{ kJ mol}^{-1}$



c) $\Delta E_{T\text{-model}} = -206.36 \text{ kJ mol}^{-1}$



f) $\Delta E_{T\text{-model}} = -200.62 \text{ kJ mol}^{-1}$

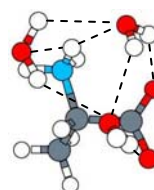
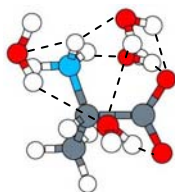
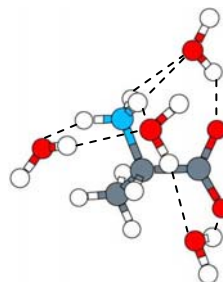


Figure B.3 Equilibrium structures of the Alaz-H₂O 1 : 3 complexes derived from T-model.

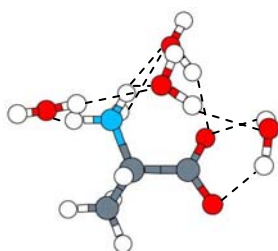
a) $\Delta E_{T\text{-model}} = -268.05 \text{ kJ mol}^{-1}$



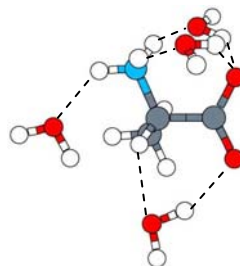
d) $\Delta E_{T\text{-model}} = -260.11 \text{ kJ mol}^{-1}$



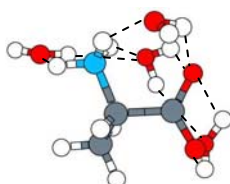
b) $\Delta E_{T\text{-model}} = -261.39 \text{ kJ mol}^{-1}$



e) $\Delta E_{T\text{-model}} = -259.97 \text{ kJ mol}^{-1}$



c) $\Delta E_{T\text{-model}} = -260.42 \text{ kJ mol}^{-1}$



f) $\Delta E_{T\text{-model}} = -259.80 \text{ kJ mol}^{-1}$

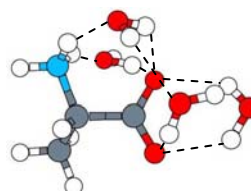


Figure B.4 Equilibrium structures of the Alaz-H₂O 1 : 4 complexes derived from T-model.

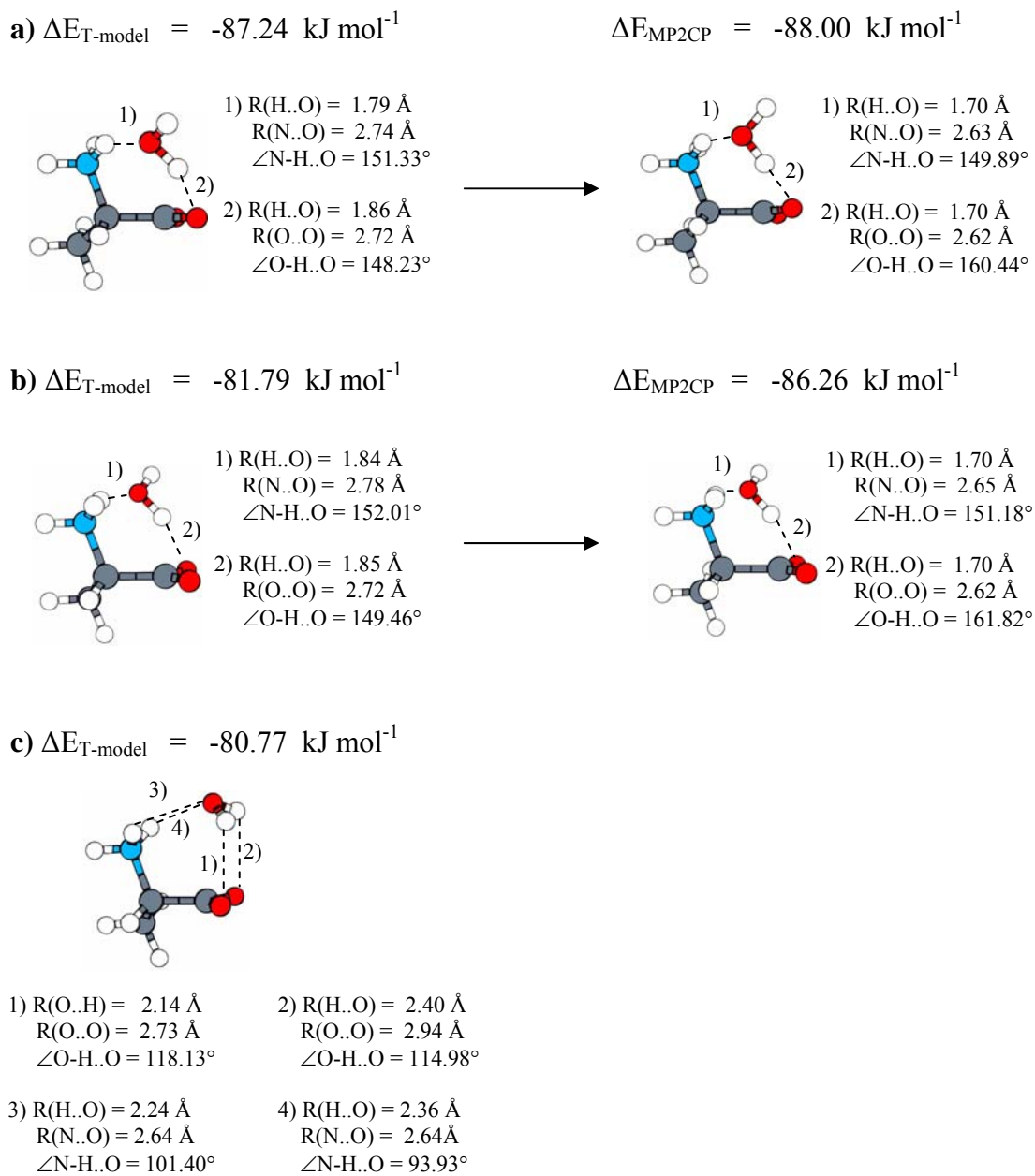
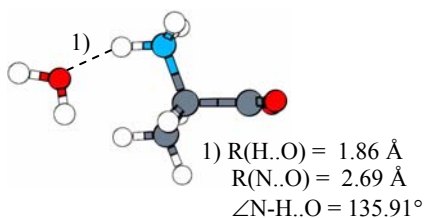
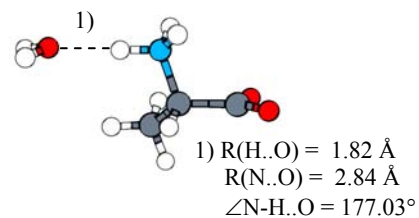


Figure B.5 The minimum energy geometries of the Alaz-R-H₂O 1 : 1 complexes obtained from T-model and MP2/6-311G(d,p) level.

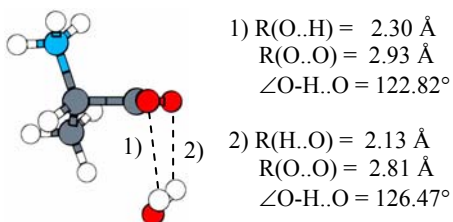
d) $\Delta E_{T\text{-model}} = -55.36 \text{ kJ mol}^{-1}$



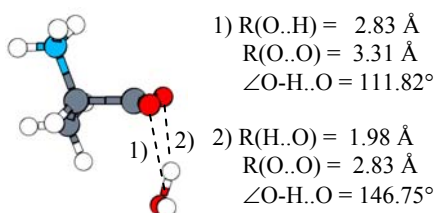
$\Delta E_{\text{MP2CP}} = -45.08 \text{ kJ mol}^{-1}$



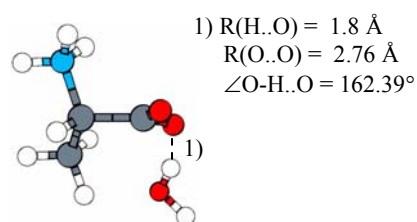
e) $\Delta E_{T\text{-model}} = -53.43 \text{ kJ mol}^{-1}$



$\Delta E_{\text{MP2CP}} = -32.01 \text{ kJ mol}^{-1}$



f) $\Delta E_{T\text{-model}} = -49.64 \text{ kJ mol}^{-1}$



$\Delta E_{\text{MP2CP}} = -37.23 \text{ kJ mol}^{-1}$

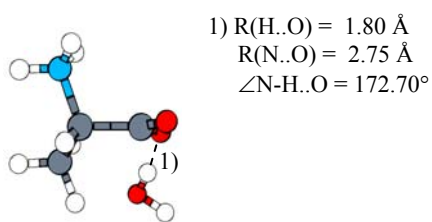


Figure B.5 (Continued).

Table B.2 Interaction energies and BSSE of Alaz-R-H₂O 1 : 1 complexes derived from the *ab initio* calculations. Energy is in kJ mol⁻¹.

Method	Structure						Mean	SD
	a	b	c*	d	e	f		
SCF-A	-96.08	-95.29	-62.21	-49.67	-45.51	-45.68		
SCFCP-A	-79.92	-77.99	-43.27	-42.37	-30.46	-36.50		
BSSE _{SCF-A}	16.16	17.30	18.94	7.30	15.05	9.18	13.99	4.67
MP2-A	-120.58	-120.09	-78.39	-58.24	-59.19	-54.90		
MP2CP-A	-88.00	-86.26	-43.76	-45.08	-32.01	-37.23		
BSSE _{MP2-A}	32.58	33.83	34.63	13.16	27.18	17.67	26.51	9.09
SCF-B	-92.17	-90.68	-58.12	-44.68	-43.51	-42.73		
SCFCP-B	-77.11	-74.82	-40.95	-36.93	-29.23	-33.91		
BSSE _{SCF-B}	15.06	15.86	17.17	7.75	14.28	8.82	13.16	3.91
MP2-B	-120.76	-120.62	-78.95	-56.24	-60.28	-56.23		
MP2CP-B	-91.49	-90.03	-48.61	-42.12	-35.50	-39.32		
BSSE _{MP2-B}	29.27	30.59	30.35	14.12	24.78	16.91	24.34	7.20
SCF-C	-77.87	-75.79	-44.49	-37.55	-31.67	-36.44		
SCFCP-C	-74.72	-72.47	-41.05	-35.91	-29.10	-34.68		
BSSE _{SCF-C}	3.15	3.32	3.44	1.64	2.57	1.76	2.65	0.79
MP2-C	-100.68	-99.71	-60.51	-45.74	-43.95	-47.69		
MP2CP-C	-89.07	-87.66	-50.38	-40.72	-36.50	-41.31		
BSSE _{MP2-C}	11.61	12.05	10.13	5.02	7.45	6.38	8.77	2.90

* single-point *ab initio* calculations made at the T-model optimized geometry

SCF-X = SCF calculations using X basis set

SCFCP-X = SCF-X with BSSE correlation

BSSE_{SCF-X} = (SCF-X) - (SCFCP-X)

MP2-X = MP2 calculation using X basis set

MP2CP-X = MP2-X with BSSE correction

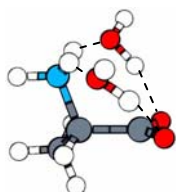
BSSE_{MP2-X} = (MP2-X) - (MP2CP-X)

X = A = *ab initio* calculations with MP2/6-311G(d,p)

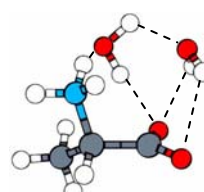
B = *ab initio* calculations with MP2/6-311G(2d,2p)//MP2/6-311G(d,p)

C = *ab initio* calculations with MP2/6-311++G(2d,2p)//MP2/6-311G(d,p)

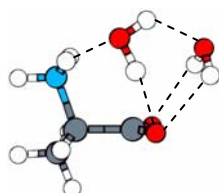
a) $\Delta E_{\text{T-model}} = -165.93 \text{ kJ mol}^{-1}$



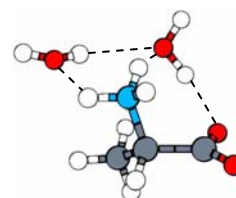
d) $\Delta E_{\text{T-model}} = -142.66 \text{ kJ mol}^{-1}$



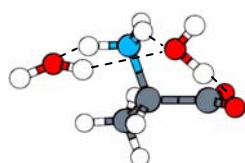
b) $\Delta E_{\text{T-model}} = -147.26 \text{ kJ mol}^{-1}$



e) $\Delta E_{\text{T-model}} = -139.31 \text{ kJ mol}^{-1}$



c) $\Delta E_{\text{T-model}} = -145.24 \text{ kJ mol}^{-1}$



f) $\Delta E_{\text{T-model}} = -139.18 \text{ kJ mol}^{-1}$

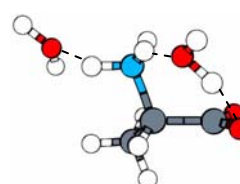
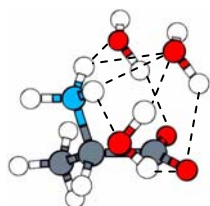
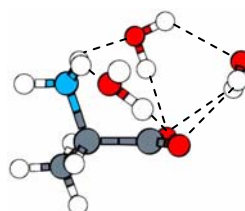


Figure B.6 Equilibrium structures of the Alaz-R-H₂O 1 : 2 complexes derived from T-model.

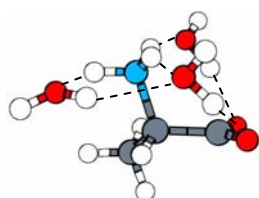
a) $\Delta E_{T\text{-model}} = -228.38 \text{ kJ mol}^{-1}$



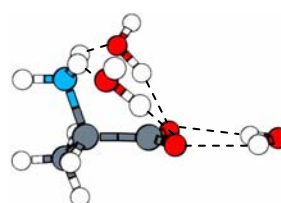
d) $\Delta E_{T\text{-model}} = -220.12 \text{ kJ mol}^{-1}$



b) $\Delta E_{T\text{-model}} = -221.63 \text{ kJ mol}^{-1}$



e) $\Delta E_{T\text{-model}} = -215.64 \text{ kJ mol}^{-1}$



c) $\Delta E_{T\text{-model}} = -220.95 \text{ kJ mol}^{-1}$

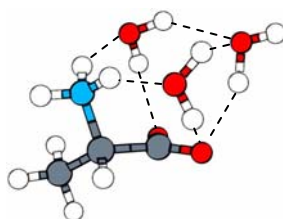
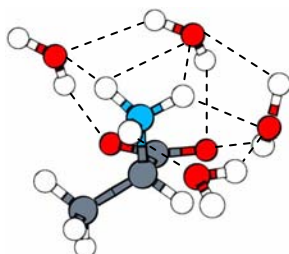
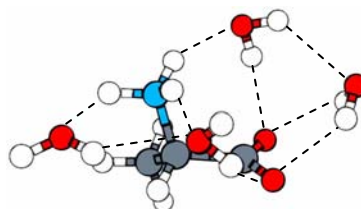


Figure B.7 Equilibrium structures of the Alaz-R-H₂O 1 : 3 complexes derived from T-model.

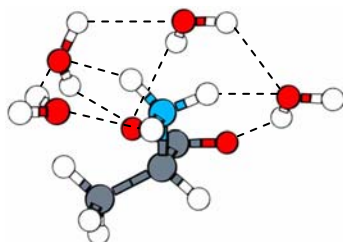
a) $\Delta E_{T\text{-model}} = -288.14 \text{ kJ mol}^{-1}$



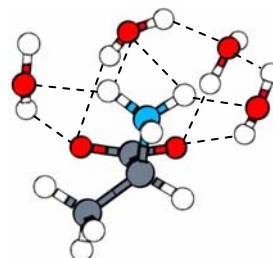
d) $\Delta E_{T\text{-model}} = -276.31 \text{ kJ mol}^{-1}$



b) $\Delta E_{T\text{-model}} = -282.28 \text{ kJ mol}^{-1}$



e) $\Delta E_{T\text{-model}} = -274.89 \text{ kJ mol}^{-1}$



c) $\Delta E_{T\text{-model}} = -281.15 \text{ kJ mol}^{-1}$

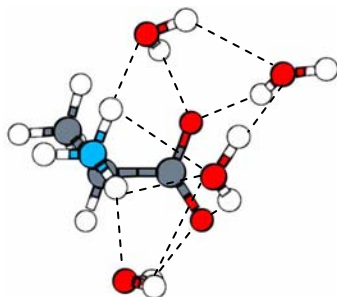


Figure B.8 Equilibrium structures of the Alaz-R-H₂O 1 : 4 complexes derived from T-model.

APPENDIX C
ADDITIONAL MD RESULTS ON ALAZ
IN AQUEOUS SOLUTION

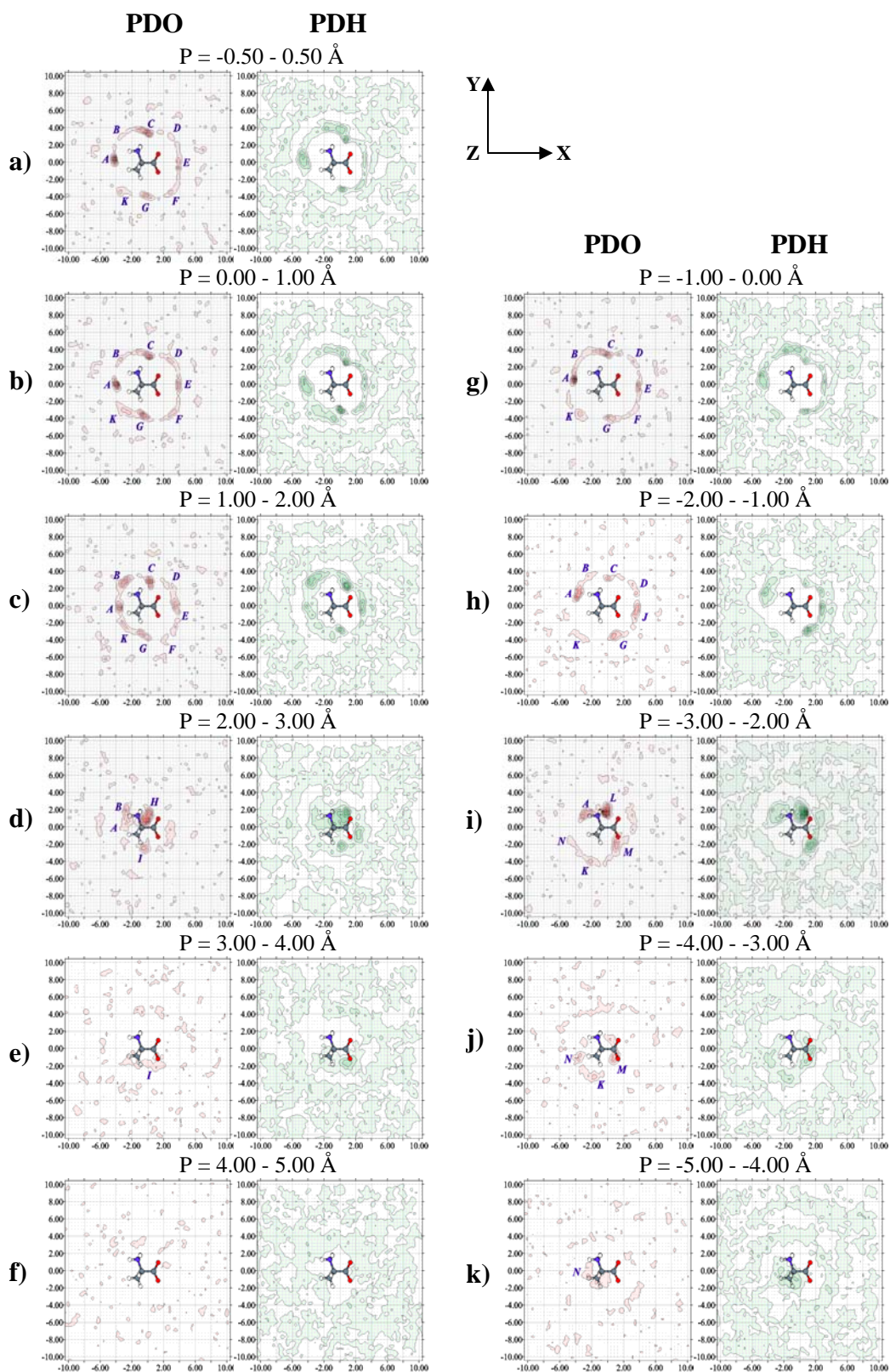


Figure C.1 PDO and PDH maps with respect to reference plane I for $[Alaz]_{aq}$ obtained from MD simulations. X-, Y- and Z-axis are in Å.

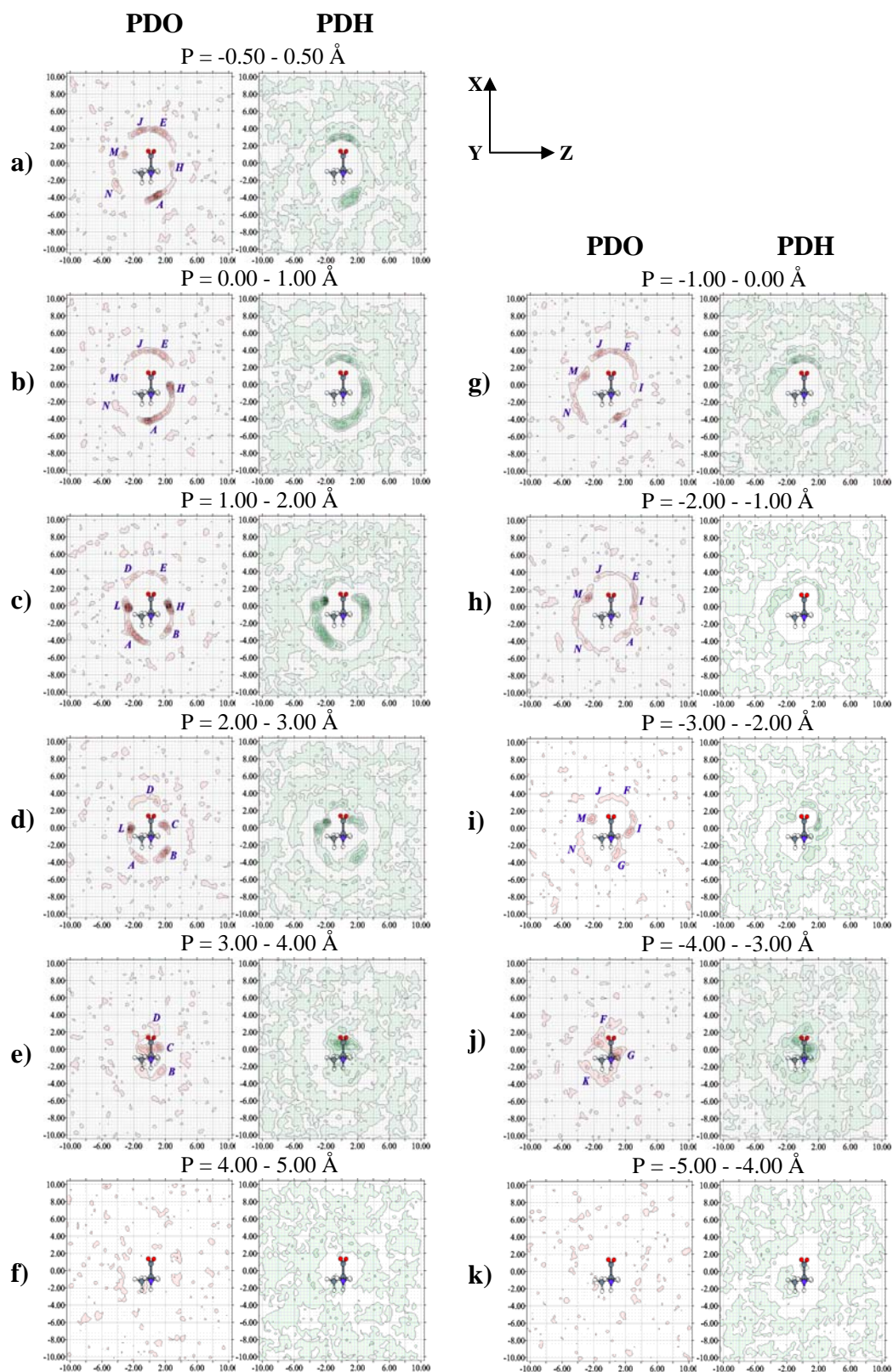


Figure C.2 PDO and PDH maps with respect to reference plane II for $[\text{Alaz}]_{\text{aq}}$ obtained from MD simulations. X-, Y- and Z-axis are in \AA .

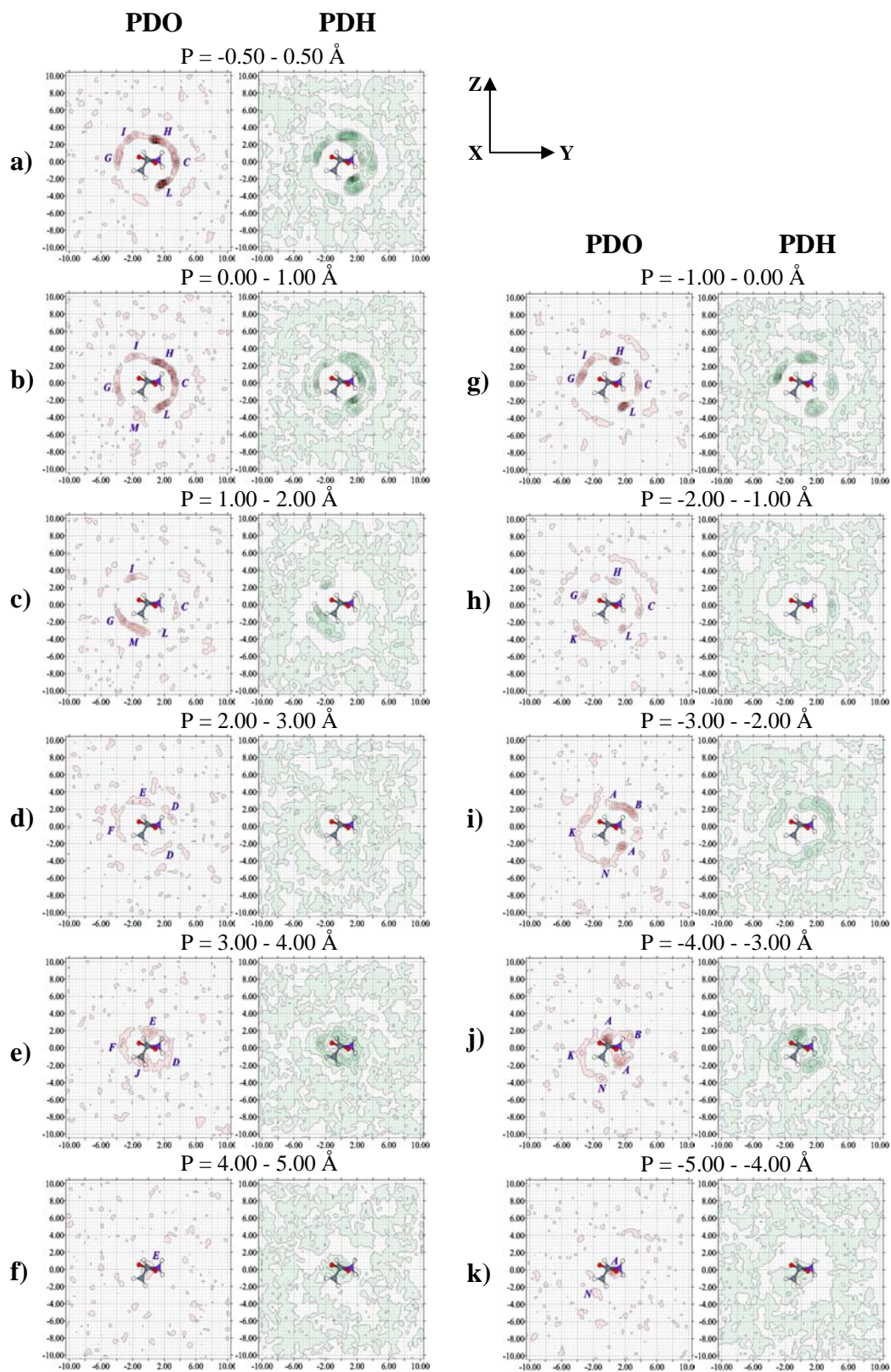


Figure C.3 PDO and PDH maps with respect to reference plane III for $[Alaz]_{aq}$ obtained from MD simulations. X-, Y- and Z-axis are in Å.

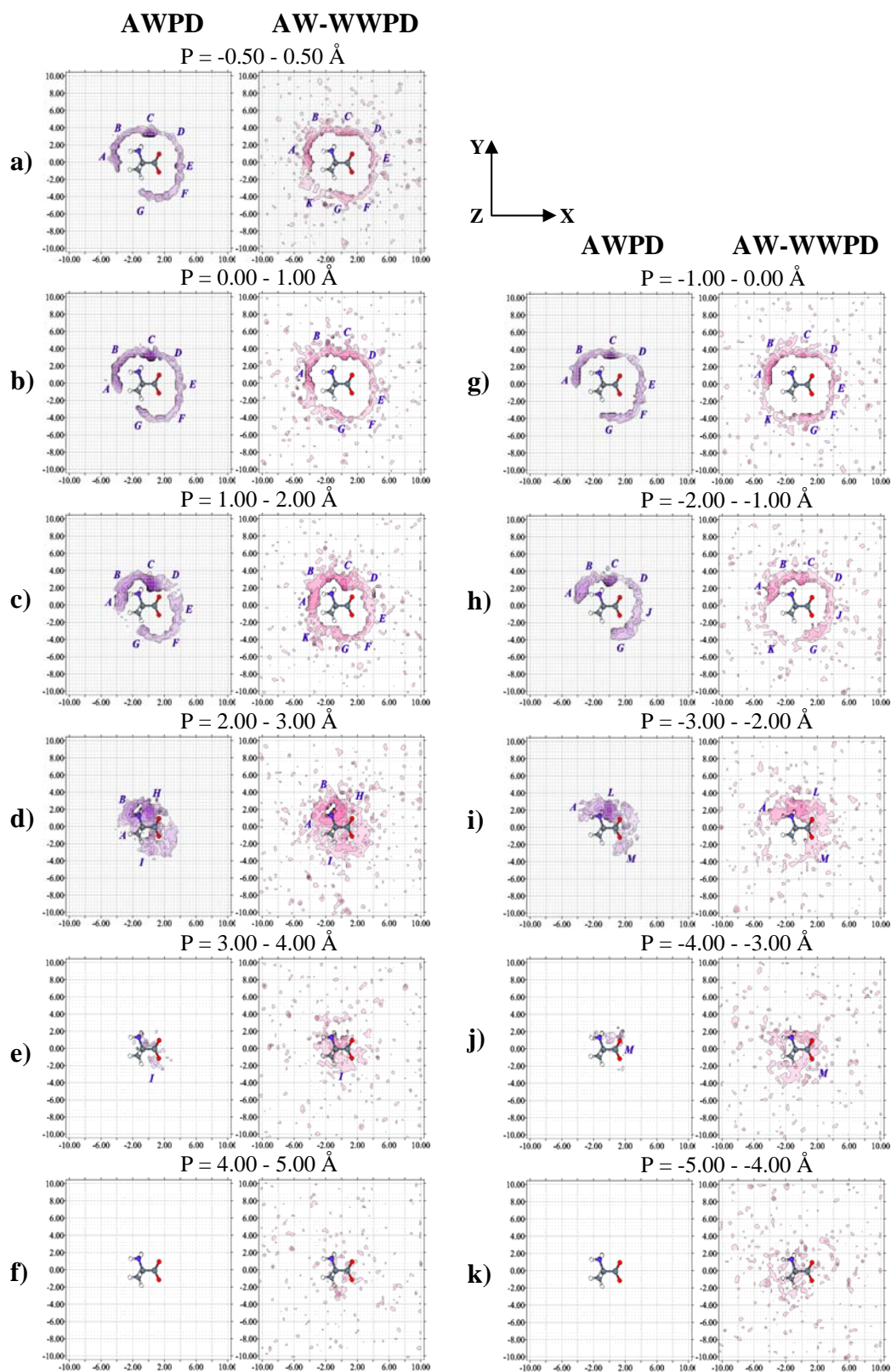


Figure C.4 AWPD and AW-WWPD maps with respect to reference plane I for $[\text{Alaz}]_{\text{aq}}$ obtained from MD simulations. X-, Y- and Z-axis are in Å.

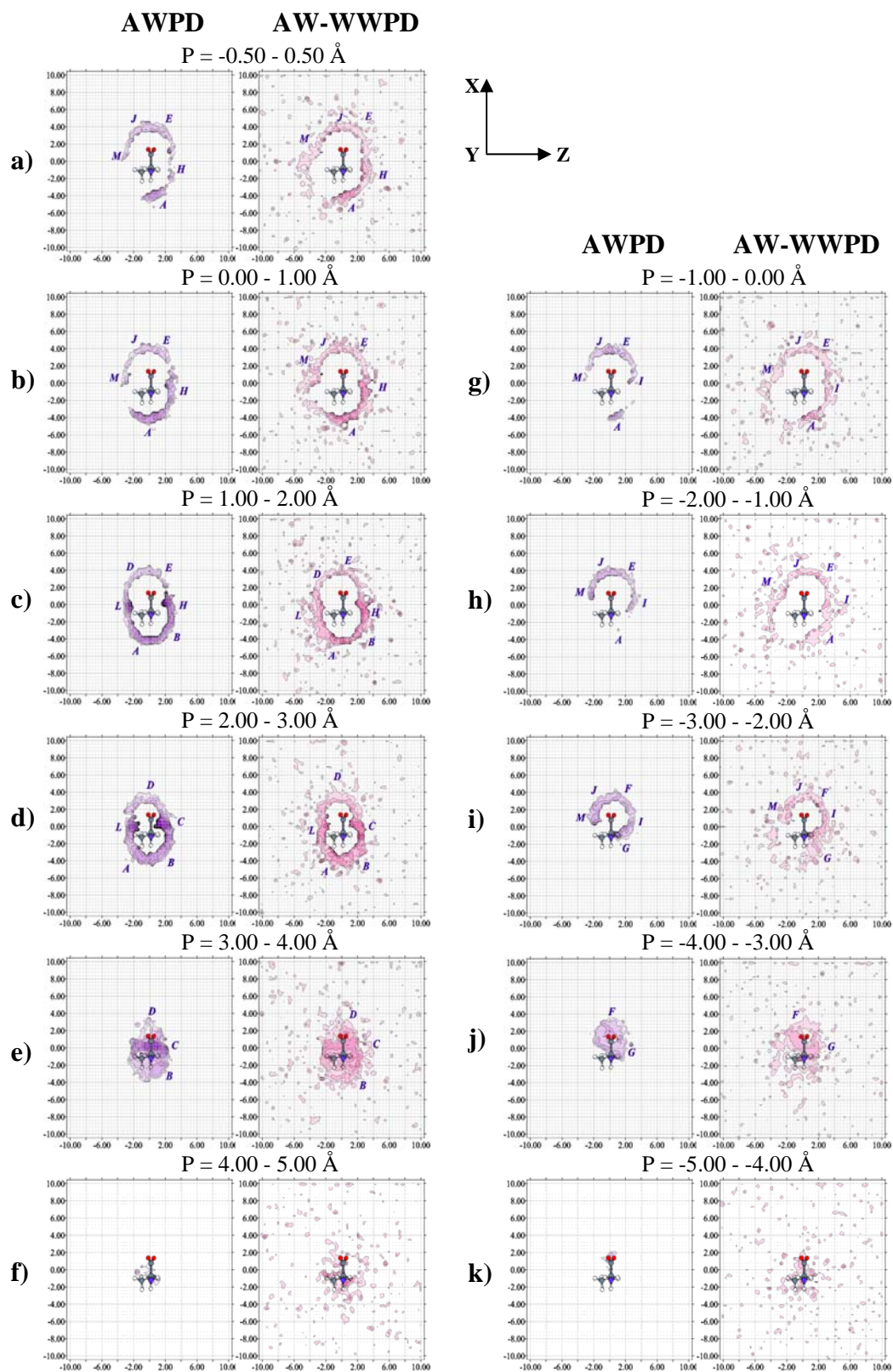


Figure C.5 AWPD and AW-WWPD maps with respect to reference plane II for $[\text{Alaz}]_{\text{aq}}$ obtained from MD simulations. X-, Y- and Z-axis are in \AA .

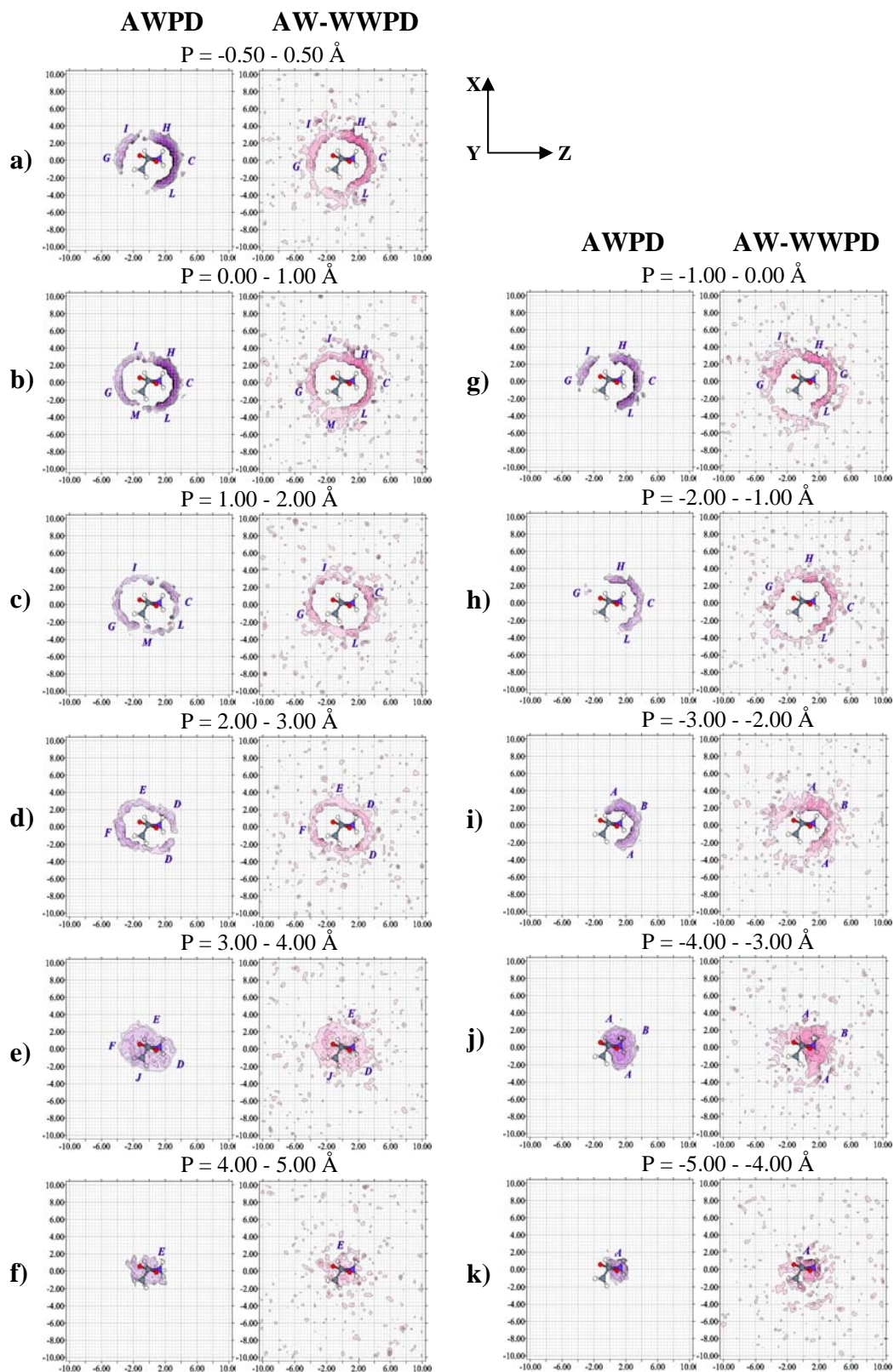


Figure C.6 AWPD and AW-WWPD maps with respect to reference plane III for [Alaz]_{aq} obtained from MD simulations. X-, Y- and Z-axis are in Å.

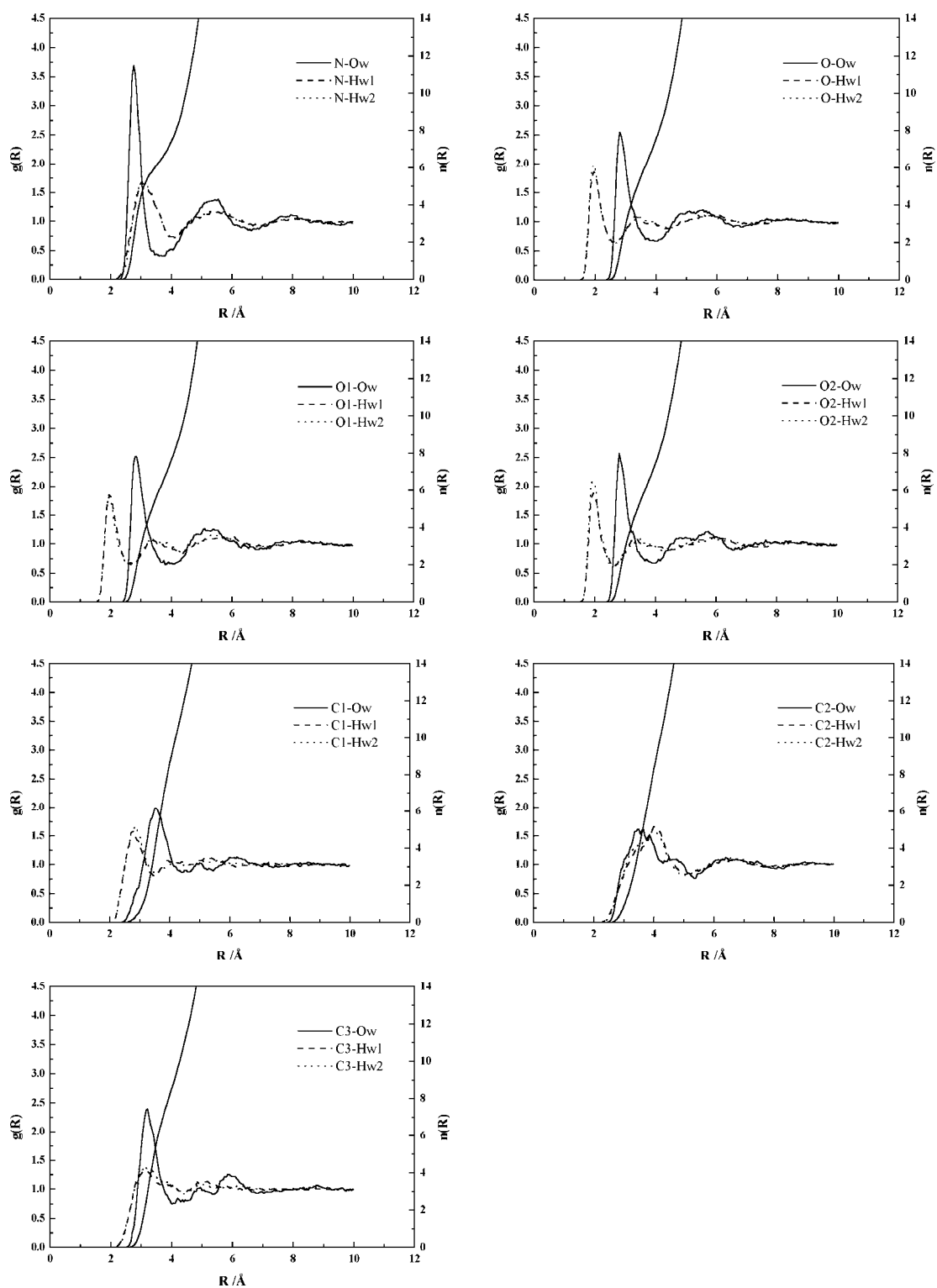


Figure C.7 $g(R)$ of $[\text{Alaz}]_{\text{aq}}$ at 298 K derived from MD simulations.

Ow, Hw1 and Hw2 are the oxygen and two hydrogen atoms of water, respectively.

APPENDIX D
ADDITIONAL MD RESULTS ON ALAZ-R
IN AQUEOUS SOLUTION

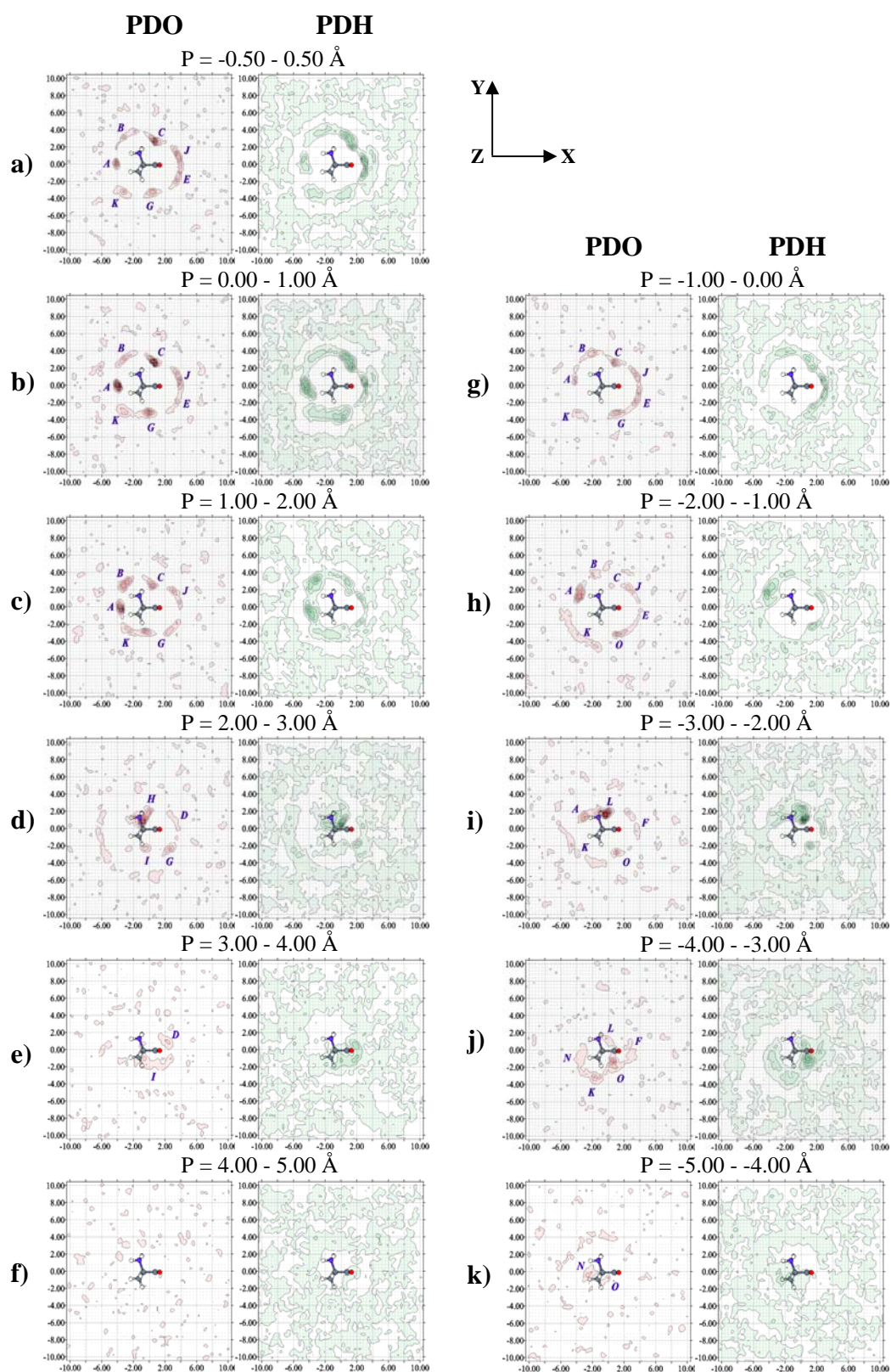


Figure D.1 PDO and PDH maps with respect to reference plane I for $[\text{Alaz-R}]_{\text{aq}}$

obtained from MD simulations. X-, Y- and Z-axis are in \AA .

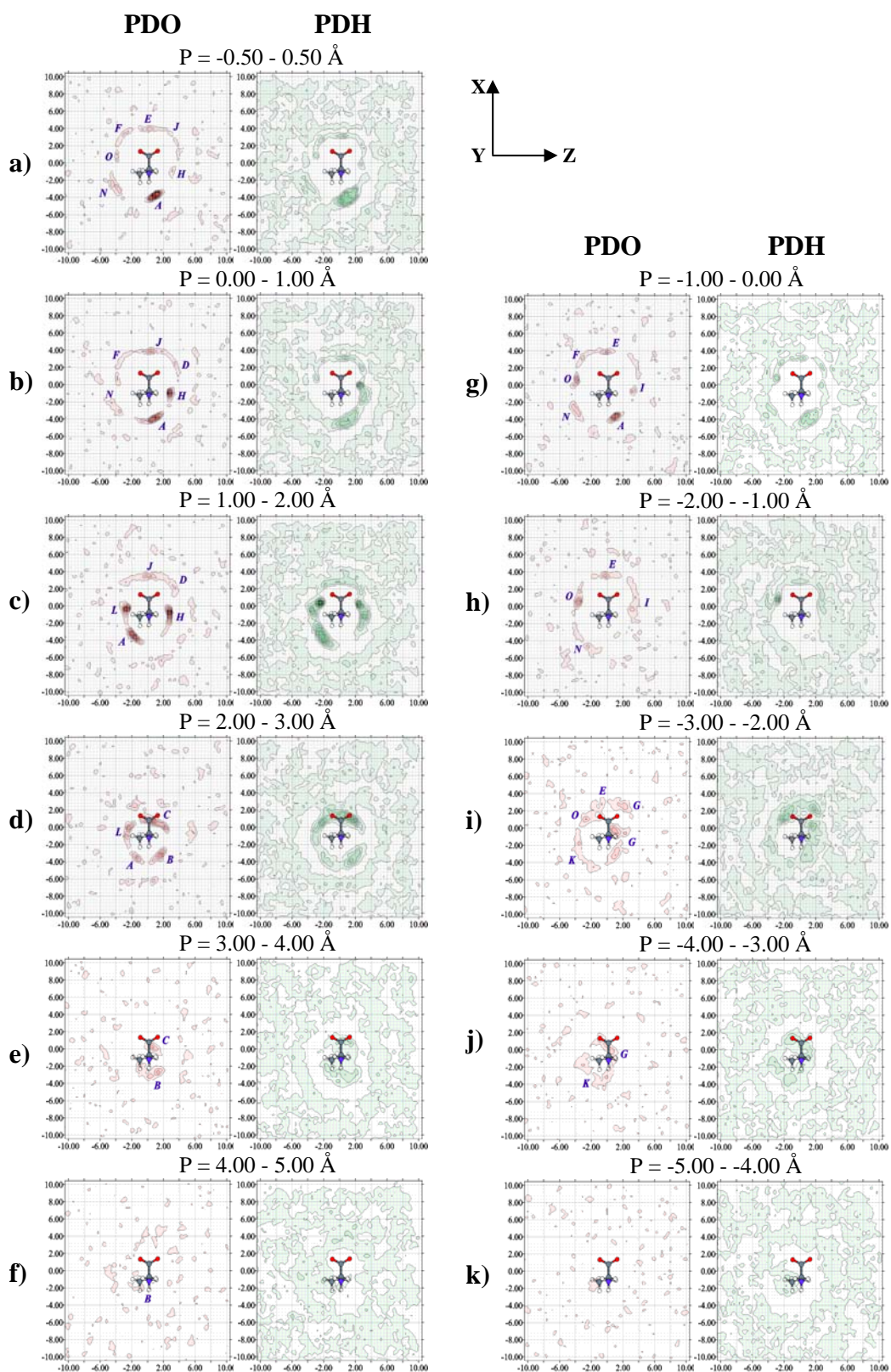


Figure D.2 PDO and PDH maps with respect to reference plane II for $[\text{Alaz-R}]_{\text{aq}}$

obtained from MD simulations. X-, Y- and Z-axis are in \AA .

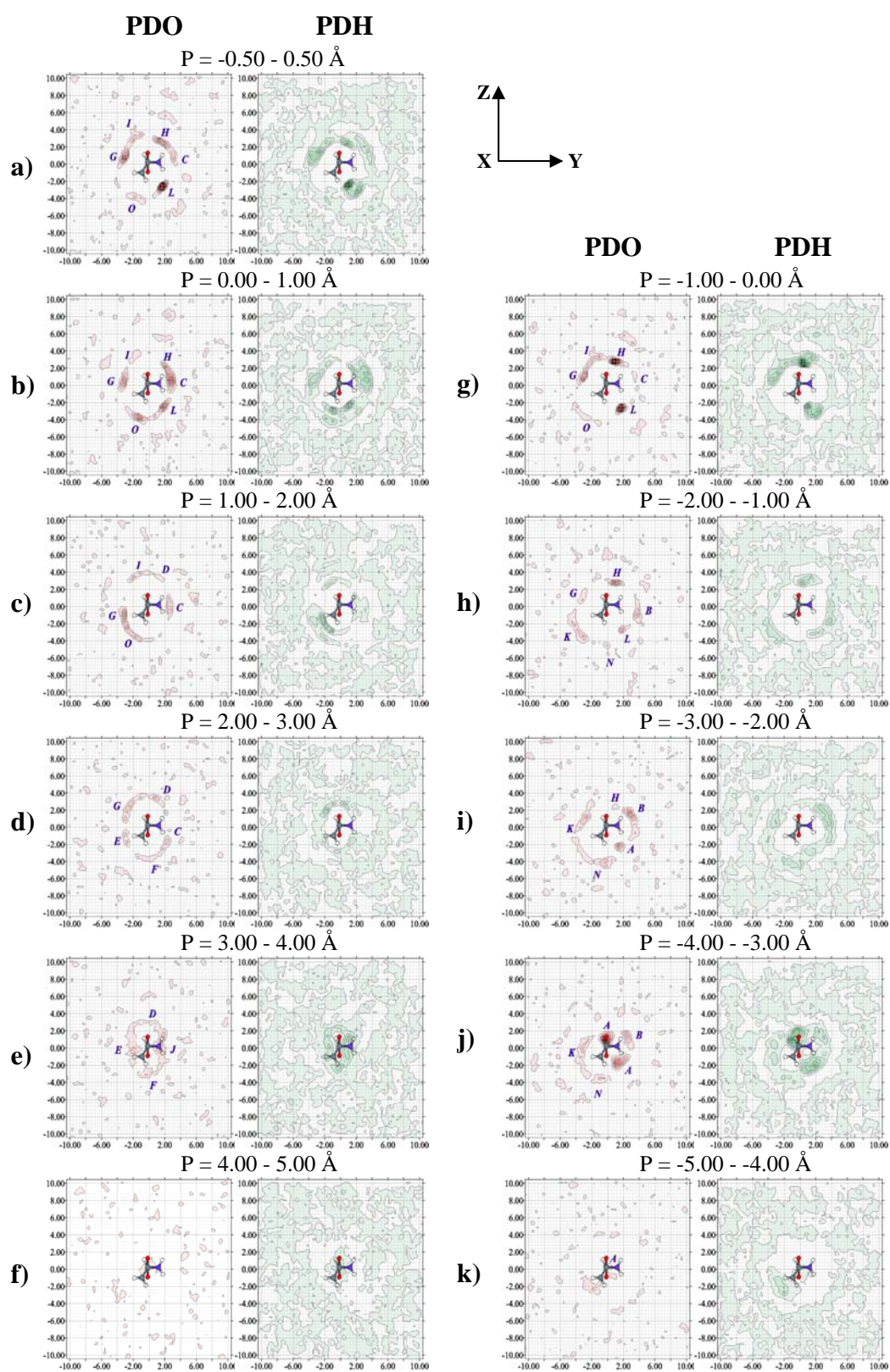


Figure D.3 PDO and PDH maps with respect to reference plane III for $[\text{Alaz-R}]_{\text{aq}}$ obtained from MD simulations. X-, Y- and Z-axis are in Å.

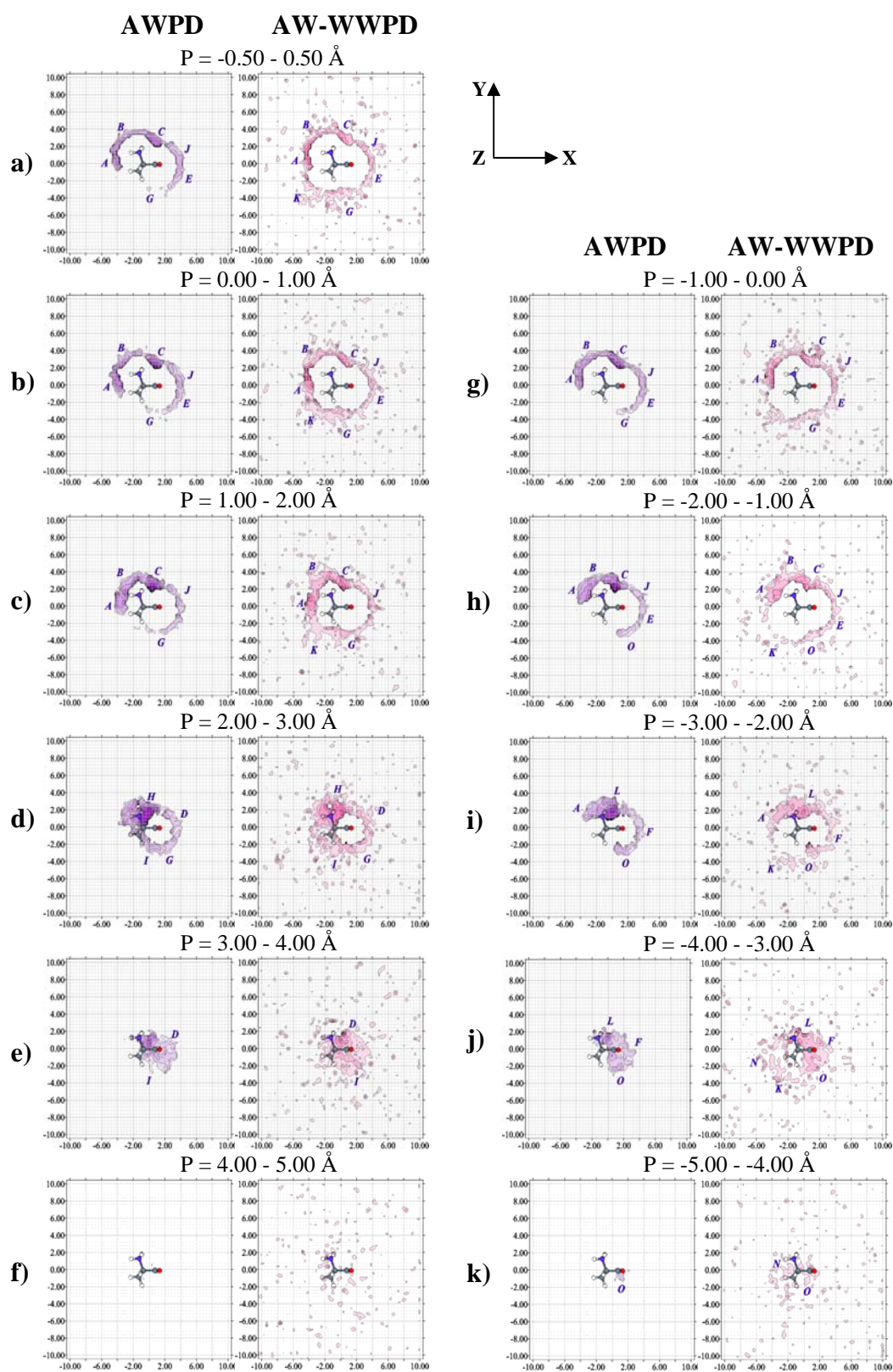


Figure D.4 AWPD and AW-WWPD maps with respect to reference plane I for $[\text{Alaz-R}]_{\text{aq}}$ obtained from MD simulations. X-, Y- and Z-axis are in \AA .

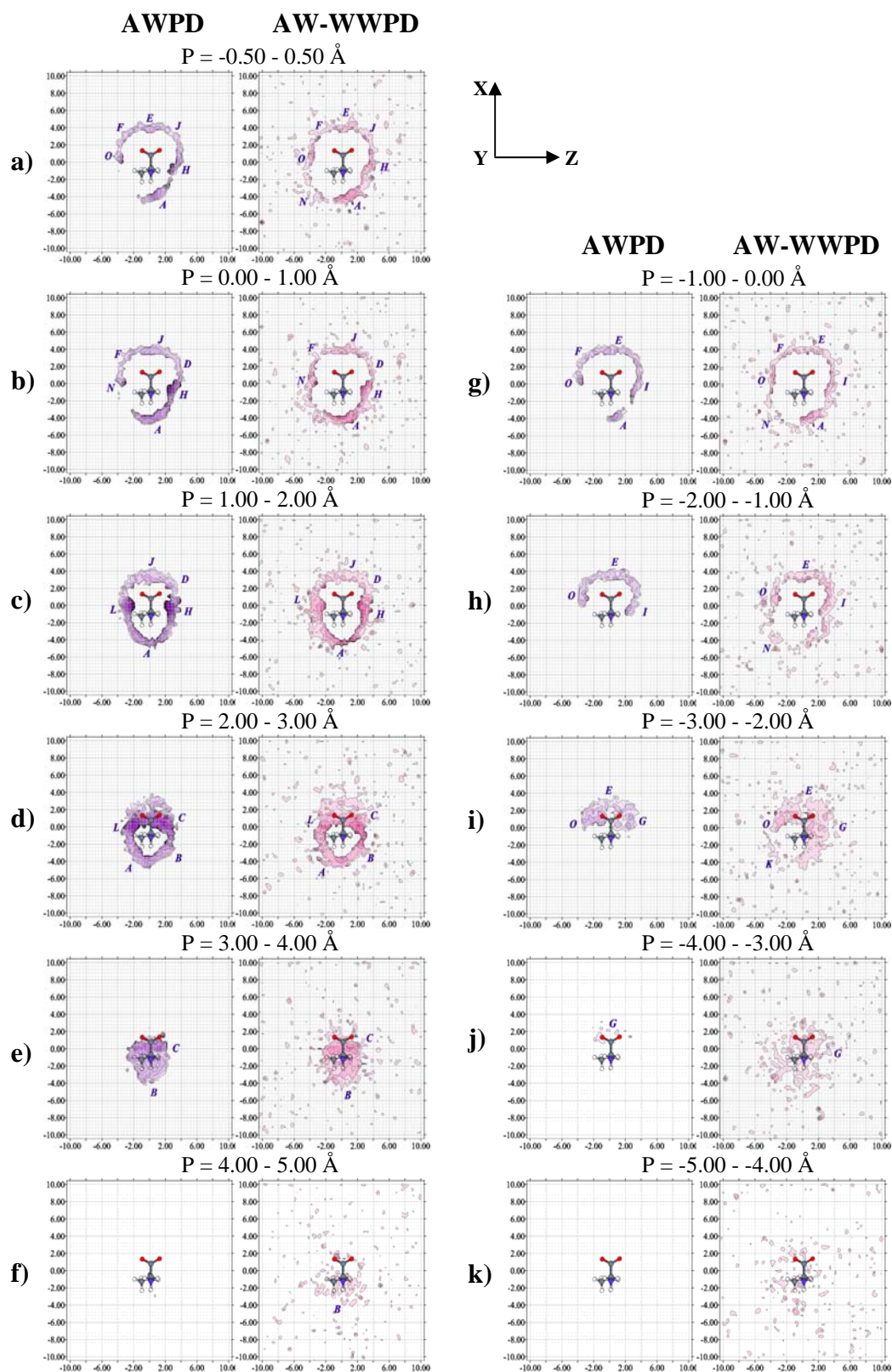


Figure D.5 AWPD and AW-WWPD maps with respect to reference plane II for $[\text{Alaz-R}]_{\text{aq}}$ obtained from MD simulations. X-, Y- and Z-axis are in Å.

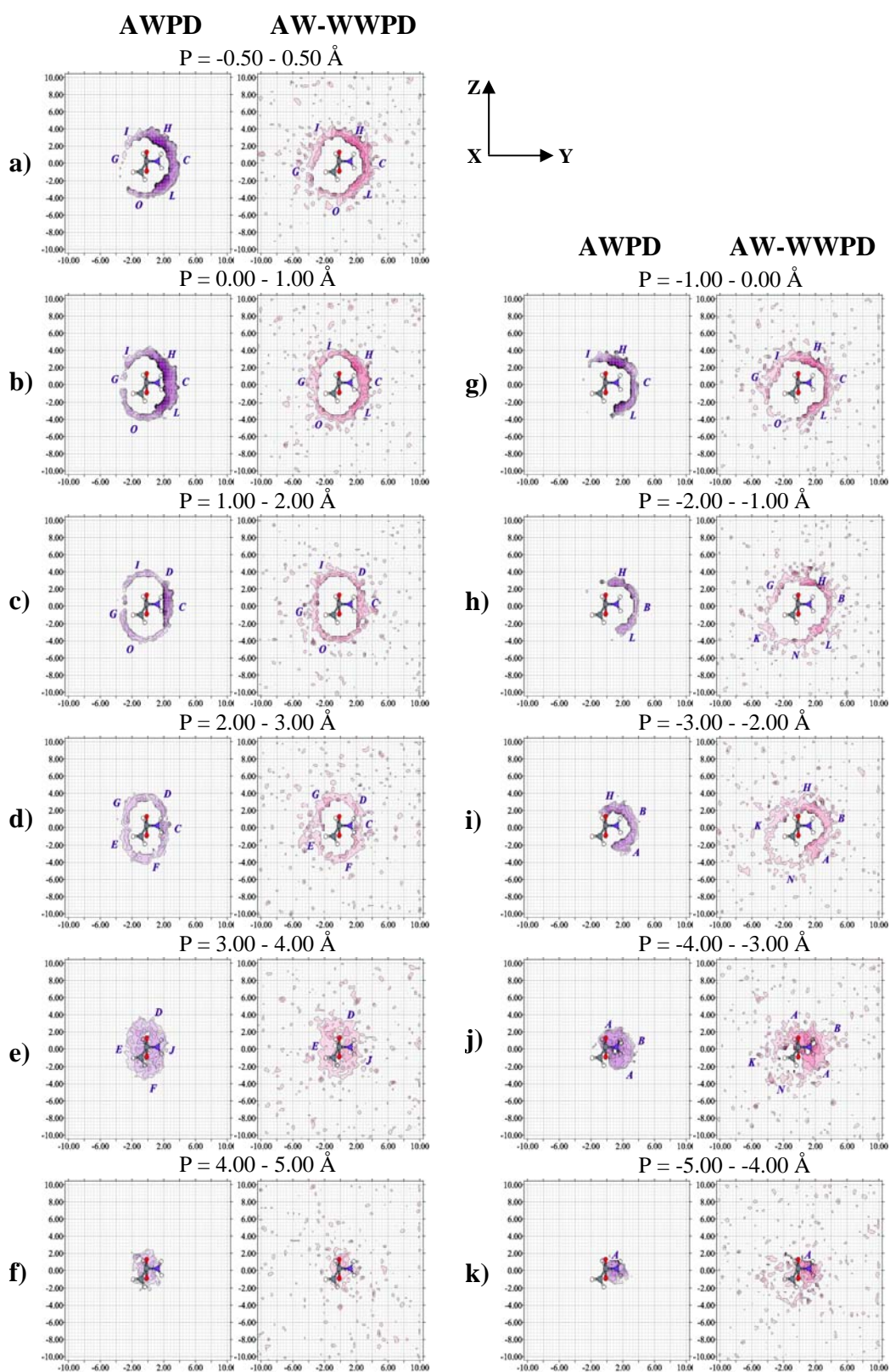


Figure D.6 AWPD and AW-WWPD maps with respect to reference plane III for $[\text{Alaz-R}]_{\text{aq}}$ obtained from MD simulations. X-, Y- and Z-axis are in Å.

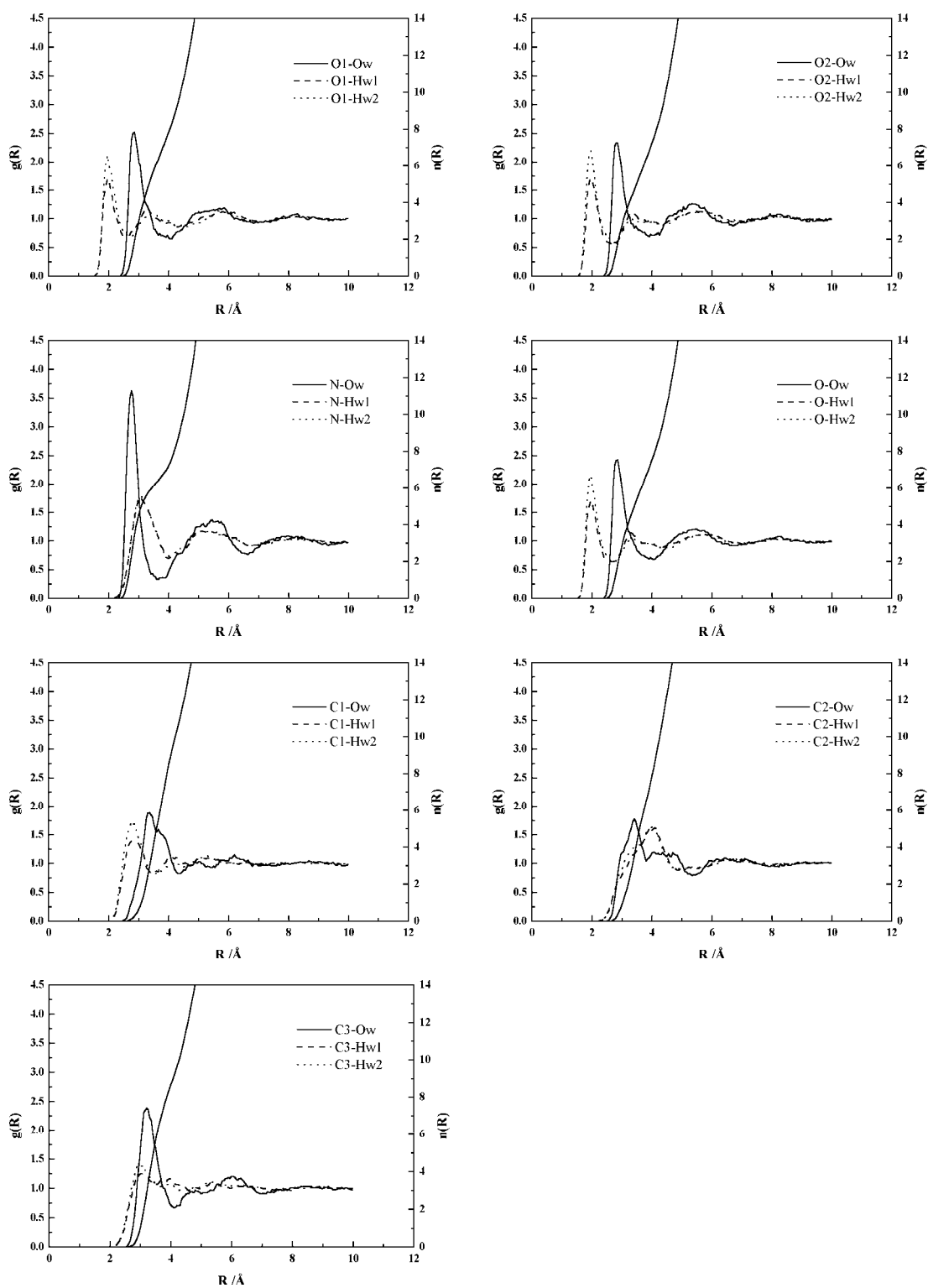


Figure D.7 $g(R)$ of $[\text{Alaz-R}]_{\text{aq}}$ at 298 K derived from MD simulations.

Ow, Hw1 and Hw2 are the oxygen and two hydrogen atoms of water, respectively.

APPENDIX E

PRESENTATION AND PUBLICATION

1. Supaporn Dokmaisrijan and Kritsana Sagarik (2-4 May 2000). "A Theoretical Investigation on Hydration-Induced Conformation of Model Amino Acids. A Progress Report", **Oral Presentation**, RGJ-Ph.D. Congress I, Felix River Kwai Resort, Kanchanaburi, Thailand.
2. Supaporn Dokmaisrijan and Kritsana Sagarik (18 May 2001). "A Theoretical Investigation on Alanine Zwitterion in Aqueous Solution", **Oral Presentation**, RGJ Seminar Series: Physical Chemistry, Kasetsart University (Pak Chong), Nakhon Ratchasima, Thailand.
3. Supaporn Dokmaisrijan and Kritsana Sagarik (21-23 July 2004). "Free Energy of Hydration for Alanine Zwitterions", **Oral Presentation**, The 8th Annual National Symposium on Computational Science and Engineering, Suranaree University of Technology, Nakhon Ratchasima, Thailand.
4. Supaporn Dokmaisrijan and Kritsana Sagarik (18-19 July 2002). "A Theoretical Investigation on Hydration Structures of Alanine Zwitterion", **Poster Presentation**, The 3rd National Symposium on Graduate Research, Suranaree University of Technology, Nakhon Ratchasima, Thailand.
5. Supaporn Dokmaisrijan and Kritsana Sagarik (10-11 August 2004). "A Theoretical Study on Relative Free Energy of Hydration of Alanine Zwitterions", **Poster Presentation**, The 4th National Symposium on Graduate Research, Lotus Hotel Pang Suan Kaew, Chiang Mai, Thailand.
6. Sagarik, K. and Dokmaisrijan, S. (2005). "A Theoretical Study of Alanine Zwitterions", **Journal of Molecular Structure (THEOCHEM)**, Vol. 718: 31-47.

CURRICULUM VITAE

Supaporn Dokmaisrijan

Education Background

1998 B.Sc. (Chemistry), Silpakorn University, Nakhon Pathom, Thailand

2005 Ph.D (Chemistry), Suranaree University of Technology,
Nakhon Ratchasima, Thailand

Experience

1996 Trainee in the Analytical Laboratory, Nitrochemical Co., Ltd.,
Samut Sakhon, Thailand

1997 Teaching assistant, Department of Chemistry, Faculty of Science,
Silpakorn University, Nakhon Pathom, Thailand

1998 Teaching assistant, School of Chemistry, Institute of Science,
Suranaree University of Technology, Nakhon Ratchasima, Thailand

2005 A short Ph.D. research at the Institute for Materials and Processes in
Energy System (IWV-3), Forschungszentrum Jülich, Jülich, F. R.
Germany

Scholarship

1998 The Royal Golden Jubilee (RGJ) Ph.D. Scholarship from Thailand
Research Fund (TRF)

Publication

Sagarik, K. and Dokmaisrijan, S. (2005). "A Theoretical Study of Alanine
Zwitterions", **Journal of Molecular Structure (THEOCHEM)** 718: 31-47.